

ATMOSPHERIC CIRCULATION AND MOISTURE TRANSPORT ASSOCIATED WITH  
LARGE-SCALE ORGANIZED CONVECTION OVER SUBTROPICAL SOUTH AMERICA

by

KYLE STEPHEN MATTINGLY

(Under the Direction of Thomas L. Mote)

ABSTRACT

Precipitation variability in the La Plata river basin of subtropical South America has wide-ranging social and economic implications. There is a well-documented out-of-phase relationship between precipitation in this region and in the South Atlantic Convergence Zone (SACZ), but few studies have investigated relationships between the SACZ and large, long-lived convective systems (LLCSs) that produce much of the annual precipitation over the La Plata basin. Additionally, the widespread presumption that these LLCSs are primarily initiated by moisture from the Amazon basin has heretofore received little scrutiny. This thesis demonstrates that active phases of the continental and oceanic portions of the SACZ have distinctly different relationships with La Plata LLCSs, and that the oceanic SACZ is more strongly related to LLCS activity over most of the La Plata basin. Results also suggest that regions other than the Amazon often contribute moisture to La Plata basin LLCSs, a finding that warrants further investigation.

INDEX WORDS: Climatology, Meteorology, Hydrology, Precipitation, Mesoscale convective systems, Monsoon, South Atlantic Convergence Zone, La Plata river, South America, Brazil, Argentina

ATMOSPHERIC CIRCULATION AND MOISTURE TRANSPORT ASSOCIATED WITH  
LARGE-SCALE ORGANIZED CONVECTION OVER SUBTROPICAL SOUTH AMERICA

by

KYLE STEPHEN MATTINGLY

B.S., Western Kentucky University, 2012

A Thesis Submitted to the Graduate Faculty of the University of Georgia in Partial Fulfillment of  
the Requirements for the Degree

MASTER OF SCIENCE

ATHENS, GA

2014

© 2014

Kyle Stephen Mattingly

All Rights Reserved

ATMOSPHERIC CIRCULATION AND MOISTURE TRANSPORT ASSOCIATED WITH  
LARGE-SCALE ORGANIZED CONVECTION OVER SUBTROPICAL SOUTH AMERICA

by

KYLE STEPHEN MATTINGLY

Major Professor: Thomas Mote

Committee: John Knox  
J. Marshall Shepherd

Electronic Version Approved:

Julie Coffield  
Dean of the Graduate School  
The University of Georgia  
August 2014

## ACKNOWLEDGMENTS

I am grateful to many people for their support and guidance during the process of completing my master's degree. I would first like to thank my advisor, Thomas Mote, for continually sharing his time and expertise with me throughout the past two years, and also for providing me with the rewarding experience of helping him teach undergraduate meteorology classes. My other committee members, John Knox and J. Marshall Shepherd, also were responsible for invaluable positive contributions to this thesis, and I would like to additionally thank them for teaching several outstanding classes that I have had the privilege to take.

I have also benefited tremendously from many other classes offered by the Geography department, and I thank the Geography faculty and staff as a whole for their commitment to excellent graduate and undergraduate education.

Special thanks also goes to Josh Durkee, who introduced me to this research topic and to the research process in general as my undergraduate advisor at Western Kentucky University, and who generously provided access to much of the data used in this thesis.

I have been lucky to be a part of a fantastic group of fellow graduate students in the Geography department. I would like to thank all of them for making the department such a fun and inspiring place to spend the past two years.

Last but not least, I owe many thanks to my family and friends for supporting / putting up with me as I worked toward my degree. I wouldn't have made it without all of you and I truly appreciate everything you have done for me.

## TABLE OF CONTENTS

	Page
ACKNOWLEDGMENTS .....	iv
LIST OF FIGURES .....	vii
LIST OF TABLES .....	xii
CHAPTER	
1 INTRODUCTION AND MOTIVATION .....	1
1.1 Study overview.....	1
1.2 Motivation .....	2
2 BACKGROUND .....	6
2.1 South American hydroclimate.....	6
2.2 Definition and regional climatology of large, long-lived convective systems .....	12
2.3 Research questions .....	13
3 DATA AND METHODOLOGY .....	25
3.1 Data sources .....	25
3.2 Methodology description.....	28
4 RESULTS .....	51
4.1 Atmospheric circulation features of SACZ and LLCS events .....	51
4.2 Continental and oceanic SACZ relationships with LLCS probability .....	57
4.3 LLCS moisture source analysis .....	64
4.4 Moisture sources and case studies of central Argentina LLCS events.....	69
5 DISCUSSION AND CONCLUSIONS .....	117

5.1 Discussion of major findings.....117

5.2 Future research .....120

REFERENCES .....122

## LIST OF FIGURES

	Page
Figure 1.1. Subtropical South America study domain.....	5
Figure 2.1. From Garreaud et al. (2009), atmospheric circulation features of the active and inactive phases of the South American monsoon .....	16
Figure 2.2. TMPA (TRMM Multisatellite Precipitation Analysis) daily mean precipitation for 45°S to 45°N during Oct–May of 1998–2007, showing the South Atlantic Convergence Zone as well as the South Pacific Convergence Zone and the South Indian / Southeast African Convergence Zone .....	17
Figure 2.3. From Nieto-Ferreira et al. (2011), daily precipitation patterns and 200-hPa height anomalies for an active period in the SESA portion of the South American Seesaw (left) and the SACZ (right) .....	18
Figure 2.4. From Vera et al. (2006a), schematic of typical 700-hPa circulation anomalies during active SESA (left) and SACZ (right) periods.....	19
Figure 2.5. From Bischof et al. (2004), map of the Brazil Current (white-outlined arrows) and sea surface temperature (shading) during Jan–Feb–Mar .....	20
Figure 2.6. MODIS Aqua-derived sea surface temperature climatology for Feb 2003–2014.....	21
Figure 2.7. TMPA (TRMM Multisatellite Precipitation Analysis) daily mean precipitation for the warm seasons (Oct–May) of 1998–2007 superimposed on shaded relief map of South America .....	22
Figure 2.8. From Jirak et al. (2003), examples of radar and satellite signatures of a mesoscale convective complex (left) and a persistent elongated convective system (right) .....	23
Figure 2.9. Spatial distribution of center points of mesoscale convective complexes (left, from Durkee and Mote 2009) and persistent elongated convective systems (right, from Mattingly 2012) over subtropical South America during the warm seasons of 1998–2007 .....	24
Figure 3.1. Sample scene of GOES infrared imagery used to compile LLCS dataset .....	37

Figure 3.2. Comparison of HYSPLIT back trajectories generated using NCEP-NCAR Reanalysis 1 (solid lines) and ERA-Interim (dashed lines) data for 25 randomly selected times and locations during the POR.....	38
Figure 3.3. Description of SACZ events during Jan 2006 from archived <i>Climanálise</i> bulletin published by the Brazilian Center for Weather Forecast and Climatic Studies (CPTEC) .....	39
Figure 3.4. Daily mean precipitation for the warm seasons (Oct–May) of 1998–2007 from the TRMM Multisatellite Precipitation Analysis (TMPA) .....	40
Figure 3.5. Standard deviation of daily precipitation for the warm seasons (Oct–May) of 1998–2007 from the TRMM Multisatellite Precipitation Analysis (TMPA).....	41
Figure 3.6. Time series of “percent domain” and “domain-average” TMPA precipitation and CFSR fields (850-hPa convergence, 700-hPa vertical velocity, 250-hPa divergence) considered for SACZ identification during the 2005–2006 warm season over the continental (top) and oceanic (bottom) SACZ domains .....	42
Figure 3.7. Mean 850-hPa convergence for all 6-hourly CFSR timesteps during the warm seasons (Oct–May) of 1998–2007 .....	43
Figure 3.8. Mean 700-hPa vertical velocity for all 6-hourly CFSR timesteps during the warm seasons (Oct–May) of 1998–2007 .....	44
Figure 3.9. Mean 250-hPa divergence for all 6-hourly CFSR timesteps during the warm seasons (Oct–May) of 1998–2007 .....	45
Figure 3.10. Distribution of daily precipitation summary statistics (top row: percentage of domain points receiving precipitation, middle row: domain-average precipitation, bottom row: $\log_{10}$ transformation of domain-average precipitation) over SACZ domains: continental (left column), oceanic (middle column), combined continental and oceanic (right column) .....	46
Figure 3.11. Percentage of days during each warm season month from 1998–2007 that were classified as having an active continental SACZ (red bars) or oceanic SACZ (blue bars).....	47
Figure 3.12. Locations of La Plata domains defined for composite atmospheric flow analysis of LLCs events .....	48
Figure 3.13. Locations of sub-domains defined for LLCs moisture source analysis.....	49

Figure 3.14. Locations of central Argentina LLCS domain (orange box) and South American Low-Level Jet domain (blue box) defined for moisture source analysis of central Argentina LLCS events.....	50
Figure 4.1. Median precipitable water (fill; $\text{kg m}^{-2}$ ) and 925-hPa wind (arrows; $\text{m s}^{-1}$ ) for subsets of SACZ activity: (a) continental and oceanic SACZ both inactive, (b) continental SACZ active only, (c) oceanic SACZ active only, (d) continental and oceanic SACZ both active.....	79
Figure 4.2. Composite PWAT and 925-hPa wind anomalies (percentile departure from Oct–May 1998–2007 climatological median) across subsets of SACZ activity described in Fig. 4.1.....	80
Figure 4.3. As in Fig. 4.1 but for subsets of La Plata domain LLCS activity: (a) no active LLCS in La Plata domain, (b) active LLCS anywhere in domain, (c) active LLCS in East La Plata domain only, (d) active LLCS in West La Plata domain only.....	81
Figure 4.4. As in Fig. 4.2 but for subsets of La Plata domain LLCS activity described in Fig. 4.3.....	82
Figure 4.5. Composite PWAT and 925-hPa wind anomalies across subsets of SACZ (columns) and La Plata LLCS (rows) activity.....	83
Figure 4.6. Median 300-hPa geopotential height (contour lines; $\times 10^{-1}$ m), wind (arrows; $\text{m s}^{-1}$ ), and divergence (fill; $\times 10^5 \text{ s}^{-1}$ ) for subsets of SACZ activity described in Fig. 4.1.....	84
Figure 4.7. Composite anomalies of 300-hPa height (contour lines), wind (arrows), and divergence (fill) across subsets of SACZ activity described in Fig. 4.1.....	85
Figure 4.8. As in Fig. 4.6 but for subsets of LLCS activity described in Fig. 4.3.....	86
Figure 4.9. As in Fig. 4.7 but for subsets of LLCS activity described in Fig. 4.3.....	87
Figure 4.10. Composite 300-hPa height, wind, and divergence anomalies across subsets of SACZ (columns) and La Plata LLCS (rows) activity.....	88
Figure 4.11. $0.25^\circ \times 0.25^\circ$ gridded probability of LLCS occurrence for each month during the Oct–May austral warm season (based on 1998–2007 study period).....	89
Figure 4.12. $0.25^\circ \times 0.25^\circ$ gridded probability of LLCS occurrence across SACZ phases: (a) neither SACZ active, (b) continental active only, (c) oceanic active only, and (d) both active.....	90

Figure 4.13. Logistic regression predicted daily LLCS probability for “continental” representative point (left side plots) and “oceanic” representative point (right side plots) across all percentiles of oceanic SACZ precipitation (top plots) and continental SACZ precipitation (bottom plots).....	91
Figure 4.14. $0.25^\circ \times 0.25^\circ$ gridded logistic regression coefficient for continental SACZ precipitation .....	92
Figure 4.15. As in Fig. 4.14 except for oceanic SACZ precipitation logistic regression coefficient .....	93
Figure 4.16. Logistic regression predicted probability of LLCS occurrence across combinations of representative “low” and “high” continental (top row) and oceanic (bottom row) SACZ precipitation percentiles (10 <sup>th</sup> and 90 <sup>th</sup> ) with precipitation over the other domain held constant at its median.....	94
Figure 4.17. Difference between the respective absolute values of the continental and oceanic SACZ precipitation coefficients .....	95
Figure 4.18. Median precipitable water ( $\text{kg m}^{-2}$ ) and 925-hPa wind vectors ( $\text{m s}^{-1}$ ) for each month of the austral warm season (Oct–May) during the 1998–2007 study period.....	96
Figure 4.19. Map of HYSPLIT modeled 120-hour parcel back trajectories at 10 meters above ground level for all 6-hourly merged LLCS cloud shields.....	97
Figure 4.20. As in Fig. 4.19 but for 1000m AGL trajectories .....	98
Figure 4.21. As in Figs. 4.19 and 4.20 but for 2500 AGL trajectories .....	99
Figure 4.22. Density of all 10m AGL LLCS back trajectories.....	100
Figure 4.23. As in Fig. 4.22 but for 1000m AGL trajectories .....	101
Figure 4.24. As in Fig. 4.23 except for 2500m AGL trajectories .....	102
Figure 4.25. HYSPLIT modeled 120-hour parcel back trajectories at 10 meters AGL for all 6-hourly merged LLCS cloud shields grouped by sub-domains: (a) West La Plata, (b) East La Plata, (c) Amazon, (d) Continental SACZ, (e) Oceanic SACZ, (f) Oceanic other.....	103
Figure 4.26. As in Fig. 4.25 except for 1000m AGL trajectories .....	104
Figure 4.27. As in Figs. 4.25 and 4.26 except for 2500m AGL trajectories.....	105

Figure 4.28. Trajectory density plots for the “West La Plata” sub-domain grouped by hours preceding LLCS valid time: 96–120 hours before LLCS time (leftmost column), 72–96 hours before (second column from left), 48–72 hours before (middle column), 24–48 hours before (second column from right), and 0–24 hours before (rightmost column) .....	106
Figure 4.29. As in Fig. 4.28 except for “East La Plata” sub-domain.....	107
Figure 4.30. As in Figs. 4.28–4.29 except for “Oceanic other” domain.....	108
Figure 4.31. As in Figs. 4.28–4.30 except for “Continental SACZ” domain .....	109
Figure 4.32. As in Figs. 4.28–4.31 except for “Oceanic SACZ” domain.....	110
Figure 4.33. As in Figs. 4.28–4.32 except for “Amazon” domain .....	111
Figure 4.34. Percentage of central Argentina LLCS events during each warm season month that fell each SALLJ connection category: no levels (no HYSPLIT modeled back trajectories at any of the three levels for any of the LLCS’s 6-hourly timesteps passed through the SALLJ domain), 1 level (back trajectory at 1 of 3 levels passed through the SALLJ domain), 2 levels (back trajectories at 2 of 3 levels passed through the SALLJ domain), 3 levels (back trajectories at all 3 levels passed through the SALLJ domain) .....	112
Figure 4.35. Distribution of central Argentina LLCS maximum cloud shield area across same categories of SALLJ connection as in Fig. 4.34 .....	113
Figure 4.36. As in Fig. 4.35 except for distribution of LLCS duration .....	114
Figure 4.37. Precipitable water (fill; $\text{kg m}^{-2}$ ) and 925-hPa wind vectors ( $\text{m s}^{-1}$ ) for four timesteps during Oct 2001 case study LLCS event: (a) 0000 UTC 15 Oct 2001, (b) 1200 UTC 15 Oct 2001, (c) 0000 UTC 16 Oct 2001, (d) 1200 UTC 16 Oct 2001 .....	115
Figure 4.38. As in Fig. 4.37 except for Apr 2004 case study LLCS event at timesteps: (a) 1800 UTC 11 Apr 2004, (b) 0600 UTC 12 Apr 2004, (c) 1800 UTC 12 Apr 2004, (d) 0600 UTC 13 Apr 2004.....	116

## LIST OF TABLES

	Page
Table 2.1. Mesoscale Convective Complex (MCC) and Large, Long-lived Convective Complex (LLCS) definitions .....	15
Table 4.1. Number of days during the Oct–May 1997–2008 POR that were classified in each SACZ category .....	73
Table 4.2. Number of 6-hourly timesteps during the Oct–May 1997–2008 POR that were classified in each LLCS category.....	74
Table 4.3. Output generated by logistic regression model for the “continental” representative point (-22.875S, -55.125W).....	75
Table 4.4. Output generated by logistic regression model for the “oceanic” representative point (-31.125S, -41.125W).....	76
Table 4.5. Number of “Central Argentina” LLCS events and their mean maximum area and duration across SALLJ connection categories .....	77
Table 4.6. Tukey’s Honestly Significant Difference Test results for differences in mean Central Argentina LLCS maximum area and duration between pairs of SALLJ connection categories .....	78

## CHAPTER 1

### INTRODUCTION AND MOTIVATION

#### **1.1 Study overview**

Subtropical South America regularly experiences some of the largest, longest-lasting, and most intense organized thunderstorms in the world. These thunderstorm complexes, known as mesoscale convective systems (MCSs), produce a substantial proportion of the region's annual precipitation (Durkee et al. 2009) and are associated with many forms of hazardous weather including large hail, damaging winds, tornadoes, and flash flooding (Maddox 1980; Tollerud and Collander 1993; Rasmussen and Houze 2011; Silva Dias 2011). MCSs in the South American subtropics are most common between the months of October–May, during the warm phase of the South American monsoon (Velasco and Fritsch 1987). Spatially, warm-season MCSs are concentrated in the La Plata river basin of southeastern South America (SESA; see Fig. 1.1), which encompasses much of southern Brazil, Paraguay, Uruguay, southern Bolivia, and northern and central Argentina (Durkee and Mote 2009; Mattingly 2012). Precipitation in this region has been shown by numerous studies (e.g. Nogués-Paegle and Mo 1997; Diaz and Aceituno 2003; Liebmann et al. 2004) to be negatively correlated with precipitation in the South Atlantic Convergence Zone (SACZ), an elongated northwest-to-southeast oriented area of clouds, precipitation, and atmospheric mass convergence often observed across southeast Brazil and the adjacent southwest Atlantic Ocean.

Despite extensive research into this “South American Seesaw” precipitation dipole (Nogués-Paegle and Mo 1997), there has been little published work on any relationships between the SACZ and MCS activity over the La Plata basin. An initial study by Durkee (2008) suggests

that periods of enhanced rainfall in the SACZ are associated with a northeastward displacement of MCSs and a shift in moisture flux from the Amazon basin toward the SACZ region. However, this analysis of MCS – SACZ relationships was somewhat limited in examining only a subset of quasi-circular MCSs known as mesoscale convective complexes (MCCs), and in its use of a SACZ definition that does not account for differences in location of SACZ episodes. Another significant finding of Durkee (2008) was the existence of MCSs in the higher latitudes of central Argentina that may develop in the absence of moisture flux from the Amazon River basin via the South American Low-Level Jet (SALLJ). This suggests the canonical assumption that the SALLJ is the primary moisture source for organized convection over the La Plata basin may not be valid in all cases.

These gaps in understanding of the atmospheric drivers of large-scale organized convection over the La Plata basin hold wide-ranging implications and warrant further investigation. Therefore, the objective of this thesis is to more thoroughly explore atmospheric circulation patterns and moisture transport regimes associated with the formation of these large, long-lived convective systems (LLCSs) in subtropical South America and their relationships with SACZ activity. Particular emphasis is placed upon LLCs in central Argentina that may receive moisture from sources other than the Amazonian SALLJ.

## **1.2 Motivation**

The La Plata river basin is the fifth largest in the world, with an areal extent of approximately 3.6 million km<sup>2</sup>. It is one of the world's centers of food production, and the regional economy is largely based on agriculture. According to the Food and Agriculture Organization of the United Nations, both Brazil and Argentina rank among the world's top ten producers of numerous agricultural products, including soybeans, maize, and beef (FAO 2014), and these two countries rank second and third, respectively, behind the United States as

producers of genetically modified crops (Delvenne et al. 2013; Goldfarb and Zoomers 2013; ISAAA 2014). Moreover, the majority of electricity in SESA is generated by hydropower plants on the region's numerous rivers (the Itaipú hydroelectric plant on the Paraná River alone generates over 95% of Paraguay's electricity and 24% of Brazil's), and most drinking water in the region (including that of Buenos Aires and São Paulo, the two largest cities in South America) is supplied by these rivers (Mechoso et al., 2001).

These facts show that subtropical South America is highly vulnerable to fluctuations in rainfall, and any shortages or excesses in precipitation hold profound economic and social implications for the region. Durkee et al. (2009) showed that MCCs contribute substantially to the region's warm-season precipitation, and Mattingly (2012) determined that non-MCC LLCs (known as persistent elongated convective systems or PECS) are much more numerous and are both larger and longer-lasting on average than their MCC counterparts. Therefore it is reasonable to surmise that LLCs account for a large proportion of regional precipitation, and fluctuations in LLC activity have wide-ranging economic and social consequences.

An improved understanding of the current relationships between LLCs, the SACZ, and atmospheric flow regimes in SESA will also be beneficial as a baseline for the assessment of past and possible future variability in regional precipitation. Vimeux et al. (2011) found that the intraseasonal variability in precipitation patterns associated with the South American Seesaw is closely related to the isotopic composition of rainfall in the Bolivian Andes, while Insel et al. (2013) and Jouzel et al. (2013) suggest that the source region of moisture is an important factor in determining the isotopic composition of precipitation that falls in the Andes. The analysis of moisture sources of SESA LLCs in this study will thus aid in the interpretation of the isotopic composition of regional precipitation samples and paleoclimate proxy records.

According to Penalba and Robledo (2010), much of the La Plata basin experienced an increasing trend in precipitation and heavy precipitation events between 1950 and 2000. Climate model simulations analyzed by Junquas et al. (2012) suggest that this trend will continue, with an increase in summer rainfall in the La Plata basin and a decrease in the SACZ region projected during the 21<sup>st</sup> Century under a midrange (SRES-A1B) global warming scenario. However, there is a great deal of uncertainty in these predictions, as most climate models have difficulty in reproducing the current large-scale atmospheric mechanisms that influence precipitation variability in SESA (Vera and Silvestri 2009). Therefore this study's contribution to the body of scientific knowledge on the large-scale dynamics and moisture source regions that drive South American hydroclimate will help provide a valuable platform for researchers to build upon as they continue to evaluate current and future trends in precipitation variability across the subtropics of South America.



**Fig. 1.1.** Subtropical South America study domain.

## CHAPTER 2

### BACKGROUND

#### **2.1 South American hydroclimate**

##### *a. The South American monsoon*

The tropical and subtropical regions of South America can be described as having a complex monsoon climate system (Nogués-Paegle et al. 2002). As with other monsoons, climate variability over most of the continental land mass (north of 35°S) is characterized by a pronounced seasonal cycle in rainfall. During austral winter, most continental precipitation occurs north of the equator near the position of the oceanic Intertropical Convergence Zone (ITCZ). A rapid southward shift in precipitation occurs during October–November, with maximum precipitation during austral summer covering a broad region of the tropical and subtropical continent extending from the southern Amazon basin to northern Argentina (Fig. 2.1). Although this seasonal shift in precipitation is forced by the low thermal inertia of the continental land surface relative to the adjacent oceans, a defining feature of monsoon systems, Garreaud et al. (2009) point out that the South American climate system is not truly monsoonal because the mean easterly low-level winds off the equatorial Atlantic never reverse direction (see Fig. 2.1). However, most scientists (e.g. Vera et al. 2006a; Carvalho et al. 2012; Vuille et al. 2012) still refer to this pronounced seasonal cycle as the “South American monsoon”, and this naming convention will be maintained in this thesis.

In the South American subtropics, a defining feature of the warm phase of the monsoon is a persistent near-surface region of low pressure centered in the lee of the Andes near 25°S (Seluchi et al. 2003), known as the “Chaco Low” due to its average position in the Chaco region

of southern Bolivia, western Paraguay, and northern Argentina. It can be identified in Fig. 2.1a by the clockwise (cyclonic) turning of the mean January 925-hPa wind vectors in the western part of the continent between 20°S and 30°S. Moisture-laden easterly winds in the Amazon basin are directed to the south by this circulation and the topographic blocking effects of the Andes. Strong episodes of this poleward flow are known as the South American Low Level Jet (SALLJ) and transport large quantities of moisture southward and southeastward to higher subtropical latitudes (Saulo et al. 2000; Vera et al. 2006b). In the upper levels of the atmosphere, latent heat release by summer convection in the Amazon basin leads to the development of a high-pressure cell known as the Bolivian High (Lenters and Cook 1997), which clearly appears in Fig. 2.1c as a counterclockwise (anticyclonic) circulation in the 300-hPa winds over the western two-thirds of the continent between 10°S and 25°S. Downstream of this feature, an upper-level cyclonic circulation appears as a clockwise flow of the 300-hPa winds over the northeast coast of Brazil (Fig. 2.1c).

b. *The South Atlantic Convergence Zone and the South American Seesaw*

The South Atlantic Convergence Zone (SACZ) is a prominent northwest-to-southeast oriented band of enhanced warm-season convection extending diagonally from the central Amazon basin into the Atlantic Ocean. It is a hallmark feature of the warm phase of the South American monsoon and is one of several large-scale subtropical southern hemisphere convergence zones (Fig. 2.2), including the South Pacific Convergence Zone (Vincent 1994) and the South Indian / Southeast African Convergence Zone (Cook 2000; McHugh and Rogers 2001). The SACZ appears suddenly at the onset of the monsoon as a result of an abrupt change in the structure and propagation of mid-latitude cold frontal systems penetrating northward into the South American subtropics (Nieto-Ferrera et al. 2011). Once this transition occurs,

subsequent SACZ events are triggered by the intrusion of synoptic-scale extratropical disturbances into the subtropics, which become stationary and combine with large-scale moisture flux from the Amazon to enhance convergence for a number of days (Gan et al. 2004; Muza et al. 2009). Although the area affected by the SACZ is relatively consistent on an interannual basis, individual SACZ events during each warm season vary substantially in location, duration, and intensity (Muza et al. 2009, de Oliveira Vieira et al. 2012; Romatschke and Houze 2013). In particular, Carvalho et al (2004) and Muza et al. (2009) have shown that atmospheric circulation patterns during enhanced SACZ events over the land mass of central and southeastern Brazil (the “continental” SACZ region) are distinct from those associated with SACZ events over the western Atlantic Ocean (the “oceanic” SACZ region), and that continental and oceanic SACZ events often occur independently of one another.

Once the warm-season SACZ is established, the “Seesaw” between precipitation in the SACZ region and southeastern South America (SESA) oscillates on average time scales of 10–15 days throughout the warm season (Liebmann et al. 2004). During periods of enhanced precipitation in SESA, a strong SALLJ located east of the Andes enhances moisture flux from the Amazon region to the subtropics and low-level zonal easterly wind anomalies over the central Amazon basin of Brazil serve to decrease the strength of low-level convergence in the SACZ region. During periods of enhanced SACZ precipitation, low-level westerly wind anomalies over tropical Brazil enhance low-level convergence in the SACZ, and moisture flux to the La Plata basin is cut off. In the upper levels of the atmosphere, enhanced precipitation in SESA is associated with a cyclonic circulation anomaly over central Argentina and Chile and an anticyclonic anomaly over the southern Atlantic Ocean near the coast of southern Brazil, with these features reversed during enhanced SACZ periods. Figures 2.3 and 2.4 summarize

precipitation and atmospheric circulation patterns associated with each phase of the South American Seesaw.

*c. Extratropical air intrusions and mid-latitude Rossby waves*

Although this study is primarily concerned with organized convection related to the warm phase of the tropical and subtropical South American monsoon, the variability of LLCS and SACZ activity in SESA is also affected by extratropical atmospheric mechanisms. Mid-latitude cold air surges along the east side of the Andes typically occur at one- to two-week intervals throughout the year over subtropical South America (Garreaud 2000). During the warm season, these cold air intrusions often organize MCSs along their leading edge as they enter subtropical South America, and they can play a role in the formation of SACZ events when their progress slows along the southeastern coast of Brazil (Siqueira et al. 2005; Nieto-Ferriera et al. 2011).

Extratropical atmospheric processes are particularly prominent in the higher latitudes of central and southern Argentina, where precipitation variability is influenced more directly by transient mid-latitude baroclinic waves than by the monsoonal regime (Garreaud et al. 2009). In this region, westerly winds associated with the southern hemisphere mid-latitude jet stream prevail throughout the troposphere during all seasons, and precipitation is largely produced by extratropical cyclones whose paths are determined by the extratropical Rossby wave train (Lenters and Cook 1999; Vera et al. 2002). Given that Durkee et al. (2008) found MCC events in central Argentina that were potentially disconnected from the SALLJ and several studies (e.g. Hoke et al. 2013; Viale and Garreaud 2014) have determined that the moisture source of precipitation along both the eastern and western slopes of the Argentinian Andes can often be traced to the Pacific Ocean, it is possible that some proportion of LLCs in central Argentina are formed by the uplift of Pacific moisture by extratropical cyclones.

d. *South Atlantic ocean characteristics*

An important feature of the oceanic circulation along the eastern coast of South America is the Brazil Current, a weak western boundary current that transports warm water from the equatorial Atlantic poleward along the coasts of Brazil and Uruguay from around 10°S to 38°S latitude (Bischof et al. 2004). It borders the eastern coast of Brazil closely for most of its length, and then is diverted offshore by the cold Malvinas Current flowing northward from the Antarctic region as it approaches the Rio de la Plata estuary (Fig. 2.5). The region where these two currents collide, known as the Brazil-Malvinas Confluence Zone, is one of the most energetic areas in the world's oceans (Saraceno et al. 2004; Pezzi et al. 2005).

Sea surface temperatures (SSTs) in the Brazil Current typically range from 18°C to 28°C, with highest SSTs occurring during the height of the warm season (January through March) in the northern part of the current off the east coast of Brazil (Bischof et al. 2004). These warm season SSTs are comparable to slightly below those observed in the equatorial Atlantic waters from which the Brazil Current originates (Fig. 2.6; Bischof et al. 2003). This observation, along with the documented high rates of oceanic and atmospheric boundary layer mass exchange in the region of the Brazil Current (Pezzi et al. 2009), suggests that the warm waters off the eastern coast of South America may serve as a prominent moisture source region for precipitation in SESA. Indeed, Doyle and Barros (2002) found that anomalously warm SSTs along the eastern coast of South America north of 40°N were associated with an enhancement of precipitation over northern Argentina, Uruguay, and southern Paraguay and a decrease in SACZ activity during the summer, while anomalously cool SSTs in the same region favored enhanced SACZ activity and a decrease in La Plata basin precipitation. A similar relationship between anomalously warm coastal South America SSTs and enhanced precipitation in Uruguay and southern Brazil was

demonstrated by both Diaz et al. (1998) and Bombardi et al. (2014). Additionally, Travasso et al. (2003) concluded that positive South Atlantic SST anomalies are associated with increased maize and wheat yields over much of northern Argentina and are a more robust predictor of yields than ENSO variability for most of the region.

e. *Summary of warm season precipitation patterns*

Figure 2.7, which displays mean TMPA (TRMM Multisatellite Precipitation Analysis; defined in section 3.1b) daily precipitation superimposed on a shaded relief map of South America, provides an overview of the aspects of South American warm season hydroclimate discussed in this section and allows for the discussion of a few other interesting precipitation features. The continental and oceanic portions of the SACZ clearly appear as a northwest-to-southeast oriented band of higher daily average precipitation extending from the Amazon basin southeastward into the Atlantic Ocean. Notably, the highest precipitation values in the continental SACZ region coincide with the highest elevations of the Brazilian Highlands (Kodama et al. 2012), and these continental average daily precipitation totals are substantially higher than the average totals in the oceanic SACZ.

The highest daily average precipitation totals in the La Plata basin occur along the western slopes of the southern extension of the Brazilian Highlands in the Brazilian states of Paraná, Santa Catarina, and Rio Grande do Sul, and in adjacent regions of far northeastern Argentina and southern Paraguay. There is also a prominent area of high daily average precipitation along the eastern coast of Brazil's Paraná state near the city of Paranaguá, which can likely be attributed to convergence of moisture from the Brazil Current along the narrow coastal plain forced by the steep slopes of the Brazilian Highlands a few miles inland. Just to the northeast of this precipitation maximum, between the cities of Curitiba and São Paulo (see Fig.

1.1), the Brazilian Highlands taper to a narrow sliver of elevated terrain near the coast; this gap in the Highlands likely serves as a pathway for moisture flux from the South Atlantic to the La Plata basin on the continental side of this narrow divide. Finally, it is worth noting the pronounced drop in average daily precipitation from the Amazon Basin to the La Plata basin in east central Bolivia. The topographic divide between these basins is relatively low, but it nevertheless forms a distinct boundary between the humid Amazon basin and the more arid La Plata basin.

## **2.2 Definition and regional climatology of large, long-lived convective systems**

A large proportion of prior research pertaining to mesoscale convective systems has focused on a subclass of long-lasting MCSs that are quasi-circular at the time of their maximum cloud shield extent, known as mesoscale convective complexes (MCCs). Based on characteristics derived from infrared satellite imagery, Maddox (1980) defined cloud-top temperature, cloud shield area, cloud shield eccentricity, and duration criteria that a contiguous area of deep convection must meet to be classified as an MCC. Subsequent studies (e.g., Augustine and Howard, 1988; Jirak et al., 2003; Durkee and Mote, 2009) have slightly altered the original cloud shield area criteria (see Table 2.1), but Maddox's requirement that cloud shield eccentricity must be  $\geq 0.7$  at the time the system reaches its maximum extent has continued to be widely employed in MCC research. This arbitrary requirement (Maddox stated that the shape requirement "was arbitrarily specified to preclude classification of linear type systems as MCCs") has resulted in comparatively little analysis of large, long-lived convective systems that are quasi-linear at their time of maximum extent. Anderson and Arritt (1998) provided one of the first such studies, keeping all criteria in the MCC definition except the shape requirement to provide a climatology of "persistent elongated convective systems" (PECSs) in the U.S. during

1992–93. PECSs are the same as MCCs in every respect except for their  $\leq -52^{\circ}\text{C}$  contiguous cloud shield eccentricity at maximum extent, which for PECSs must be between 0.2 and 0.7 (see Fig. 2.8). This thesis will use a combined dataset of both MCCs and PECSs in subtropical South America to analyze their associated circulation patterns; together, MCCs and PECSs will be referred to as large, long-lived convective systems (LLCSs).

Several previous studies have detailed the characteristics of LLCSs in the subtropical South America (SSA) study region. Velasco and Fritsch (1987) found that MCCs in the region during 1981–1983 were spatially concentrated in Paraguay and adjacent areas of southern Brazil, southern Bolivia, northern Argentina, and northern Uruguay. Durkee and Mote (2009) compiled a more extensive sample of MCCs encompassing the warm seasons (October–May) of 1998 through 2007; their results were in agreement with Velasco and Fritsch (1987) regarding the spatial concentration of MCCs in Paraguay and adjacent countries, and they also determined that MCCs in SSA are, on average, both larger and longer-lasting than MCC events in North America. Mattingly (2012) extended this climatological analysis to PECSs for the same temporal and spatial domains as Durkee and Mote (2009), finding that PECS events occur more frequently than MCCs in SSA and are larger and longer-lasting on average than their MCC counterparts. The spatial distribution of PECSs is similar to that of MCCs (Fig. 2.9). Together, these studies show that LLCSs in SSA occur most frequently in the La Plata river basin, and that quasi-linear events (PECSs) account for a substantially larger proportion of the LLCS population than quasi-circular MCCs.

### **2.3 Research questions**

The objective of this thesis is to provide a more thorough analysis of atmospheric circulation and moisture transport across the South American subtropics associated with the

formation of LLCs, and to determine how these circulation patterns are related to SACZ activity. Specifically, this study addresses the following research questions:

- How do lower- and upper-tropospheric atmospheric circulation patterns related to LLC development over the La Plata basin vary across oceanic and continental SACZ episodes and times with no SACZ present?
- Does enhanced precipitation in both the continental and oceanic SACZ always simultaneously coincide with reduced LLC probability in the La Plata basin, or is this relationship more complex?
- Is the SALLJ the only moisture source for LLCs in the La Plata basin? How do moisture source regions associated with LLCs vary for LLCs located over different regions of subtropical South America?
- Can LLCs occur over the higher latitudes of central Argentina in the absence of moisture transport from the Amazon via the SALLJ? If so, how common are these “non-SALLJ” events and how do their characteristics compare to “SALLJ” LLCs?

**Table 2.1.** Mesoscale Convective Complex (MCC) and Large, Long-lived Convective Complex (LLCS) definitions. MCC definition established by Maddox (1980), with cloud top temperature modification described in Augustine and Howard (1988).

**Mesoscale Convective Complex (MCC) and Large, Long-lived Convective System (LLCS) Characteristics**

---



---

<b>Size:</b>	Interior contiguous cold–cloud region with IR temperature of $\leq -52$ °C must have an area of $\geq 50\,000$ km <sup>2</sup>
<b>Initiation:</b>	Size definition first satisfied
<b>Duration:</b>	Size definition must be met for $\geq 6$ hours
<b>Maximum Extent:</b>	Contiguous cold–cloud shield (IR temperature $\leq -52$ °C) reaches maximum size
<b>Shape:</b>	<p><b>MCC:</b> Eccentricity (minor axis/major axis) <math>\geq 0.7</math> at time of maximum extent</p> <p><b>LLCS:</b> Eccentricity (minor axis/major axis) <math>\geq 0.2</math> at time of maximum extent</p>
<b>Termination:</b>	Size definition no longer satisfied

---

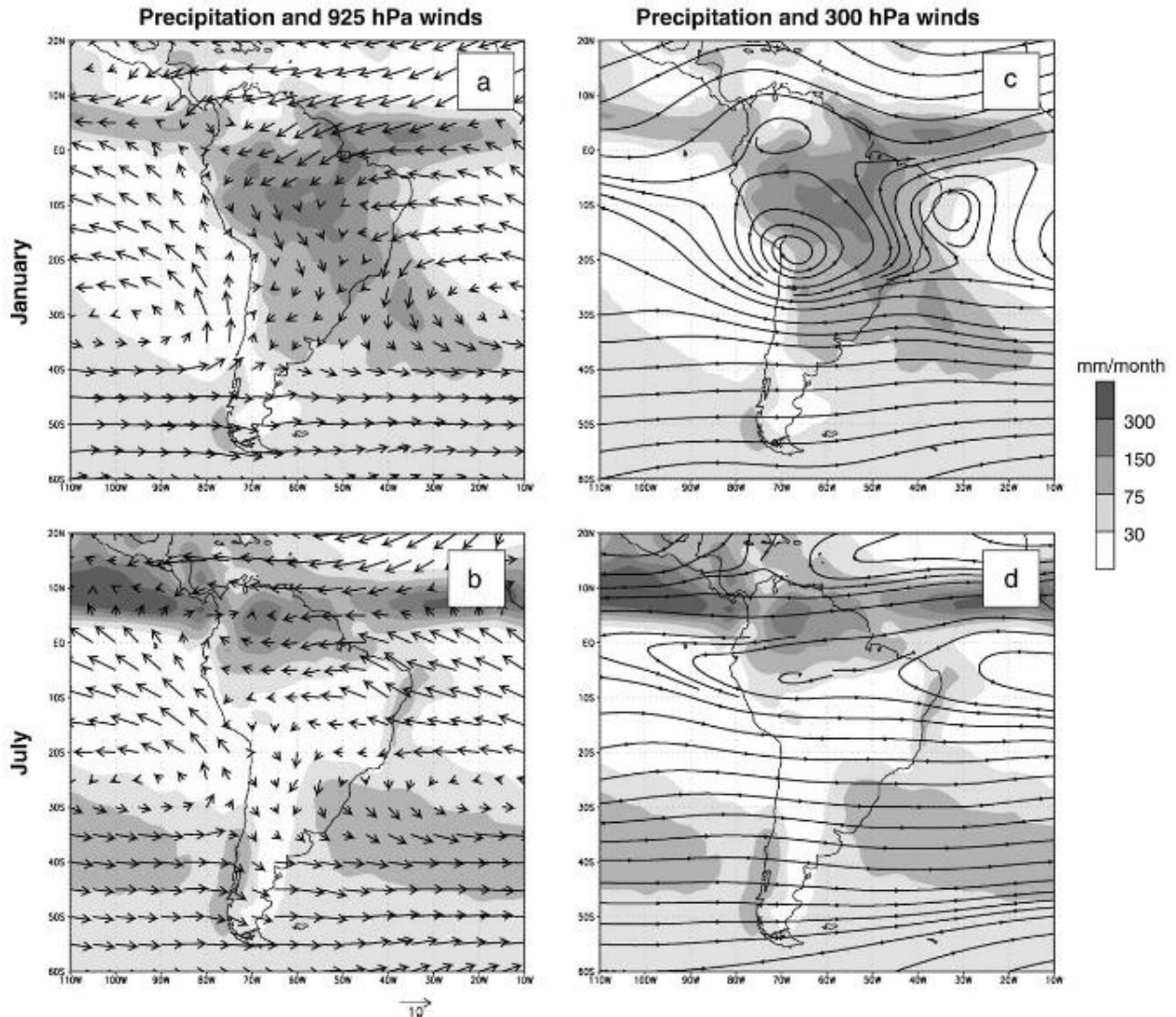


**Fig. 2.1.** From Garreaud et al. (2009), atmospheric circulation features of the active and inactive phases of the South American monsoon. Left panels (a and b): mean 925-hPa wind vectors and precipitation during Jan (top) and July (bottom). Right panels (c and d): mean 300-hPa streamlines and precipitation during Jan (top) and July (bottom).

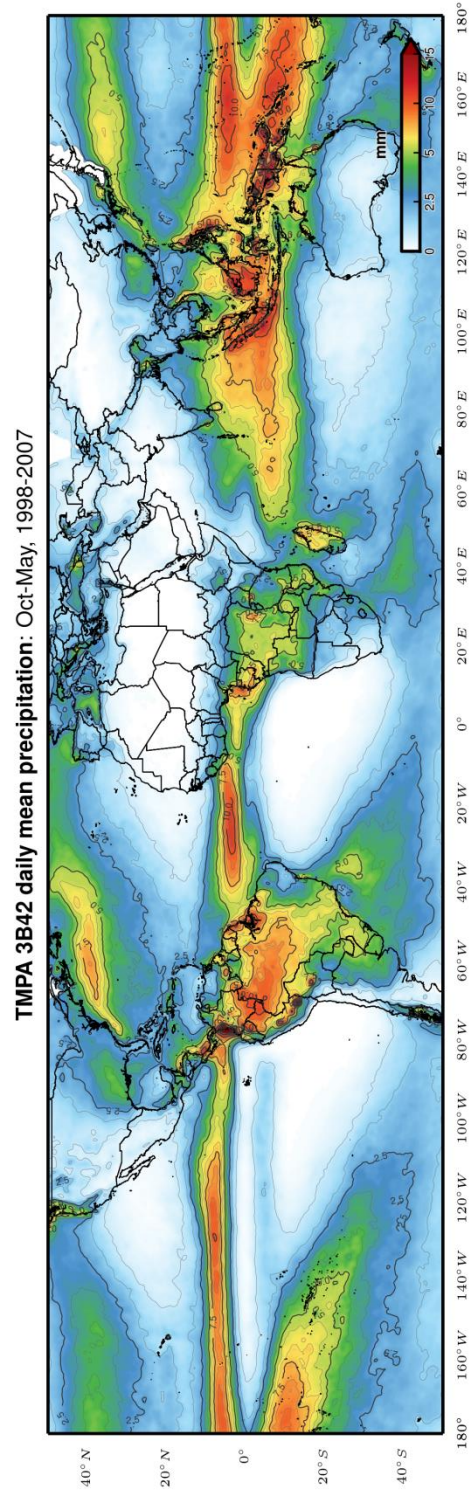


**Fig. 2.2.** TMPA (TRMM Multisatellite Precipitation Analysis) daily mean precipitation for 45°S to 45°N during Oct–May of 1998–2007, showing the South Atlantic Convergence Zone as well as the South Pacific Convergence Zone and the South Indian / Southeast African Convergence Zone.

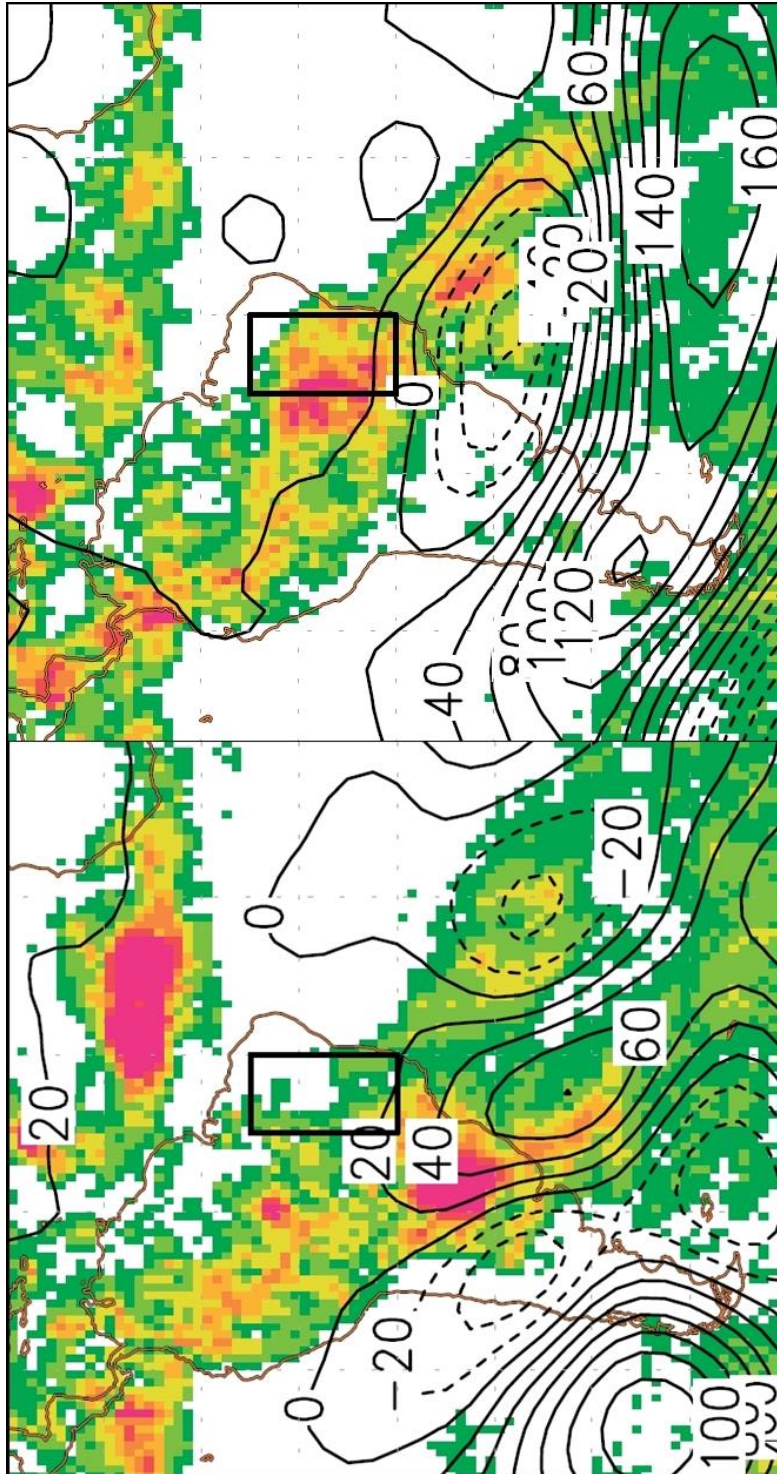


**Fig. 2.3.** From Nieto-Ferreira et al. (2011), daily precipitation patterns and 200-hPa height anomalies for an active period in the SESA portion of the South American Seesaw (left) and the SACZ (right).

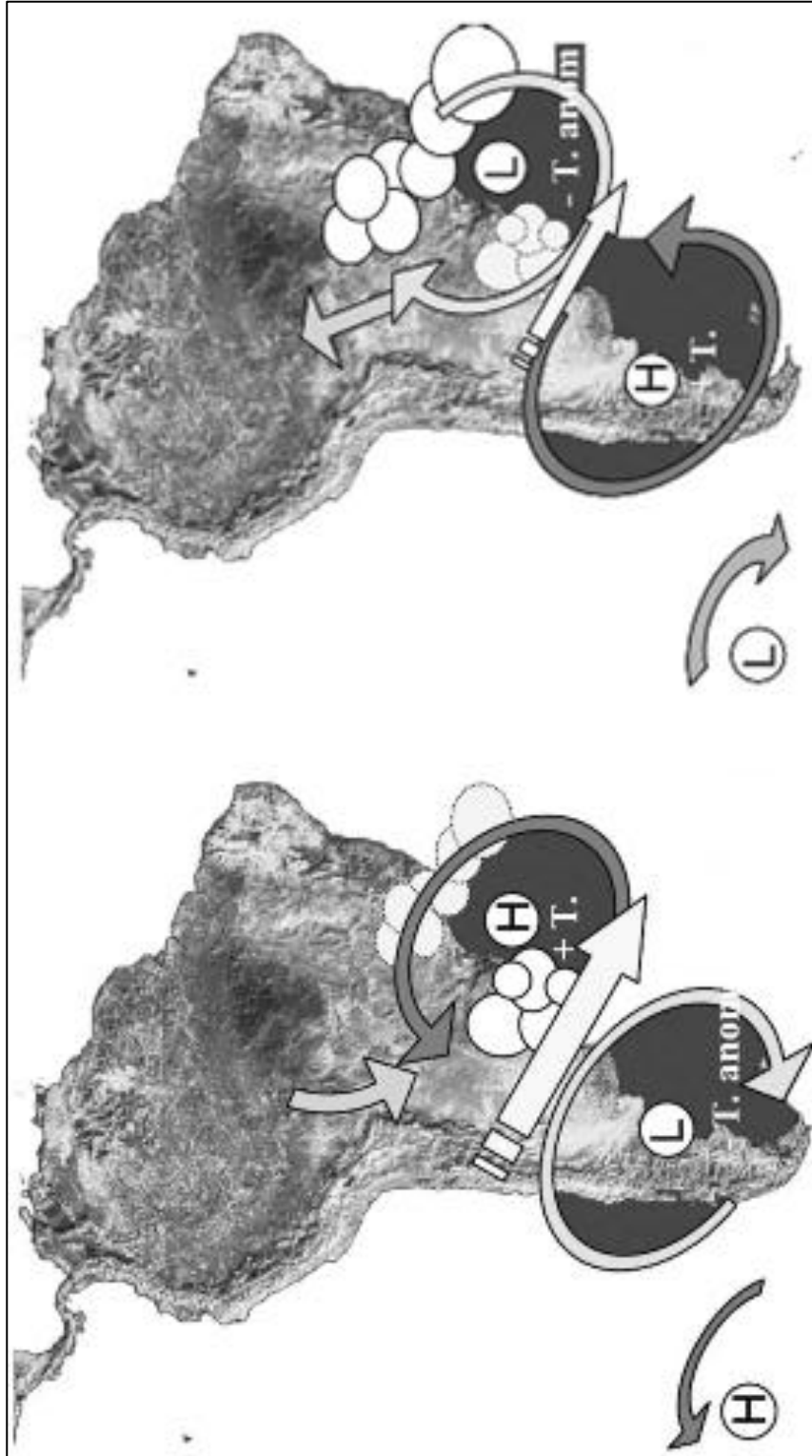


**Fig. 2.4.** From Vera et al. (2006a), schematic of typical 700-hPa circulation anomalies during active SESA (left) and SACZ (right) periods.

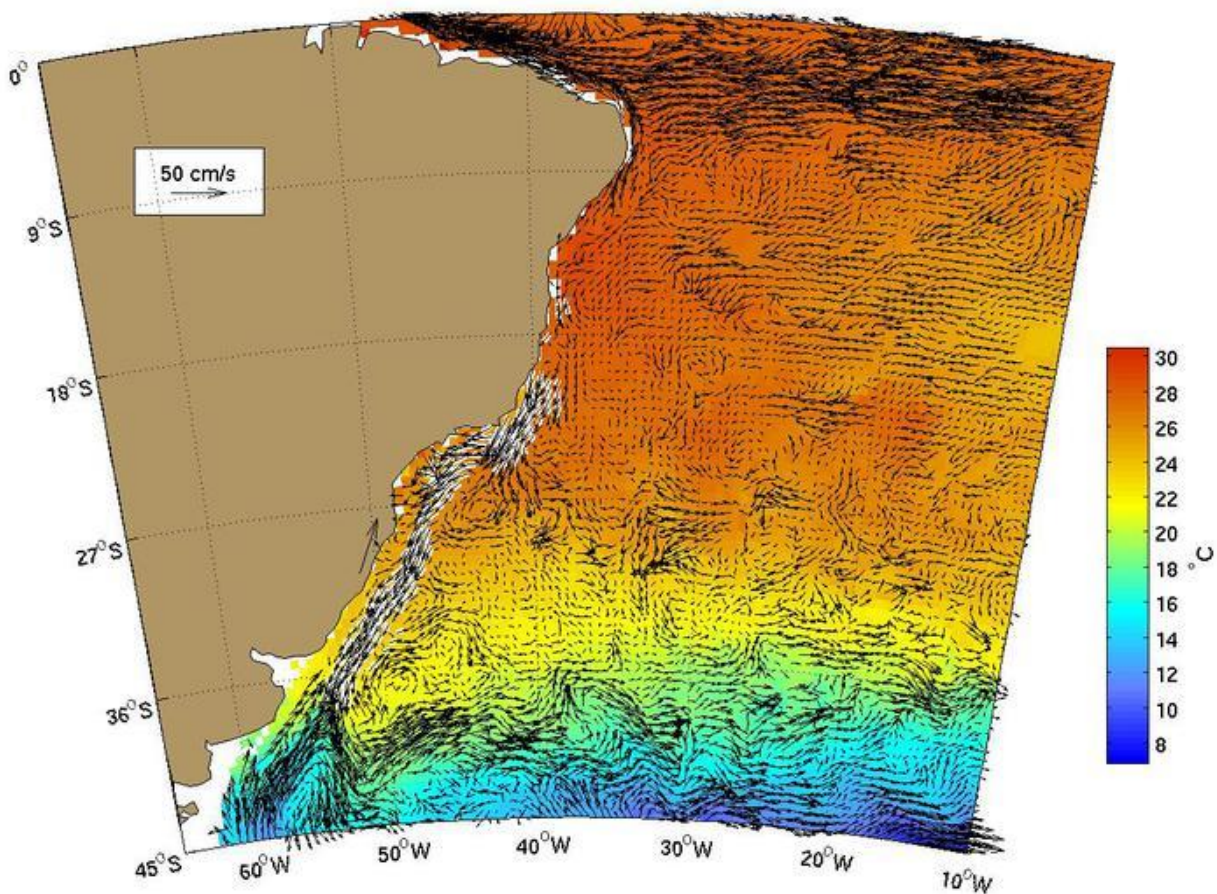


**Fig. 2.5.** From Bischof et al. (2004), map of the Brazil Current (white-outlined arrows) and sea surface temperature (shading) during Jan–Feb–Mar.

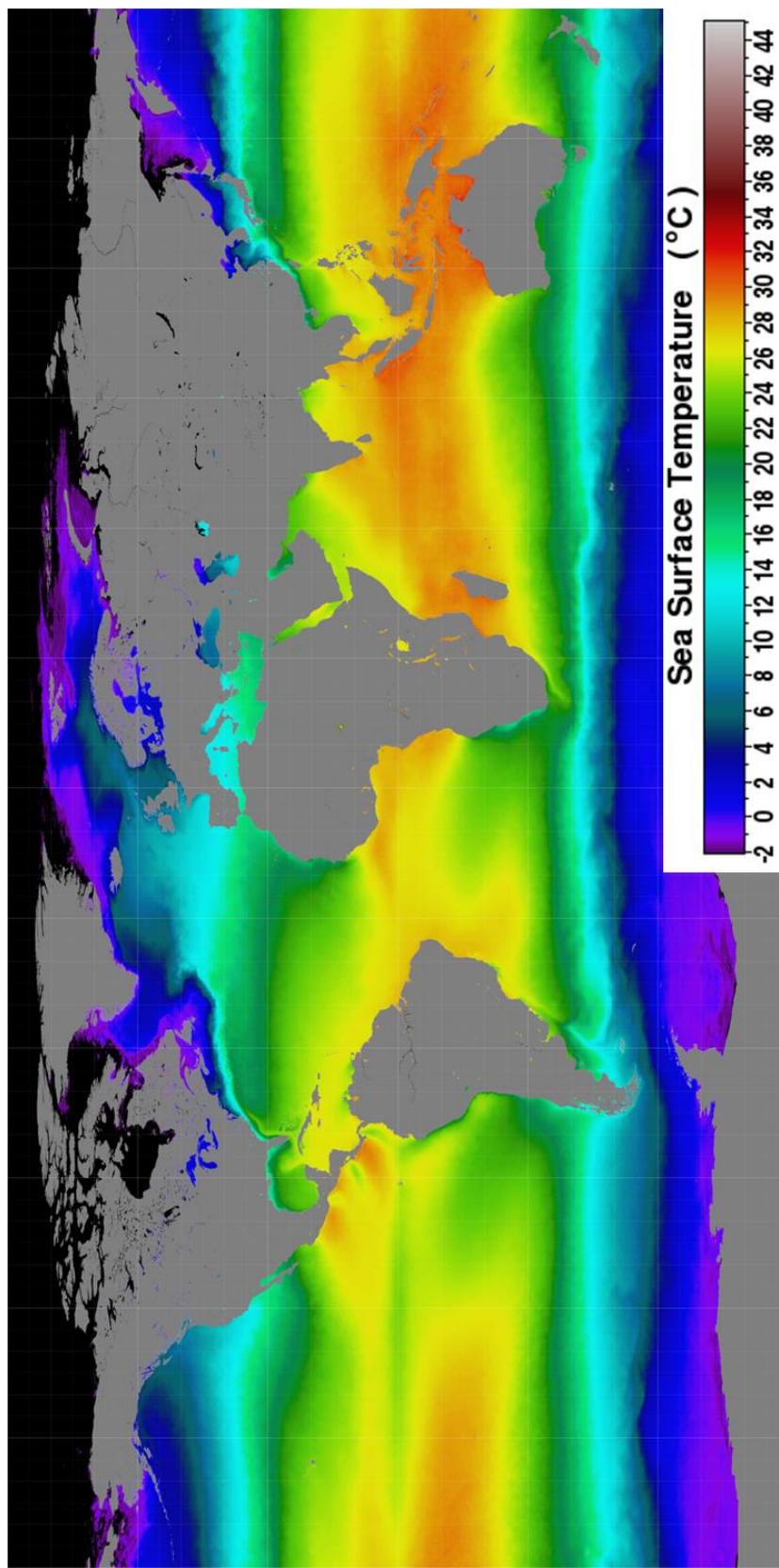


**Fig. 2.6.** MODIS Aqua-derived sea surface temperature climatology for Feb 2003–2014.

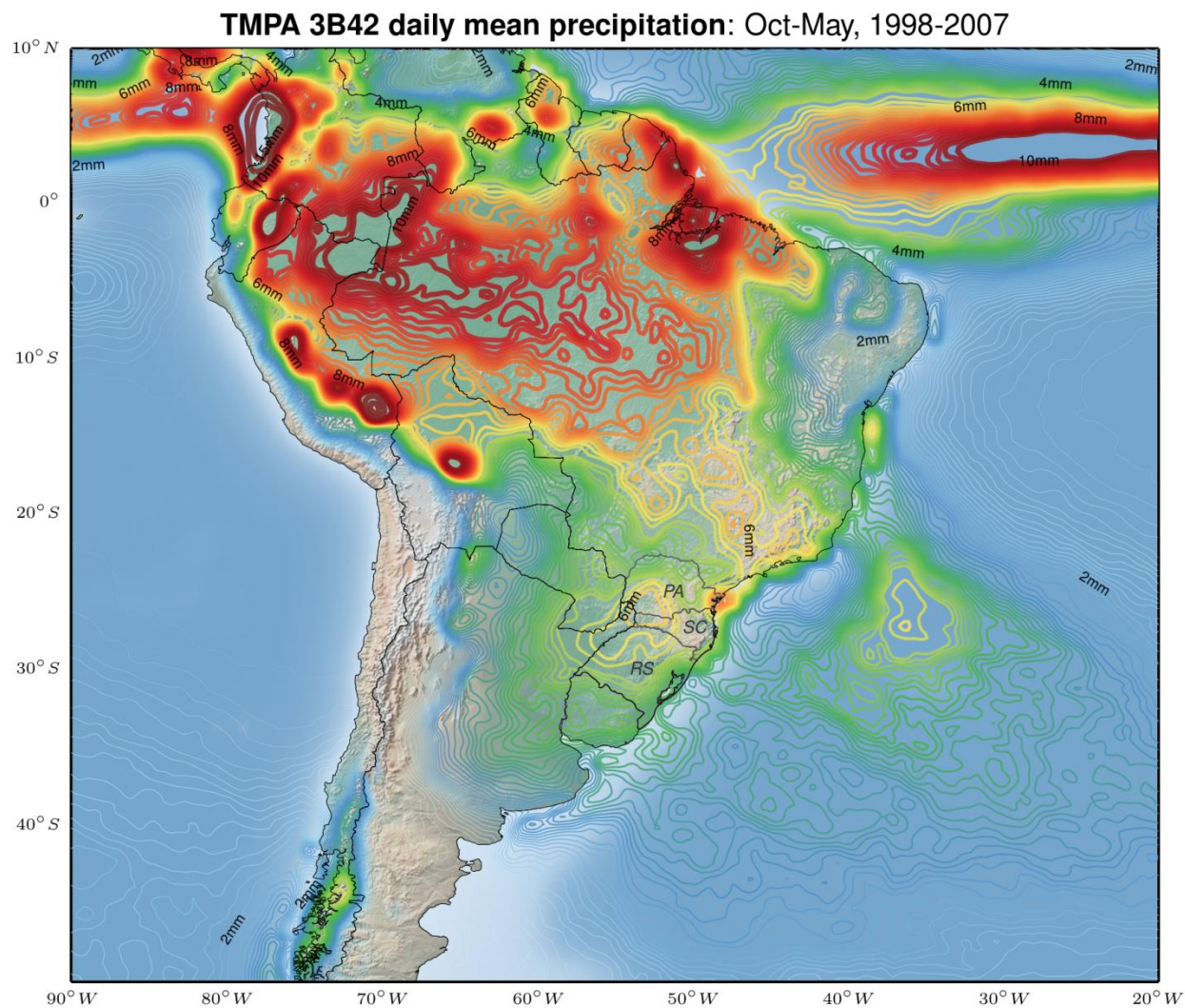


**Fig. 2.7.** TMPA (TRMM Multisatellite Precipitation Analysis) daily mean precipitation for the warm seasons (Oct–May) of 1998–2007 superimposed on shaded relief map of South America. Labeled are the three states in southern Brazil referenced in the text: Paraná (PA), Santa Catarina (SC), and Rio Grande do Sul (RS).

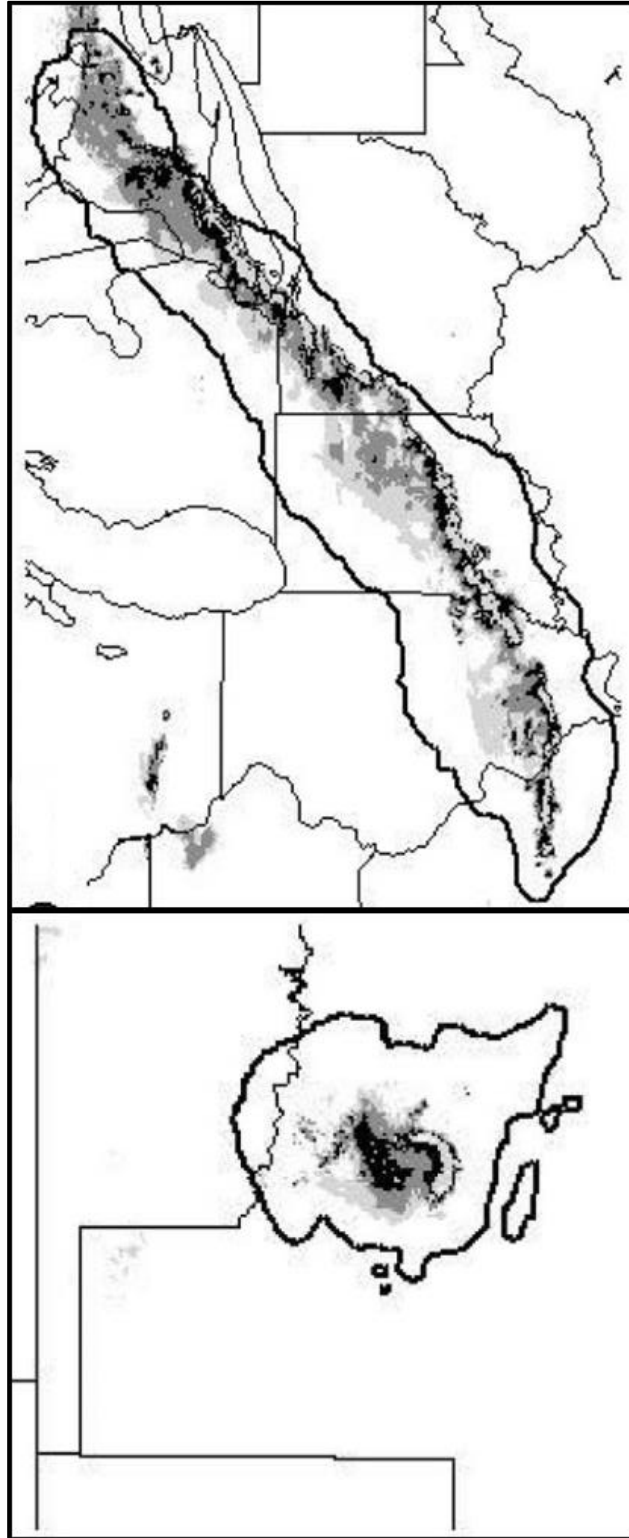


**Fig. 2.8.** From Jirak et al. (2003), examples of radar and satellite signatures of a mesoscale convective complex (left) and a persistent elongated convective system (right). Black outline shows the contiguous  $\leq -52^{\circ}\text{C}$  cloud top area in each image.

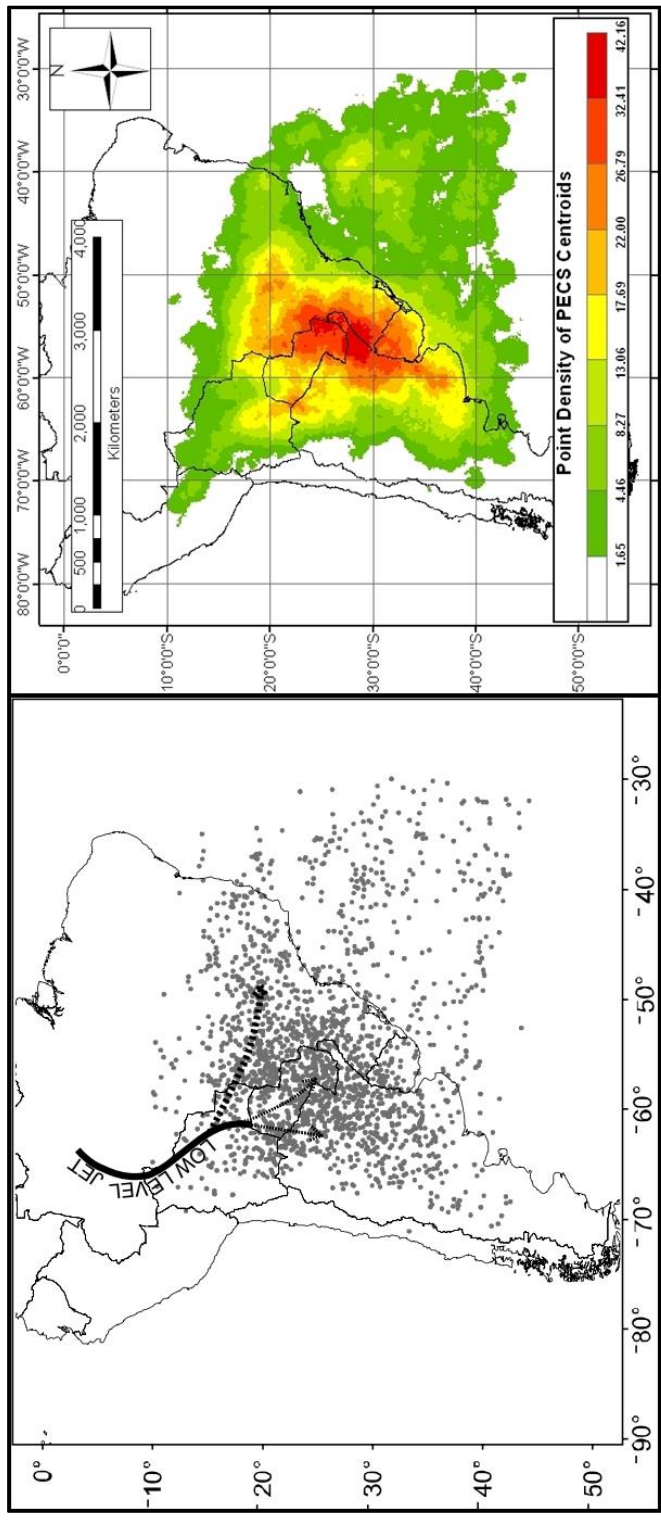


**Fig. 2.9.** Spatial distribution of center points of mesoscale convective complexes (left, from Durkee and Mote 2009) and persistent elongated convective systems (right, from Mattingly 2012) over subtropical South America during the warm seasons of 1998–2007.

## CHAPTER 3

### DATA AND METHODOLOGY

#### 3.1 Data sources

##### *a. LLCS dataset*

The LLCS dataset used for this study was developed by Durkee and Mote (2009) for their SSA MCC research, and the climatological characteristics of the PECSs in this dataset were analyzed by Mattingly (2012). This dataset consists of 1616 LLCSs (330 of which are MCCs) identified during the austral warm seasons (October–May) of 1998–2007 using 4-km infrared geostationary satellite imagery (GOES-8 and GOES-12). Imagery was generally available at 3-hour time increments. An automated cloud-top identification procedure similar to that of Augustine (1985) was used to identify each cloud shield that met the LLCS size criteria (see Table 2.1), then a combination of empirical orthogonal function (EOF) analysis of pixel coordinates and manual observation of image sequences was used to determine the track and characteristics of individual LLCS events (Fig. 3.1). Systems had to intersect the study domain of 70° to 40° W, 20° to 40° S (see Fig. 1.1) at some point in their life cycle to be included in the dataset. A more thorough description of this identification and tracking process can be found in Durkee and Mote (2009).

The final output consisted of a set of characteristics attributed to each LLCS for each time step in its life cycle, including  $\leq -52$  °C contiguous cloud shield area, latitude and longitude coordinates of cloud shield centroids, and eccentricity of the cloud shield. These properties were then used to determine the duration and maximum cloud shield extent of each discrete LLCS event.

*b. TMPA precipitation data*

The precipitation data used to identify SACZ events were obtained from the Tropical Rainfall Measuring Mission Multisatellite Precipitation Analysis (TMPA), archived and distributed by NASA's Goddard Earth Sciences (GES) Data and Information Services Center (DISC). TMPA provides  $0.25^\circ \times 0.25^\circ$  gridded precipitation estimates for latitudes between  $50^\circ\text{N}$  and  $50^\circ\text{S}$  at 3-hourly intervals for the period 1998–present (Huffman et al. 2007). These precipitation estimates are generated by calibrating passive microwave and visible / infrared brightness temperature measurements from a variety of low-earth orbiting and geostationary satellites to the high-resolution but spatially limited observations collected by the Precipitation Radar (PR), Microwave Imager (TMI), and visible / infrared scanner (VIRS) instruments aboard the Tropical Rainfall Measuring Mission (TRMM) Satellite. The specific product employed in this analysis is the TMPA version 7 3B42 daily precipitation estimate, originally released in 2012 and publically available through NASA's Mirador data portal (<http://mirador.gsfc.nasa.gov/>).

*c. Climate Forecast System Reanalysis*

Data from the National Centers for Environmental Prediction's Climate Forecast System Reanalysis (CFSR) version 2 were used to visualize and quantify differences in atmospheric circulation patterns over the study region. Completed in 2010, CFSR version 2 is a third-generation coupled atmospheric-ocean-land surface-sea ice reanalysis that provides global fields for the period 1979–present (Saha et al. 2010). Its high spatial ( $0.5^\circ \times 0.5^\circ$  or  $\sim 38\text{km}$ ) and vertical (37 atmospheric pressure levels) resolution, approaching that of regional reanalyses such as the North American Regional Reanalysis and Arctic Systems Reanalysis, enables CFSR fields to resolve fine-scale atmospheric features over the complex terrain of subtropical South America. However, it must be noted that this reanalysis dataset was developed quite recently and only a

limited number of studies (e.g. Stopa and Cheung 2014; Hu et al. 2014) have evaluated its performance, so its reliability compared to older reanalysis datasets is uncertain (NCAR Staff 2013b).

*d. HYSPLIT / NCEP-NCAR Reanalysis 1*

The Hybrid Single Particle Lagrangian Integrated Trajectory (HYSPLIT) Model, developed by NOAA's Air Resources Laboratory (ARL), was used to simulate the path taken by air parcels at various levels of the atmosphere into the centroids of LLCS cloud shields. HYSPLIT computes air parcel trajectories and dispersion of atmospheric pollutants using pre-gridded meteorological data from either analyses or short-term forecasts (Draxler and Hess 1997).

In order to efficiently process the large number (5866) of parcel trajectories, the downloadable version of the HYSPLIT software was used to run the model repeatedly. The NCEP-NCAR Reanalysis 1 dataset (Kalnay et al. 1996) was used as the input data source for these analyses because it is the only publicly available reanalysis dataset pre-gridded for the HYSPLIT desktop version. Due to its antiquated data assimilation system (frozen in 1995 to ensure temporal consistency of the dataset) and coarse resolution ( $2.5^{\circ} \times 2.5^{\circ}$ ), along with relatively poor performance over the southern hemisphere (NCAR Staff 2013a), there is a substantial degree of uncertainty in the parcel trajectories computed for LLCS events. However, a comparison of HYSPLIT runs for 25 randomly selected times and locations in the SSA study domain computed with both NCEP-NCAR Reanalysis 1 data and the higher-resolution ERA-Interim reanalysis (Fig. 3.2) shows that NCEP-NCAR Reanalysis 1 appears to produce back trajectory results comparable to higher resolution datasets in most cases.

## 3.2 Methodology description

### *a. SACZ event classification*

Previous studies have used a variety of objective and subjective criteria based on precipitation or other atmospheric fields (e.g. outgoing longwave radiation, relative humidity, temperature, location of troughs / ridges) to identify SACZ events. Examples of objective SACZ identification methods include Liebmann et al. (1999), who characterized SACZ episodes using outgoing longwave radiation anomalies from the NCEP-NCAR reanalysis dataset, and Carvalho et al. (2011), who created a SACZ intensity index using combined EOF analysis of Global Precipitation Climatology Project pentad precipitation, along with specific humidity, air temperature, and zonal and meridional winds at 850-hPa from NCEP-NCAR reanalysis 1 data. Durkee (2008) defined SACZ events using the Brazilian Center for Weather Forecast and Climatic Studies (CPTEC) monthly climate bulletins (*Climanálise*) that detail occurrences of SACZ episodes between October and March (see Fig. 3.3). The subjective criteria used to define these SACZ episodes are based on the duration of precipitation over southeast Brazil and several other qualitative aspects of the atmospheric flow pattern, and do not include any information about the location or intensity of the SACZ.

Although the SACZ is often described as a continuous band of convection extending from central Brazil southeastward into the South Atlantic Ocean, a few previous studies (Carvalho et al. 2004 and Muza et al. 2009) have demonstrated that heavy precipitation events over the land mass of southeastern Brazil and the adjacent South Atlantic Ocean are often decoupled from one another. Based on these results, it was determined that this study would define separate continental and oceanic and SACZ domains to investigate whether relationships between SACZ and LLCS activity vary depending on the location of the heaviest SACZ

precipitation. As Fig. 3.4 shows, these separate SACZ domains were chosen to encompass the continental and oceanic regions with the highest average daily warm season precipitation and, in the case of the oceanic domain, where day-to-day variability in precipitation (as measured by the standard deviation of daily precipitation; see Fig. 3.5) is greatest. These continental and oceanic domains cover similar regions to those defined by previous studies (e.g. Carvalho et al. 2002 and 2004; Muza et al. 2009; de Oliveira Vieira et al. 2012) but, unlike past studies, are diagonally oriented from northwest to southeast to more effectively capture variability in the typically diagonally-oriented SACZ.

A variety of atmospheric fields, including TMPA precipitation and CFSR-derived 850-hPa convergence, 700-hPa vertical velocity, and 250-hPa divergence, were considered as candidates for identifying SACZ events over the continental and oceanic SACZ domains. A time series of these variables during the 2005–06 warm season (Fig. 3.6) shows that they generally agree in the timing of active SACZ periods. However, maps of the mean of CFSR variables over all 6-hourly timesteps during the period of record (POR) show that these fields are quite noisy and heavily influenced by the mountainous topography of southeastern Brazil in the continental SACZ domain (Figs. 3.7, 3.8, and 3.9). Due to this issue with the CFSR data and the overall objective of this study to examine atmospheric mechanisms that govern the relationship between *precipitation* variability in the SACZ and La Plata basin, daily TMPA precipitation was ultimately chosen as the SACZ identification variable.

The final steps in constructing a set of SACZ event identification criteria were to choose a summary statistic to represent daily precipitation over the SACZ domains and to consider whether any SACZ duration requirements would be included as a component of the criteria. Muza et al. (2009) and de Oliveira Vieira et al. (2012) both chose daily domain-averaged

precipitation as the summary statistic to quantify precipitation variability. However, as Fig. 3.10 shows, daily domain-averaged precipitation over both the continental and oceanic SACZ domains approximates an exponential rather than a normal distribution, and it is difficult to define a clear distinction between SACZ and non-SACZ events in the long positive tail of these distributions. Moreover, domain-averaged precipitation can be unduly influenced by high convective precipitation totals that affect a relatively small portion of the domain (especially in the topographically complex continental SACZ domain), which could detract from this study's intended analysis of the synoptic-scale atmospheric features associated with large-scale SACZ events. For these reasons, the percentage of each SACZ domain receiving any amount of precipitation on a given day (the number of domain points on the  $0.25^\circ \times 0.25^\circ$  TMPA grid receiving precipitation, divided by the total number of TMPA grid points in the domain) was chosen as the SACZ domain precipitation summary statistic. Days with percentage of domain precipitation above the 75<sup>th</sup> percentile (with respect to the distribution of all daily values during the October–May warm seasons of the 1998–2007 POR) were classified as “SACZ days” in each domain; this percentile-based definition was preferred to a standard deviation-based definition like that of de Oliveira Vieira et al. (2012) because the distribution of percentage of domain precipitation is not normal in the continental SACZ domain (see Fig. 3.10).

With regard to SACZ duration, Muza et al. (2009) implicitly included duration criteria with their choice of pentad-averaged precipitation as the identifying variable, and de Oliveira Vieira et al. (2012) explicitly required that domain-averaged precipitation in their continental SACZ domain must be present for at least three of five consecutive days to be classified as an SACZ event. However, as previously stated, this study concerns *concurrent* atmospheric flow features associated with the SACZ and La Plata basin LLCS activity, rather than features that

manifest themselves in time-averaged analyses. Additionally, Carvalho et al. (2004) found that the vast majority of SACZ events persist for less than five days, so instituting a duration threshold for SACZ event classification would likely cause many valid SACZ events to be excluded from classification as such. Therefore, days with percentage of domain precipitation above the 75<sup>th</sup> percentile are assumed to be representative of active SACZ conditions with no restrictions related to the duration of above-normal precipitation.

In total, of the 2189 days in the 1998–2007 POR, 418 were classified as active continental SACZ days and 397 were classified as active oceanic SACZ days (see Table 4.1). As Fig. 3.11 shows and the 2006–07 warm season time series in Fig. 3.6 suggests, continental SACZ events are most common during the peak of the warm season from November through March, while oceanic SACZ events have their highest relative frequency during May.

*b. Composite flow analysis of LLCS / SACZ events*

In order to analyze atmospheric flow during LLCS and SACZ events and relationships between SACZ activity and LLCSs over the La Plata basin, composites of atmospheric fields from CFSR were compiled and mapped for categories of LLCS and SACZ activity. At each 6-hourly CFSR timestep during the POR, all LLCS cloud shield outlines that were active within  $\pm 3$  hours of the timestep were examined to determine if they intersected any part of three pre-defined domains over the La Plata basin (Fig. 3.12): the “West La Plata” domain, the “East La Plata” domain, and the “Full La Plata” domain, which encompasses both the West and East La Plata domains. If any of these cloud shields intersected any part of a La Plata domain during the given 6-hourly window, the CFSR atmospheric fields for that 6-hourly timestep were included in the distribution for the domain’s “active LLCS” category (e.g. if an active LLCS cloud shield intersected the West La Plata domain, the reanalysis fields for that timestep were included in the “active West La Plata LLCS” distribution). The distribution of CFSR fields during categories of

daily SACZ activity (neither SACZ active, continental SACZ active only, oceanic SACZ active only, both continental and oceanic SACZ active) was also compiled, along with the distribution of these fields across *combinations* of LLCS and SACZ activity (e.g. active LLCS over the West La Plata domain during a day with the continental SACZ active only).

For each of these defined LLCS / SACZ subsets, composite maps and composite anomaly maps of the lower- and upper-tropospheric atmospheric flow were generated. The CFSR variables used to visualize low-level flow and atmospheric moisture were wind vectors at the 925-hPa constant pressure level, along with precipitable water (PWAT), which, as provided by the CFSR in units of kilograms per square meter, is an estimate of the area density of the water in a column in the atmosphere if all the water in the column were precipitated as rain. Upper-tropospheric flow composites were visualized using geopotential height, wind vectors, and vector divergence at the 300-hPa constant pressure level. For all composite maps, each variable displayed on the map is the median of the distribution of all 6-hourly values of that variable for the given LLCS subset. For all composite anomaly maps, each variable displayed on the map is the percentile departure of the median of the subset's distribution from the climatological median of the given variable across all 6-hourly CFSR timesteps during the POR. This median- and percentile-based composite method was preferred to a mean- and standard deviation-based approach because the climatological distribution of most of the variables at each CFSR grid point is non-normal.

*c. Logistic regression analysis of SACZ / LLCS relationships*

To further examine the relationships between SACZ precipitation and LLCS activity over the subtropical South America study region, a regression analysis was performed at all points on a  $0.25^\circ \times 0.25^\circ$  grid over a domain extending from  $-17^\circ\text{S}$  to  $-43^\circ\text{S}$  latitude and  $-73^\circ\text{W}$  to  $-37^\circ\text{W}$  longitude. This domain was chosen to extend  $3^\circ$  in all directions beyond the boundaries of the

domain that Durkee and Mote (2009) used to generate the LLCS cloud shield dataset, under the assumption that LLCS cloud shields occurring less than  $3^\circ$  outside of the domain would intersect the domain boundaries at some point in their life cycle and would be ultimately be included in the LLCS dataset. At each grid point, the respective climatological *percentile ranks* of the percentage of points in the continental and oceanic SACZ domains receiving precipitation for each of the 5849 days in the POR were used as the two predictor variables. A dummy variable indicating whether or not the grid point was located underneath any part of a LLCS cloud shield on each of the 5849 days was the predictand.

Because the chosen dependent variable of this regression was binary (a 1 or 0 indicating whether or not a given grid point was affected by an LLCS on each day in the POR), the technique of logistic regression was employed to construct a model of the probability of LLCS occurrence at each grid point as predicted by daily continental and oceanic SACZ precipitation. Logistic regression provides a more realistic model for probabilities than linear regression because its probability output is bounded between 0 and 1 (Hamilton 1992). The raw coefficients for each independent variable generated by a logistic regression model represent the predicted change in the natural logarithm of the odds of the event described by the dependent variable for a one unit change in the given independent variable; these “log-odds” coefficients can then be used to calculate predicted probabilities. The respective percentile ranks of continental and oceanic SACZ precipitation were chosen as the independent variables in this model to ensure straightforward interpretation of the model output: at a given grid point, for a one *percentile* change in percent domain precipitation, the log-odds of LLCS occurrence are predicted by the model to change by the amount given by the regression coefficient for each domain.

*d. LLCS moisture source identification*

HYSPLIT trajectories for LLCS moisture source tracking were generated at 6-hourly intervals throughout the study period due to the 6-hourly resolution of the NCEP-NCAR Reanalysis 1 data. For each 6-hourly timestep in the POR, the three hours before and after the timestep were searched to determine if any LLCs were active during that time. If there were active LLCs present, the cloud shields associated with each unique active event were merged into one polygon and HYSPLIT was used to model back trajectories for parcels terminating at the centroid of this merged polygon. Model back trajectories were generated for three parcel levels: 10 meters above ground level (AGL), 1000 meters AGL, and 2500 meters AGL. These trajectory levels were selected to provide vertical coverage across the levels of the lower troposphere (roughly 1000 hPa to 700 hPa) where the greatest quantities of atmospheric moisture are transported (Vera et al. 2006b) and are similar to those of recent studies that have employed HYSPLIT for moisture transport analysis (e.g. Feng et al. 2013; Guan et al. 2013; Wu et al. 2014). All trajectories extend backwards in time 120 hours (five days) from the given LLCS valid time, with modeled latitude / longitude trajectory coordinates generated at one hour intervals.

In order to analyze the spatial variability of moisture sources associated with LLCS events throughout subtropical South America in greater detail, the centroid coordinates of each 6-hourly merged LLCS cloud shield were grouped into six sub-domains (Fig. 3.13). For each of these sub-domains, the spatial density of modeled trajectories terminating at all 6-hourly merged LLCS cloud shields in the domain was calculated to visualize the most common air parcel pathways entering LLCs within the given sub-domain. This was accomplished by dividing a grid extending from  $-60^{\circ}\text{S}$  to  $-8^{\circ}\text{N}$  latitude and  $-90^{\circ}\text{W}$  to  $-20^{\circ}\text{W}$  longitude into  $4^{\circ} \times 4^{\circ}$  boxes and calculating the percentage of trajectories that intersected each box for each of the six sub-

domains. These trajectory density calculations were further grouped according to the number of days preceding the valid LLCS time (e.g. 120–96 hours before LLCS valid time, 96–72 hours before, etc.) to visualize the four-dimensional variability of LLCS moisture supply.

*e. Analysis of central Argentina LLCS events*

The final step of this study was a detailed examination of LLCS events in central Argentina that could possibly occur in the absence of moisture supply from the South American Low Level Jet. Each unique LLCS event with a cloud shield centroid that was located within a domain encompassing much of central and southern Argentina, central Chile, and adjacent regions of the Pacific and Atlantic oceans at any time during its life cycle was examined (Fig. 3.14). For each of the three parcel trajectory levels (10m, 1000m, and 2500m AGL), if any of the LLCS's 6-hourly modeled back trajectories at that level passed through a domain surrounding the climatological position of the South American Low Level Jet (Fig. 3.14), the LLCS was noted as demonstrating a SALLJ connection at that parcel level. The duration and maximum cloud shield area of each of these discrete central Argentina LLCS events was then analyzed across categories of SALLJ connection (e.g. no parcel trajectories passed through SALLJ domain, one parcel level trajectory passed through SALLJ domain, etc.). Finally, two case studies of central Argentina LLCS events that exemplify the complexity involved in determining the moisture sources of these systems were selected and are discussed in detail in section 4.4.

In summary, the methodology of this thesis was designed to investigate the atmospheric circulation patterns and moisture sources associated with LLCs over subtropical South America and their relationships with SACZ activity, with particular emphasis placed on central Argentina LLCS events that may occur in the absence of Amazonian moisture. The specific procedure followed was to: (1) Identify continental and oceanic SACZ events using TMPA precipitation data, (2) Map composites of atmospheric variables in order to visualize lower- and upper-

tropospheric features across categories of SACZ and LLCS activity, (3) Develop a logistic regression model to quantify the relationships between continental / oceanic SACZ activity and LLCS probability over the study region, (4) Generate HYSPLIT back trajectories to investigate LLCS moisture sources, and (5) Examine central Argentina LLCS events in greater detail using HYSPLIT back trajectories and maps of case study events. Results of these analyses are presented in section 4.

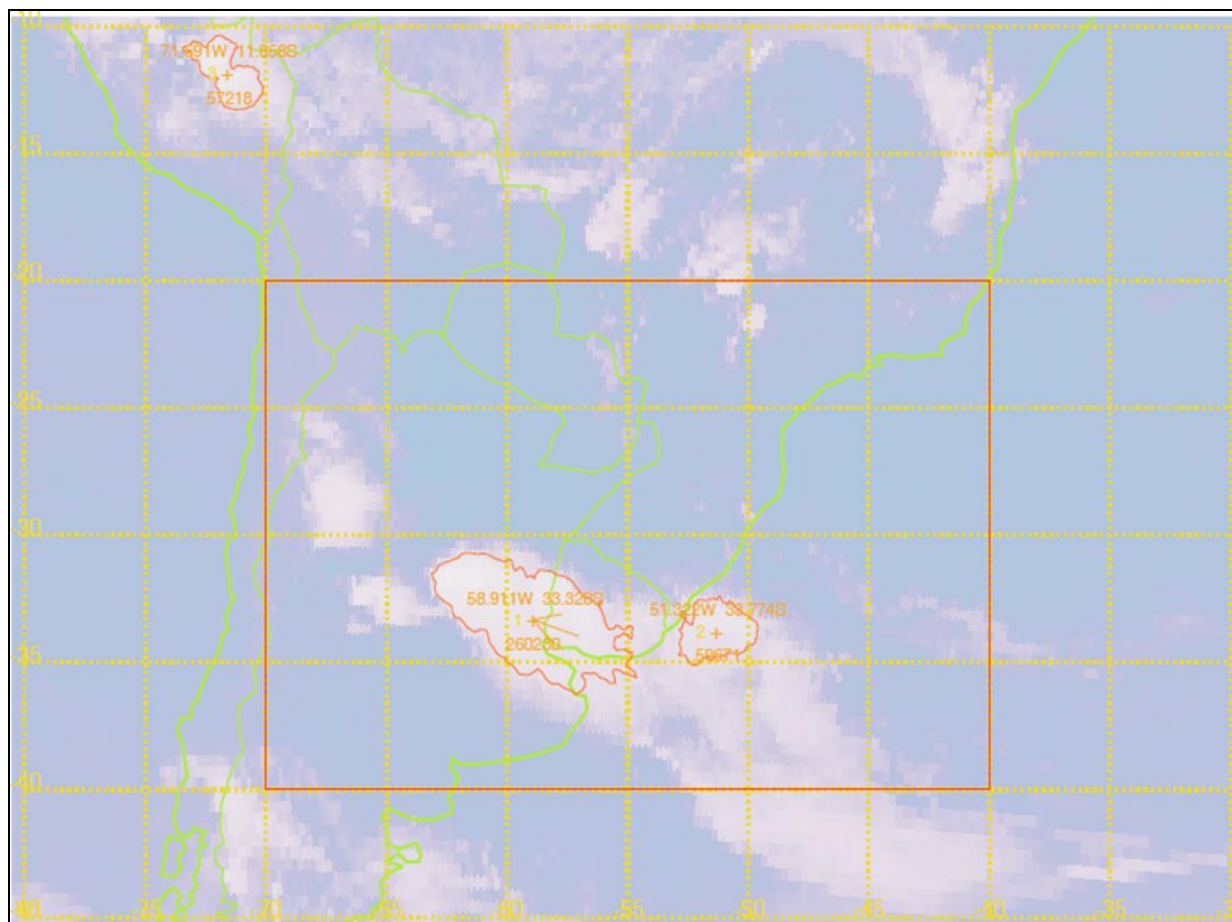


**Fig. 3.1.** Sample scene of GOES infrared imagery used to compile LLCS dataset. Outlined are contiguous regions of  $\leq -52^{\circ}\text{C}$  cloud top temperature that meet the size criterion given in Table 1.1.

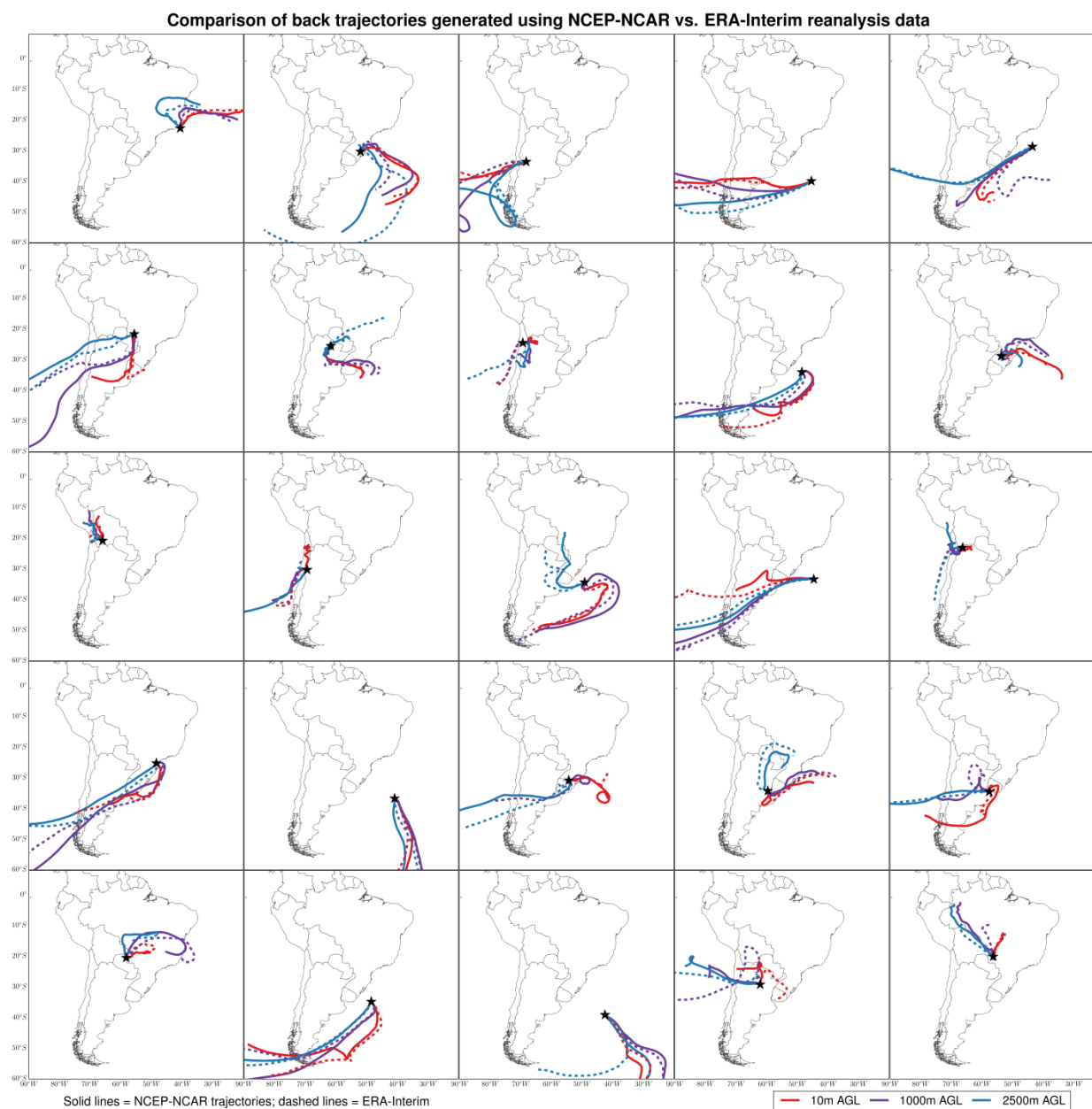
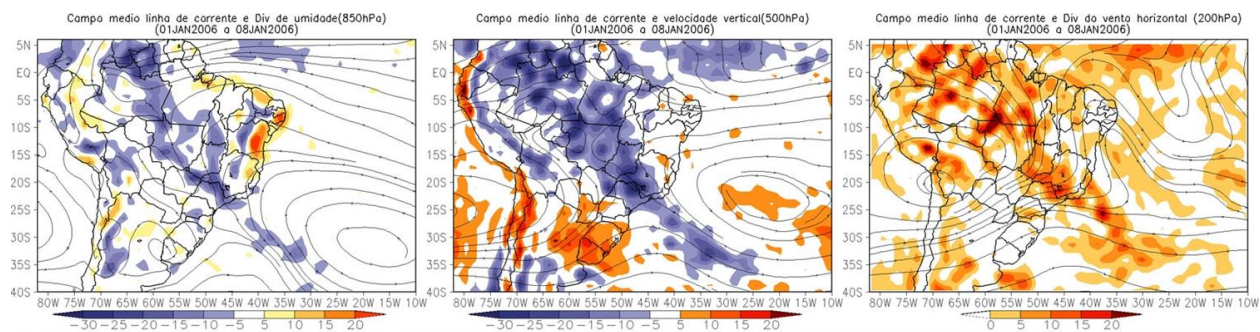


**Fig. 3.2.** Comparison of HYSPLIT back trajectories generated using NCEP-NCAR Reanalysis 1 (solid lines) and ERA-Interim (dashed lines) data for 25 randomly selected times and locations during the POR. Red lines indicate 10m AGL trajectories, purple lines 1000m AGL, and blue lines 2500m AGL. Trajectories were calculated using the Spain HYSPLIT web application (<http://www.ciecem.uhu.es/hysplit/index.php>).



### 3 - PERTURBAÇÕES ATMOSFÉRICAS SOBRE O BRASIL

#### 3.1 - Sistemas Frontais e Frontogênese

#### 3.2 - Massas de Ar Frio e Geadas

#### 3.3 - Atividade Convectiva sobre a América do Sul

##### 3.3.1 - Zona de Convergência do Atlântico Sul (ZCAS)

Em janeiro, houve a formação de dois episódios de Zona de Convergência do Atlântico Sul (ZCAS). O primeiro evento ocorreu no período de 01 a 08 e o segundo iniciou no dia 27, prolongando-se até o início de fevereiro. Este último episódio será discutido no próximo número do Boletim Climanálise.

Neste primeiro episódio, os campos médios são concordantes com o modelo conceitual da ZCAS (Figuras 24a a 24d). Houve excesso de chuva em diversas cidades, a exemplo de São Paulo, onde o acumulado mensal foi de 249,1 mm. Salienta-se a intensa região de movimento ascendente em 500 hPa (Figura 24c), associada à divergência em 200 hPa, com a definição da Alta da Bolívia e do cavado sobre o Nordeste (Figura 24d).

##### 3.3.2 - Zona de Convergência Intertropical (ZCIT)

##### 3.3.3 - Linhas de Cumulonimbus na Costa Norte/Nordeste da América do Sul

**Fig. 3.3.** Description of SACZ events during Jan 2006 from archived *Climanálise* bulletin published by the Brazilian Center for Weather Forecast and Climatic Studies (CPTEC). Maps show atmospheric fields averaged from 1 Jan 2006 through 8 Jan 2006: 850-hPa divergence (left), 500-hPa vertical velocity (center), and 200-hPa divergence (right).

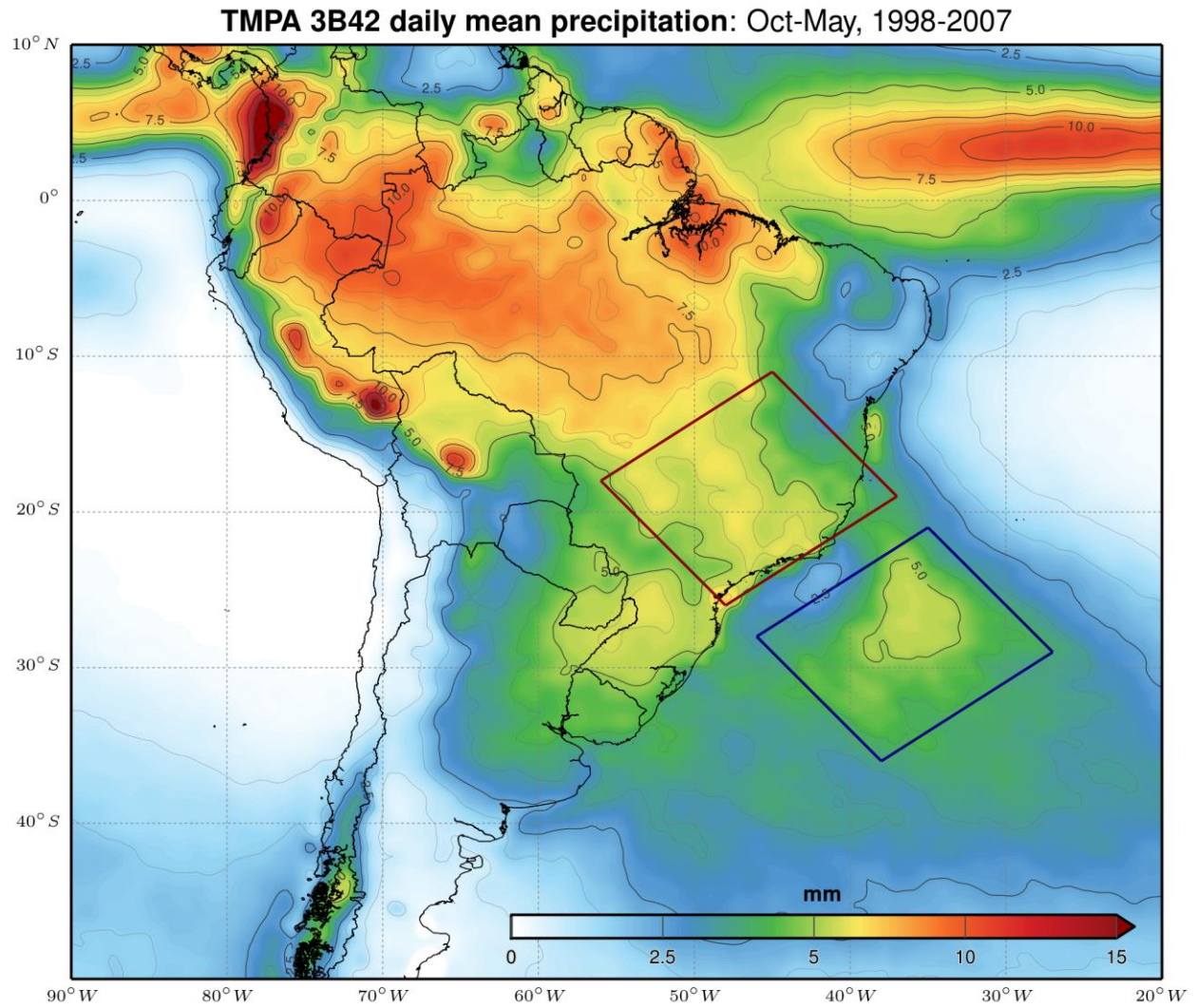


**Fig. 3.4.** Daily mean precipitation for the warm seasons (Oct–May) of 1998–2007 from the TRMM Multisatellite Precipitation Analysis (TMPA). Boxes show the designated locations of the continental SACZ domain (red box) and oceanic SACZ domain (blue box).

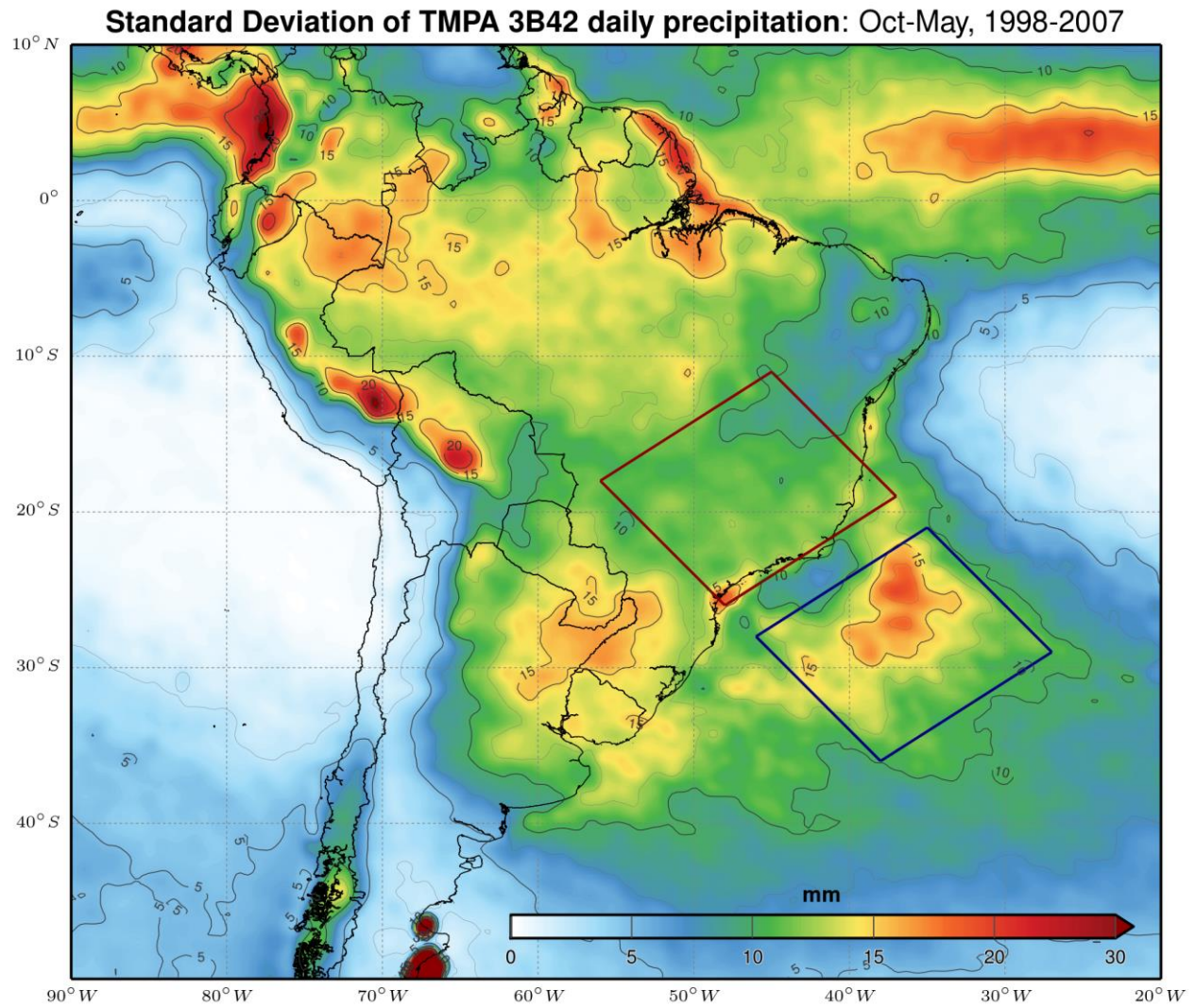


**Fig. 3.5.** Standard deviation of daily precipitation for the warm seasons (Oct–May) of 1998–2007 from the TRMM Multisatellite Precipitation Analysis (TMPA). Boxes show the designated locations of the continental SACZ domain (red box) and oceanic SACZ domain (blue box).

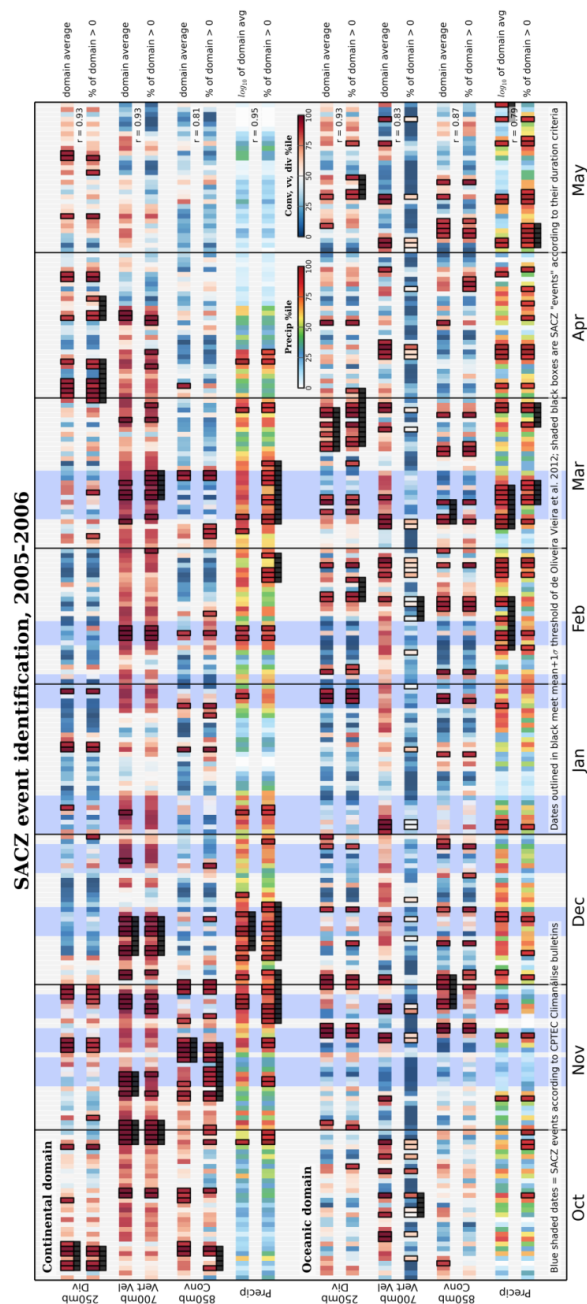


**Fig. 3.6.** Time series of “percent domain” and “domain-average” TMPA precipitation and CFSR fields (850-hPa convergence, 700-hPa vertical velocity, 250-hPa divergence) considered for SACZ identification during the 2005–2006 warm season over the continental (top) and oceanic (bottom) SACZ domains. Filled colors represent the percentile rank of each daily value relative to the 1998–2007 warm season distribution, outlined daily boxes indicate days when value exceeded one standard deviation above the climatological mean, and black boxes below time series indicate dates when the “three out of five days” duration requirement of de Oliveira Vieira et al. (2012) was met. Dates with blue shaded background were identified as SACZ events by the CPTEC *Climanalise* bulletins.

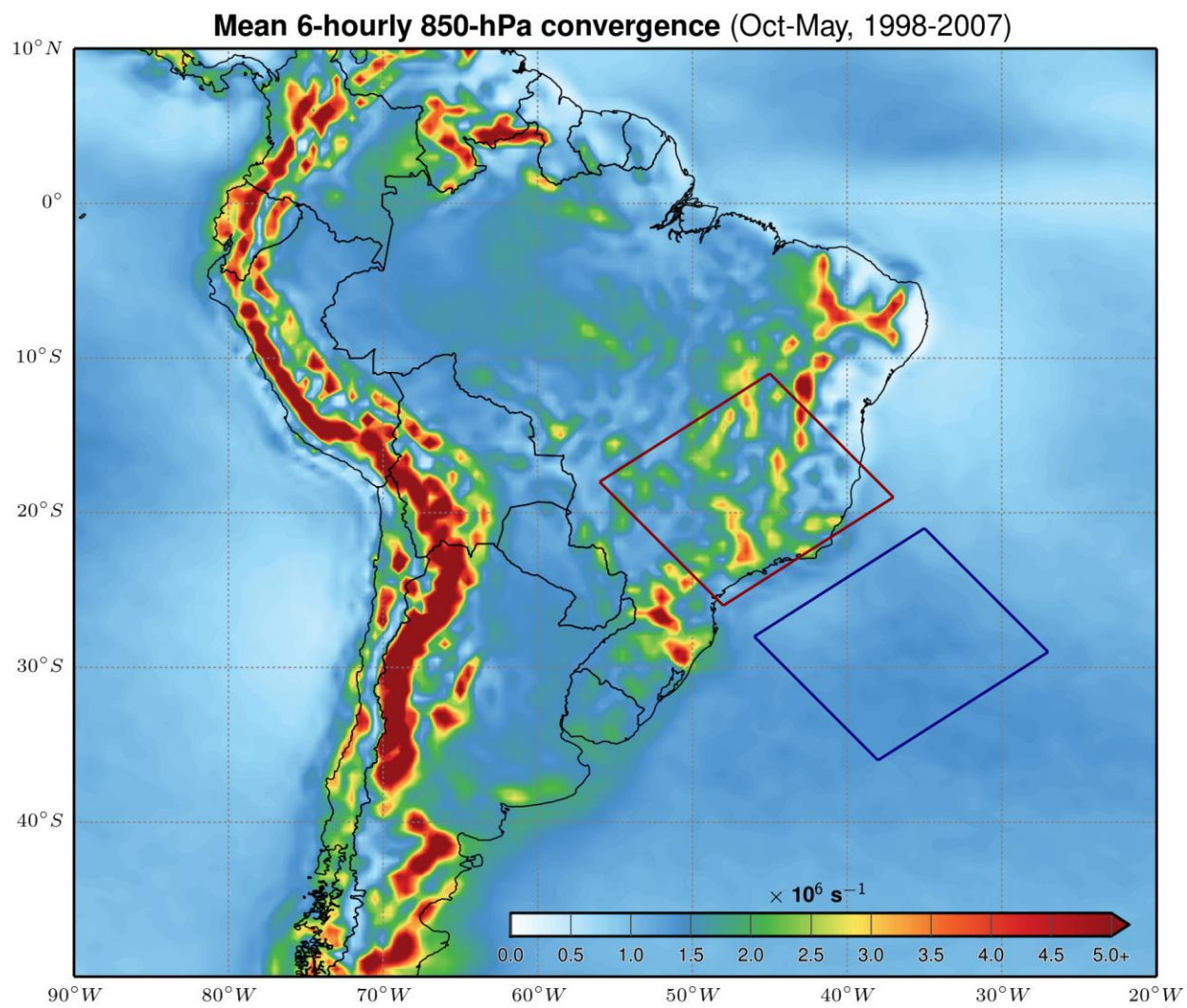


**Fig. 3.7.** Mean 850-hPa convergence for all 6-hourly CFSR timesteps during the warm seasons (Oct–May) of 1998–2007.

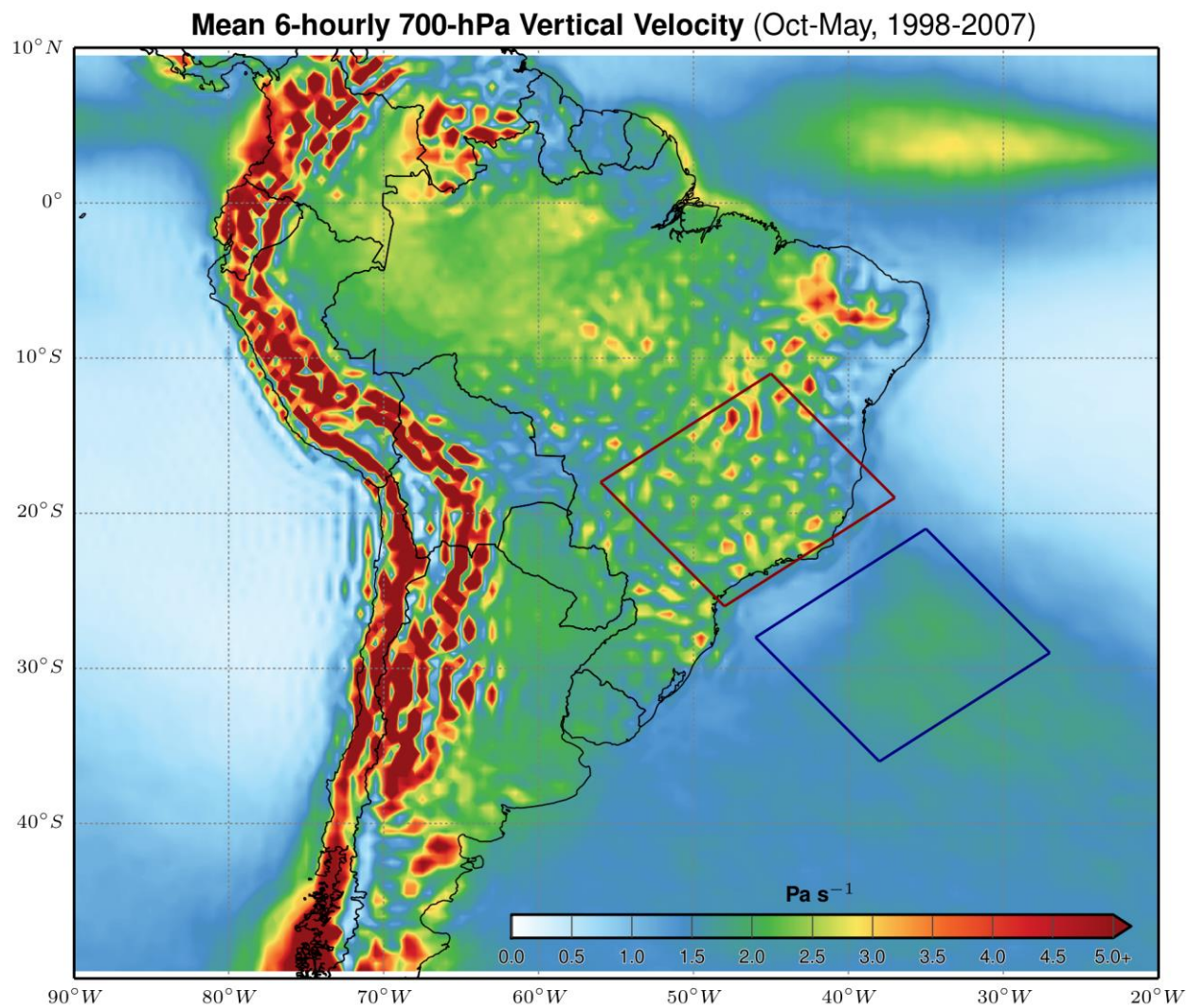


**Fig. 3.8.** Mean 700-hPa vertical velocity for all 6-hourly CFSR timesteps during the warm seasons (Oct–May) of 1998–2007.

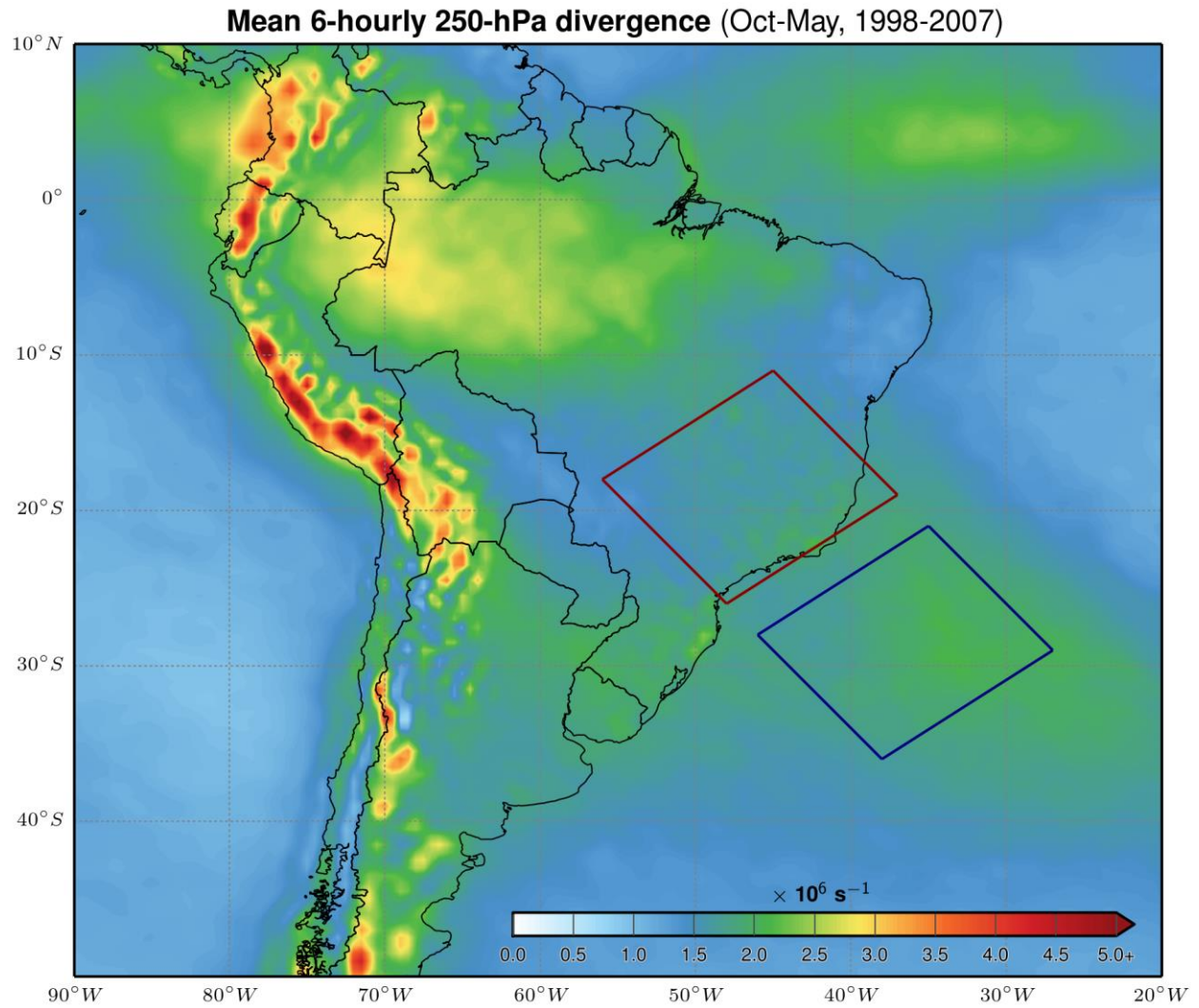


**Fig. 3.9.** Mean 250-hPa divergence for all 6-hourly CFSR timesteps during the warm seasons (Oct–May) of 1998–2007.

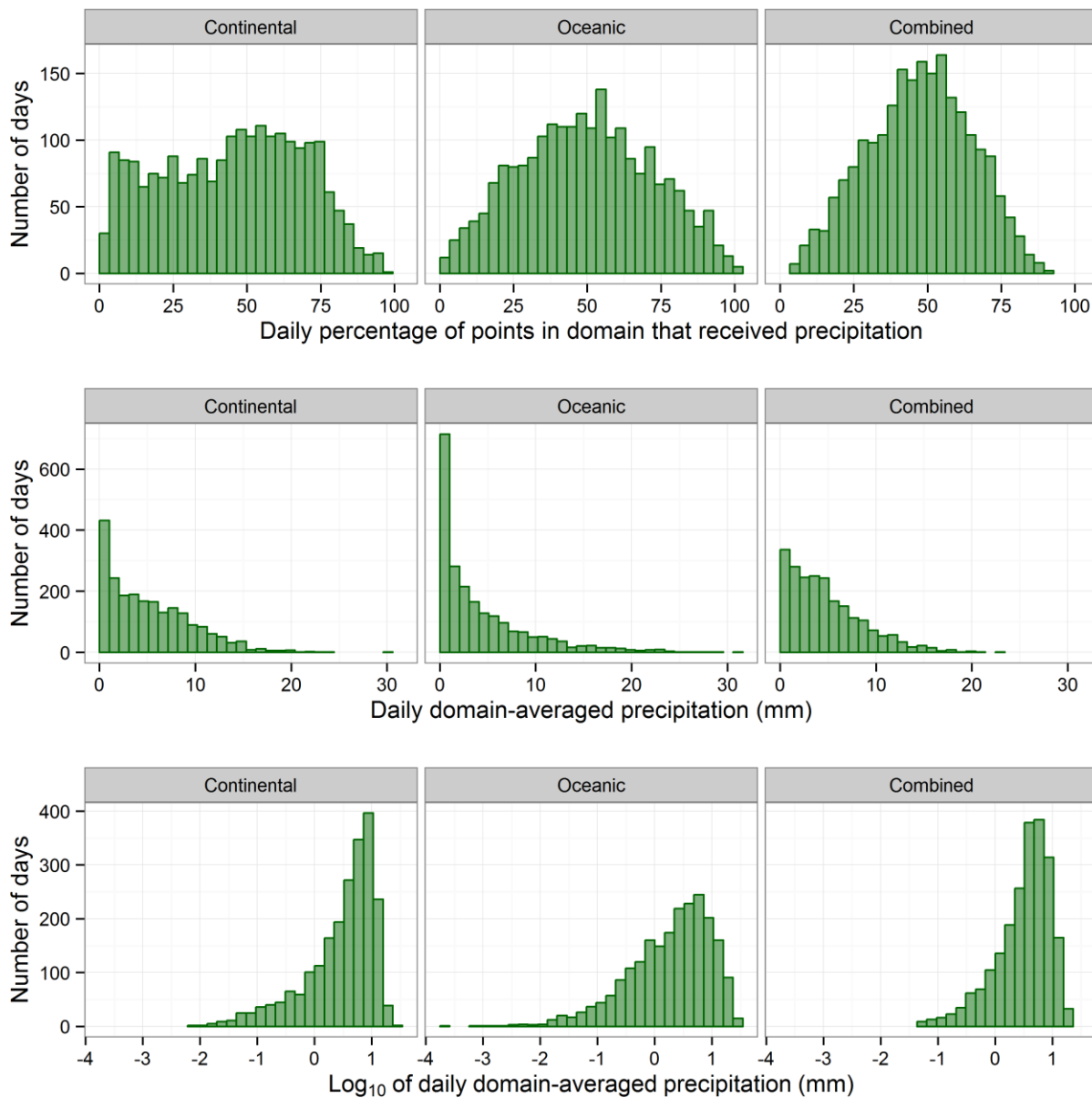


**Fig. 3.10.** Distribution of daily precipitation summary statistics (top row: percentage of domain points receiving precipitation, middle row: domain-average precipitation, bottom row:  $\log_{10}$  transformation of domain-average precipitation) over SACZ domains: continental (left column), oceanic (middle column), combined continental and oceanic (right column).

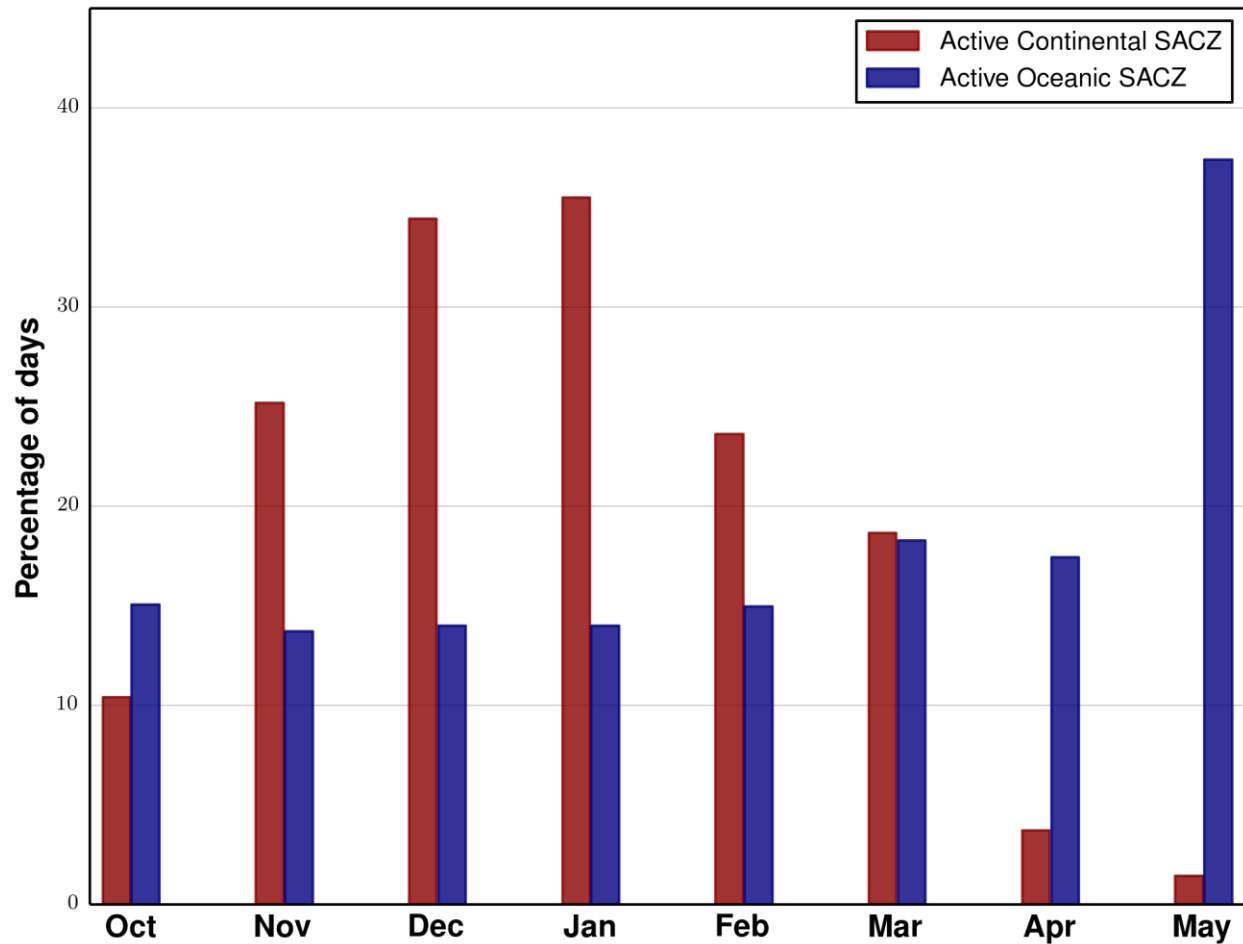


**Fig. 3.11.** Percentage of days during each warm season month from 1998–2007 that were classified as having an active continental SACZ (red bars) or oceanic SACZ (blue bars).

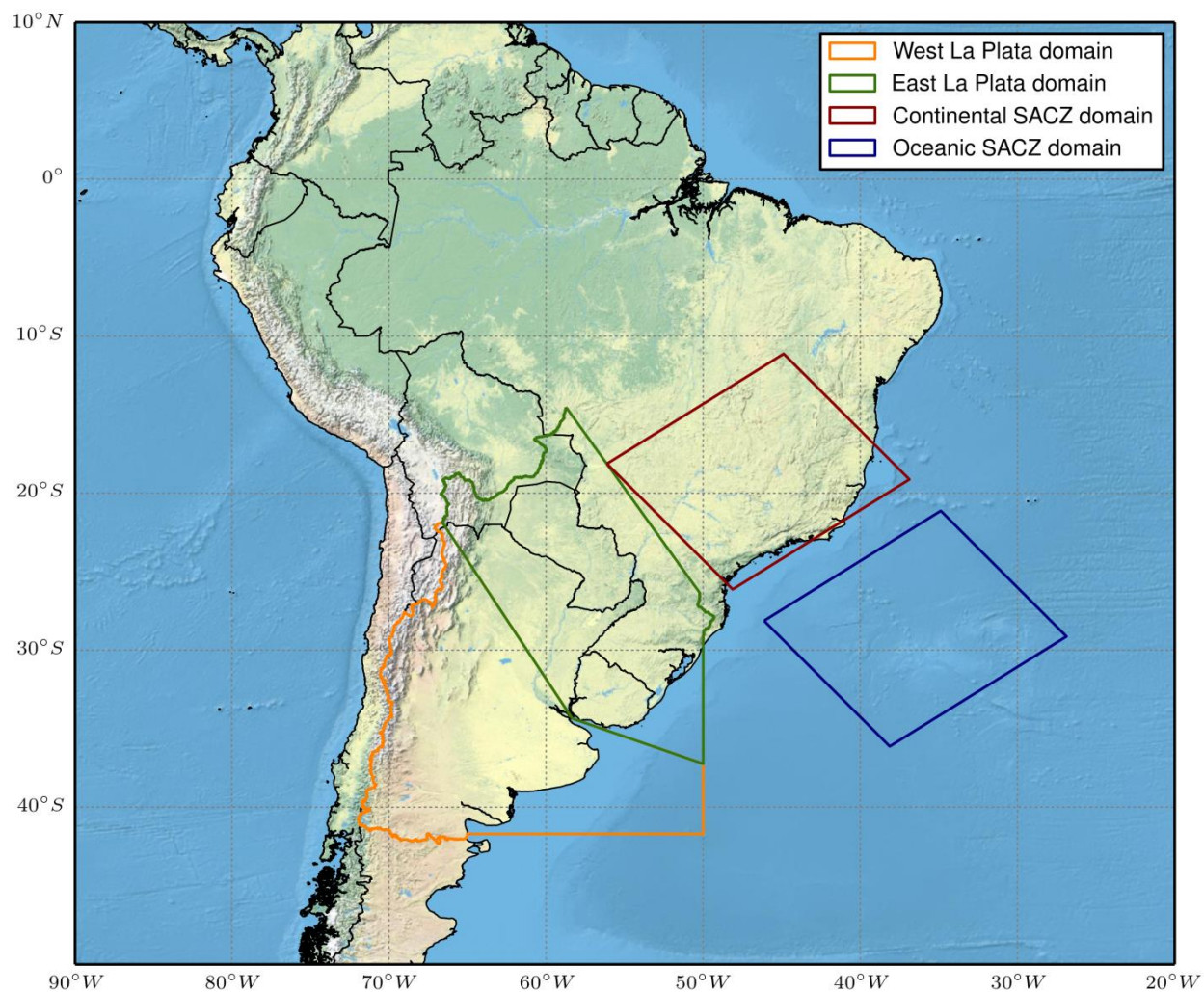


**Fig. 3.12.** Locations of La Plata domains defined for composite atmospheric flow analysis of LLCS events. Note that these La Plata domain names were created for the sake of convenience and are not accurate from a hydrological perspective. Also shown are the continental and oceanic SACZ domains.

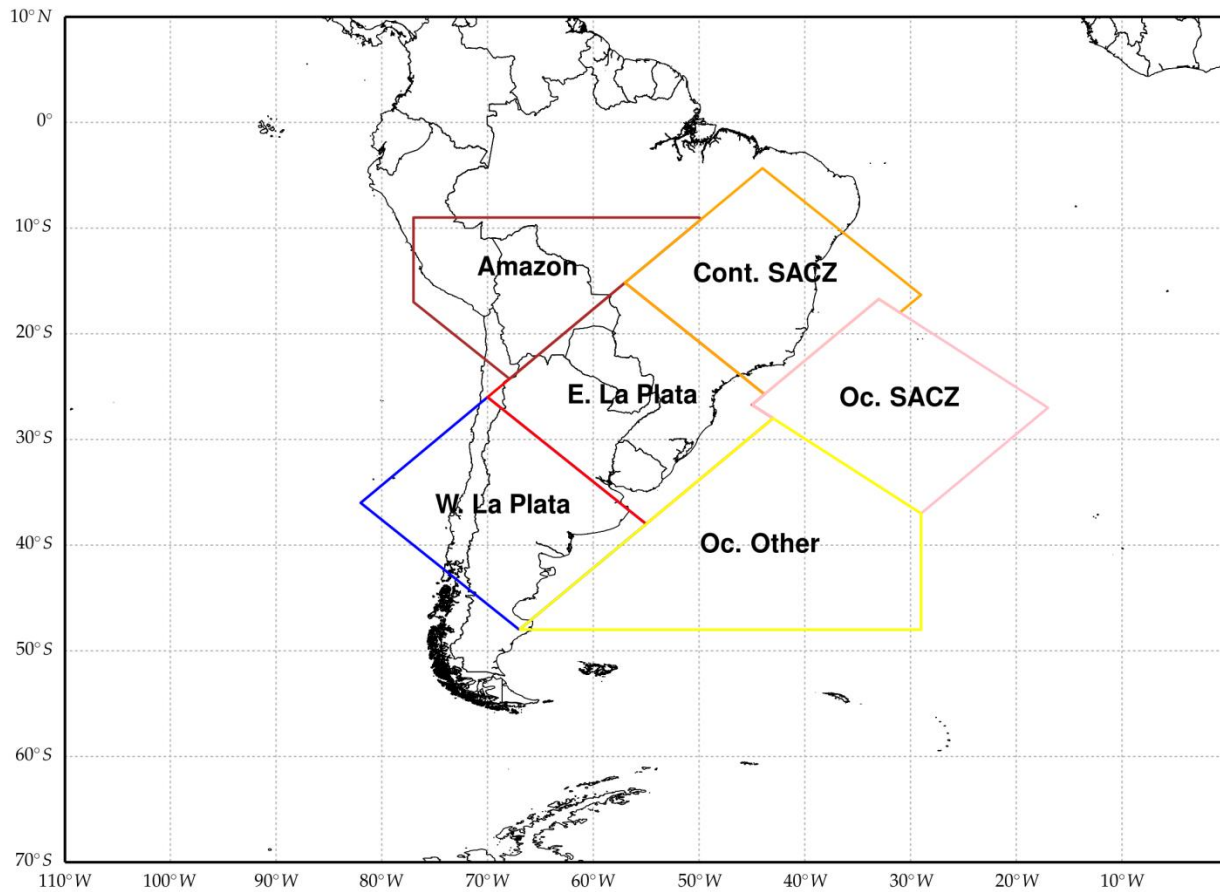


**Fig. 3.13.** Locations of sub-domains defined for LLCS moisture source analysis. Note that the locations of the La Plata and SACZ domains are slightly different than those defined for SACZ event identification and composite flow analysis.

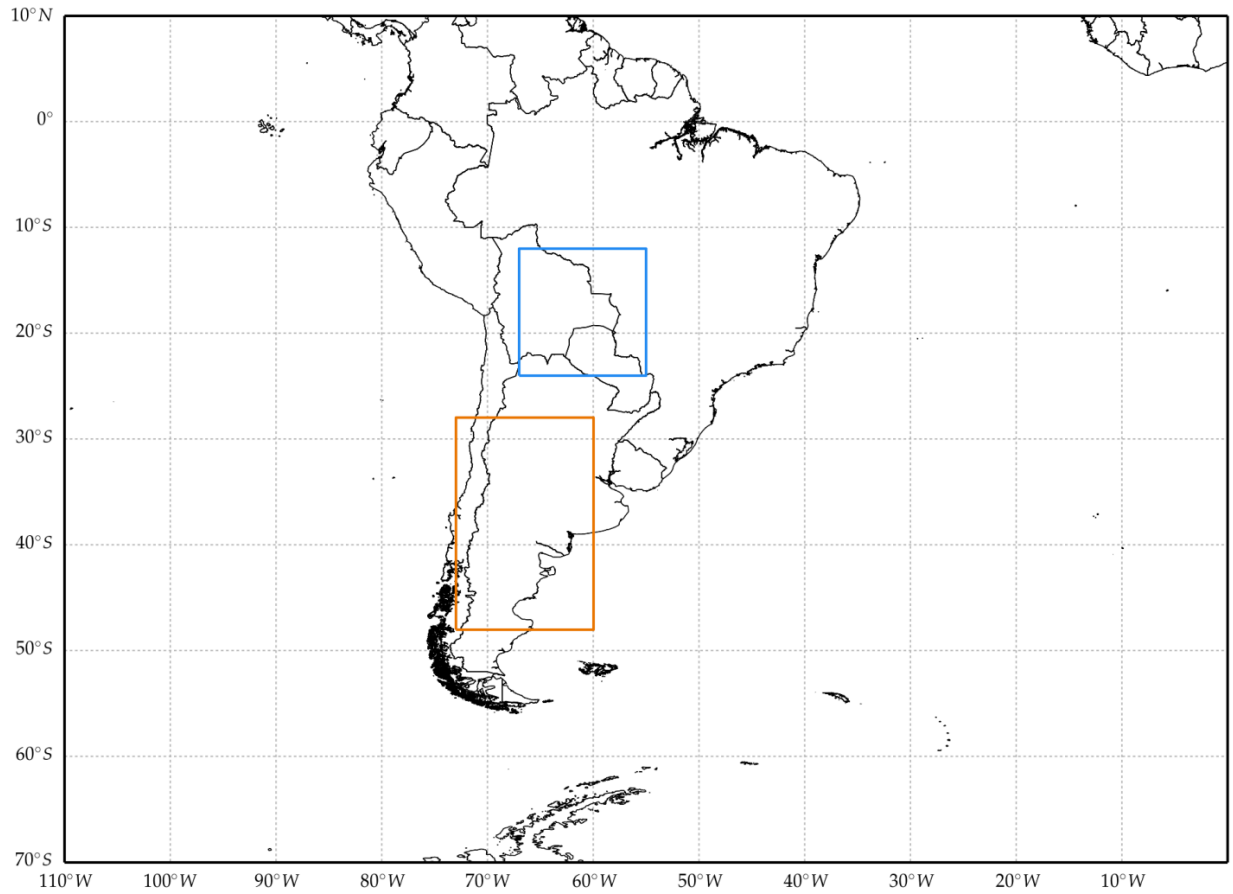


**Fig. 3.14.** Locations of central Argentina LLCS domain (orange box) and South American Low-Level Jet domain (blue box) defined for moisture source analysis of central Argentina LLCS events.

## CHAPTER 4

### RESULTS

Presentation of results follows the order of the methodology narrative in chapter 3. First, composite lower- and upper-tropospheric atmospheric circulation features associated with SACZ and LLCS events are discussed in section 4.1. The insights into SACZ – La Plata basin LLCS relationships provided by the logistic regression model are detailed in section 4.2, followed by an evaluation of LLCS moisture sources in section 4.3. Finally, the moisture sources of central Argentina LLCSs are analyzed in section 4.4, and case studies of two central Argentina LLCS events are presented to illustrate the multiple source regions that provide moisture to these systems.

#### **4.1 Atmospheric circulation features of SACZ and LLCS events**

##### *a. Lower troposphere*

On two-thirds of days (67%) during the study period, precipitation over the both the continental and oceanic SACZ domains was below their respective climatological 75<sup>th</sup> percentiles (Table 4.1). As Fig. 4.1a shows, these “continental and oceanic SACZ inactive” events were characterized by easterly low-level flow and relatively meager atmospheric moisture (PWAT values of 30–35 kg m<sup>-2</sup>) over the continental and oceanic SACZ domains. These days also featured northerly low-level flow from the Amazon basin southward into the La Plata basin, with cyclonic (clockwise) curvature of the 925-hPa flow around the Chaco Low in southern Bolivia. The location of the South Atlantic subtropical cyclone near 30°S off the coast of Brazil resulted in northeasterly low-level flow over the Brazil Current that was diverted around both sides of the Highlands in southern Brazil before ultimately reaching the La Plata basin. As a

result of these low-level circulation patterns, median PWAT values during these inactive SACZ days were approximately 5% above the climatological median over the central La Plata basin and 5% below normal over both the continental and oceanic SACZ regions (Fig. 4.2a).

On active continental SACZ days (Figs. 4.1b, 4.2b), moist northerly SALLJ flow from the Amazon was diverted eastward toward the Highlands of central Brazil and the southeastern Brazil coast, resulting in PWAT above the 75<sup>th</sup> percentile over the continental SACZ domain. On these “continental SACZ only” days, PWAT was slightly below normal over a small section of the La Plata basin in northern Argentina, but there was still evidence of northeasterly flow over the Brazil Current toward the La Plata basin and PWAT across most of the La Plata basin and southward into central Argentina was well above normal (Fig. 4.2b). On “oceanic SACZ only” days, however, the median location of the subtropical anticyclone shifted to the coast of eastern Argentina, and southerly low-level flow over the Brazil Current and much of the South American continent resulted in PWAT values below the 25<sup>th</sup> percentile over the La Plata basin (Figs. 4.1c, 4.2c). Days with both continental and oceanic SACZ active (Figs. 4.1d, 4.2d) also featured an anticyclone over eastern Argentina and below-normal moisture over most of the La Plata basin, but, unlike on “active oceanic SACZ only” days, northwesterly low-level winds prevailed over the Amazon and supplied moisture to the continental SACZ region.

With regard to La Plata LLCS activity, a majority (58%) of 6-hourly timesteps during the POR (Table 4.2) had no LLCS over any part of the La Plata basin domain (see Fig. 3.12). These “no active La Plata LLCS” times were characterized by an anticyclone located along the coast of eastern Argentina and a lack of northerly low-level flow from the Amazon basin or easterly low-level flow from the Brazil Current to supply moisture to the La Plata basin (Fig. 4.3a). As a result, PWAT values were well below normal over the La Plata basin and the western Amazon

basin during these times, with slightly above normal PWAT over eastern Brazil and central and southern Argentina (Fig. 4.4a). These patterns were reversed during the 42% of 6-hourly timesteps where LLCs were active over any part of the La Plata basin, with northerly flow from the Amazon basin and northeasterly flow from the Brazil Current resulting in PWAT values exceeding 15% above normal over the central La Plata basin (Figs. 4.3b, 4.4b). During timesteps where a LLC was only active over the East La Plata domain, the center of highest PWAT anomalies was located over northeastern Argentina and adjacent regions of southern Paraguay, southwestern Brazil, and northern Uruguay, with northwesterly 925-hPa wind anomalies to the east of the Bolivian Andes associated with the SALLJ (Fig. 4.4c). During “active West La Plata LLC only” timesteps, the center of highest PWAT anomalies shifted southwest into central Argentina and southern Uruguay (Fig. 4.4d), and a pronounced Chaco Low resulted in northeasterly SALLJ flow over northern Argentina (Fig. 4.3d). An area of above-normal PWAT also extended from the Pacific Ocean toward the western coast of Chile (Fig. 4.4d), hinting that the Pacific may be a moisture source for some LLC events in the “West La Plata” domain (see sections 4.3 and 4.4).

A comparison of the four columns of Fig. 4.5 reveals that low-level atmospheric circulation tended to be more favorable for La Plata basin LLC activity on days with no SACZ present (first column) and during continental-only SACZ phases (second column). A LLC occurred somewhere in the full La Plata domain on 47% and 43% of these days, respectively. In contrast, La Plata LLCs occurred on just 20% of days when the oceanic SACZ only was active (third column) and 27% of days with the continental and oceanic SACZ both active (fourth column). Continental-only SACZ phases were associated with above normal moisture across the southern Amazon basin southeastward into the Brazilian Highlands, and it appears from Fig. 4.5j

that LLCs occurring over the East La Plata domain during continental-only SACZ phases were fed by the same northwesterly Amazonian moisture flux as the SACZ. Continental-only SACZ days when a LLC occurred over the West La Plata domain (Fig. 4.5n) featured a bifurcation of this Amazonian moisture transport into an eastern pathway directed toward the SACZ region and a western pathway flowing down the eastern flank of the Andes toward central Argentina, with northeasterly 925-hPa wind anomalies over the Brazil Current also suggestive of moisture transport from the South Atlantic Ocean to the La Plata basin. Rich Amazon moisture was also present on the days when both the continental and oceanic SACZ were active (fourth column), but southerly wind flow over the La Plata basin decreased moisture availability in that region. Oceanic-only SACZ days (third column) typically featured below normal moisture across most of continental South America, which is likely a product of the tendency of oceanic SACZ events to occur more often during spring and fall as opposed to mid-summer like the continental SACZ (see Fig. 3.11).

*b. Upper troposphere*

Composite upper-tropospheric conditions on days when neither the continental nor the oceanic SACZ was active were characterized by generally zonal 300-hPa flow, with the signature of the Bolivian High evident in counterclockwise curvature of wind vectors over eastern Bolivia and western Brazil (Fig. 4.6a). An area of above-normal 300-hPa divergence extended over most of the La Plata basin, with anomalously negative 300-hPa divergence indicative of sinking tropospheric air over southeastern Brazil and the adjacent Atlantic Ocean (Fig. 4.7a). The only substantial change to these upper tropospheric composite features for continental-only SACZ events (Figs. 4.6b and 4.7b) was the appearance of an area of below-normal 300-hPa geopotential height and cyclonic flow off the northeast coast of Brazil, identified in previous literature as the “Nordeste Low” (Chen et al. 1999).

During oceanic-only SACZ events, in contrast, a trough of low pressure extended from the La Plata basin southeastward across the South Atlantic Ocean (Fig. 4.6c). Pronounced height anomalies of up to 30% below normal coincided with a cyclonic upper-level circulation over southern Brazil and the Brazil Current, resulting in strong upper-level divergence extending from the southeast coast of Brazil southeastward well into the South Atlantic Ocean (Fig. 4.7c). A similar upper-level cyclonic circulation was observed on days with both SACZ domains active (Fig. 4.6d). However, negative height anomalies were of lesser magnitude and confined to a smaller region of the southern Brazil coast on these days (Fig. 4.7d), with positive height anomalies in the Bolivian High region and evidence of the Nordeste Low off the coast of northeastern Brazil.

Upper-tropospheric composites for 6-hourly timesteps with no active LLCS over any part of the La Plata domain (Figs. 4.8a and 4.9a) reveal a ridge of high pressure over the subtropical Andes and the western La Plata basin, with anomalously low 300-hPa height and cyclonic curvature of wind vectors indicating a low pressure trough centered over the coast of southern Brazil. These features were reversed during times with an active La Plata LLCS, with an Andes trough and a downstream upper-level anticyclone resulting in anomalously strong upper-tropospheric divergence over most of the La Plata basin (Figs. 4.8b and 4.9b). When LLCS activity was only present over the East La Plata basin, the coupled cyclone-anticyclone were both shifted slightly to the northeast (Figs. 4.8c and 4.9c), causing a concentration of strongest divergence in northern Argentina, Paraguay, and southern Brazil. Active West La Plata LLCS composites (Figs. 4.8d and 4.9d), as expected, show a southwestward shift in these circulation features – the axis of a strong trough was aligned with the central and southern Argentinian Andes, and the resultant divergence was located over central Argentina and Uruguay.

Similar to the lower-tropospheric circulation composites described above, maps of 300-hPa anomalies across all subsets of LLCS and SACZ activity (Fig. 4.10) reveal the upper-tropospheric conditions that lead to more favorable conditions for La Plata LLCS development during inactive and continental-only SACZ phases, compared to both-active and oceanic-only phases. During inactive SACZ phases, La Plata basin LLCS activity was associated with a well-defined cyclonic disturbance in the mid-latitude jet stream over the subtropical Andes (bottom three maps in column 1). Upper tropospheric composites for La Plata LLCS events during continental-only SACZ phases (bottom three maps in column 2), meanwhile, showed a Nordeste trough and positive height anomalies across most of the South American continent. These features represent a monsoonal large-scale circulation that is quite different from the aforementioned “Andes trough” pattern but is also favorable for La Plata LLCS formation, particularly over the northeastern sections of the La Plata basin.

In contrast, oceanic-only SACZ events (column 3) were associated with a more amplified upper-tropospheric atmospheric circulation pattern, with negative height anomalies over the La Plata basin indicating an upper-level trough and convergence in place. An exception to this general rule occurred on the rare occasions when an active West La Plata LLCS coincided with an oceanic-only SACZ day (Fig. 4.10o); during these times, positive height anomalies over central Argentina located between negative anomalies over both the subtropical Andes and the southeast coast of Brazil signaled a highly meridional jet stream pattern with multiple Rossby waves supporting separate areas of upper-level divergence over central Argentina and the oceanic SACZ region. Taken as a whole, these upper-level composites again reflect the tendency for continental-only SACZ phases to occur during the summer peak of the monsoon season,

while oceanic-only SACZ events are more likely to result from the dynamic extratropical circulation of austral spring and fall.

#### **4.2 Continental and oceanic SACZ relationships with LLCS probability**

Previous studies (Velasco and Fritsch 1987; Durkee and Mote 2009; Mattingly 2012) have noted that MCS activity in subtropical South America exhibits a large degree of temporal and spatial variability throughout the austral warm season. A map of the daily probability of LLCS occurrence across the study region for all warm season months (Fig. 4.11) shows that LLCS probability gradually increased from early spring to midsummer (October through January) and decreased sharply to a May minimum thereafter. Spatially, the zone of highest LLCS frequency shifted from the western slopes of the Highlands of far southern Brazil during October to encompass a belt extending from eastern Paraguay through the western sections of the continental SACZ region during January. It then migrated southward across southern Paraguay, northern and central Argentina, Uruguay, and adjacent regions of the South Atlantic Ocean throughout the remainder of the warm season.

In analyzing these patterns of LLCS variability and the atmospheric circulation features associated with LLCS events over the La Plata basin during various SACZ phases (section 4.1), the question naturally arises: How is the probability of LLCS development in SESA related to the activity of the SACZ? An examination of daily LLCS probability across the same SACZ phase categories employed in the atmospheric composite analyses (Fig. 4.12) reveals that spatial variability in LLCS probability was linked to these SACZ classifications in a manner consistent with the atmospheric circulation features described in the previous section. LLCS probability was highest over the central La Plata basin during inactive SACZ phases, with relatively high LLCS probability over the western part of the continental SACZ domain during continental-only SACZ days and higher LLCS probability over both SACZ domains on days with both SACZ

active. During oceanic SACZ phases, the maximum LLCS probability was substantially lower than the other three SACZ classifications, with highest LLCS probabilities only around 10% over the oceanic SACZ domain and relative maxima around 8% over central Argentina and southwestern Brazil.

While these maps of LLCS probability across various SACZ phases provide a useful first impression of the relationships between SACZ activity and subtropical South America LLCS occurrence, they are dependent on categorical classification of SACZ events and do not conclusively answer any questions about the “South American Seesaw” inverse relationship between SACZ and La Plata basin precipitation. In order to determine whether this precipitation dipole is also reflected in LLCS activity in the region, the results of the gridded logistic regression model described in section 3.2c are examined. Recall from section 3.2c that the predictor variables of this regression model at each  $0.25^\circ \times 0.25^\circ$  grid point are the respective climatological percentile ranks of continental and oceanic SACZ domain precipitation for each day in the POR, and the predictand is a dummy variable indicating whether or not the grid point was located underneath any part of a LLCS cloud shield on each day.

Figure 4.13 provides an overview of the logistic regression technique and an example of the model results at two example domain points: a “continental” point (red star on Fig. 4.13) located near the continental SACZ domain in the region of highest climatological LLCS probability, and an “oceanic” point (blue star) located within the oceanic SACZ domain in an area of relatively low climatological LLCS probability. For each point, two representative graphs of model-predicted daily LLCS probability are plotted; these predicted LLCS probabilities were calculated using the raw model-output coefficients for the continental and oceanic SACZ precipitation variables at each point given in Table 4.3 (“continental” domain point) and Table

4.4 (“oceanic” domain point). On the first graph for each point (near the top of the map), model-predicted daily LLCS probability is plotted as a function of *continental* SACZ precipitation ranging continuously from its 0<sup>th</sup> to 100<sup>th</sup> percentile, with *oceanic* SACZ precipitation held constant at its 10<sup>th</sup> (blue line), 50<sup>th</sup> (green line), and 90<sup>th</sup> (red line) percentiles. On the second graph for each point (near the bottom of the map), model-predicted daily LLCS probability is plotted as a function of *oceanic* SACZ precipitation ranging continuously from its 0<sup>th</sup> to the 100<sup>th</sup> climatological percentile, with *continental* SACZ precipitation held constant at its 10<sup>th</sup> (blue line), 50<sup>th</sup> (green line), and 90<sup>th</sup> (red line) percentiles.

These graphs show that at the “oceanic” representative point (right two plots on map), LLCS probability increases with increasing oceanic SACZ precipitation in a nonlinear fashion, as LLCS probabilities below 5% in the 0–60<sup>th</sup> oceanic SACZ precipitation percentiles increase markedly to near 10% as oceanic SACZ precipitation approaches its maximum. These plots also show that LLCS probability at this “oceanic” representative point is, as expected, much more closely related to precipitation in the oceanic SACZ domain than precipitation in the continental SACZ domain: the curves of predicted LLCS probability according to continental SACZ precipitation (top right) have essentially zero slope, and the p-value of the continental SACZ precipitation coefficient is an insignificant 0.6 (Table 4.4).

At the “continental” representative point, however, model results indicate that variations in continental and oceanic SACZ domain precipitation are equally influential in predicting LLCS probability. Table 4.3 shows that the raw log-odds coefficients for continental and oceanic SACZ precipitation are 0.010 and -0.012, respectively. This means that a 1% increase in daily precipitation over the continental SACZ domain is predicted by the regression model to result in an increase of 0.010 in the log-odds of LLCS occurrence at that point, while a 1% increase in

daily precipitation over the oceanic SACZ domain is expected to cause a decrease of 0.012 in the log-odds of LLCS occurrence. As the graphs of predicted LLCS probability show (left two plots on map), the positive slope of the predicted LLCS probability curves across the range of continental SACZ precipitation (top left) is roughly equal in magnitude to the negative slope of the predicted LLCS probability curves across the range of oceanic SACZ precipitation (bottom left). Moreover, the large gap between the continental SACZ precipitation probability curves for oceanic precipitation held constant at its 10<sup>th</sup>, 50<sup>th</sup>, and 90<sup>th</sup> percentiles (top left) shows that the LLCS probability across the range of continental precipitation at this point is strongly modulated by oceanic SACZ activity.

This analysis of continental and oceanic SACZ precipitation relationships with LLCS probability can be extended from the two example points presented above to each  $0.25^\circ \times 0.25^\circ$  grid point in the specified domain (described in section 3.2c) by plotting the spatial variability of the raw model log-odds coefficient for continental SACZ precipitation (Fig. 4.14) and oceanic SACZ precipitation (Fig. 4.15). For each map, the plotted values are the expected change in the log-odds of daily LLCS occurrence at the given point for a one percentile change (relative to the October–May 1998–2007 climatological distribution) in the percentage of the continental (Fig. 4.14) or oceanic (Fig. 4.15) SACZ domain receiving precipitation on a given day. Positive coefficient values indicate that an increase in continental / oceanic SACZ domain precipitation is predicted to result in increased LLCS probability, while negative coefficient values indicate that LLCS probability is modeled to decrease with increasing precipitation over the specified domain.

Figure 4.14 shows that, unsurprisingly, increased precipitation over the continental SACZ domain was associated with an increase in LLCS probability over the entire continental SACZ domain, with the strongest positive effect over the northeastern sections of the domain.

Continental SACZ precipitation also showed a positive relationship with LLCS probability over much of the oceanic SACZ domain and along an arc extending westward from western Brazil through southern Bolivia and northern Paraguay, and southward along the eastern flank of the Andes into northwestern and central Argentina. A negative relationship between continental SACZ precipitation and LLCS probability extended across far southern Brazil, southern Paraguay, northeastern Argentina, Uruguay, southeastward into the South Atlantic Ocean, with a separate region of negative continental SACZ influence located over the Andes of south-central Argentina. A map of the raw oceanic SACZ precipitation coefficient (Fig. 4.15), meanwhile, showed a negative relationship between oceanic SACZ precipitation and LLCS probability over much of subtropical South America, particularly in the central La Plata basin region of northern Argentina, southern Paraguay, far southern Brazil, Uruguay, and the adjacent South Atlantic Ocean. Strong positive relationships between oceanic SACZ precipitation and LLCS probability were found over the oceanic SACZ domain, with a less pronounced positive relationship over southeastern sections of the continental SACZ domain and the same section of south-central Argentina where continental SACZ precipitation was shown to be inversely related to LLCS probability.

Another way to visualize these modeled relationships is displayed in Fig. 4.16, which shows the spatial variability of model-predicted daily LLCS probability across combinations of representative “low” and “high” continental and oceanic SACZ precipitation percentiles (10<sup>th</sup> and 90<sup>th</sup>) with precipitation over the other domain held constant at its median. Highest probabilities of LLCS occurrence over western Brazil, northeast Paraguay, and western Bolivia were modeled for the “high continental SACZ precipitation” case, while predicted LLCS probability over the central La Plata basin in southern Paraguay, northern Uruguay, far southern

Brazil, and far northeastern Argentina was maximized in the “low oceanic SACZ precipitation” case. Much lower LLCS probabilities occurred during the “high oceanic SACZ precipitation” case, which again reflects the tendency for oceanic SACZ events to occur in accordance with low LLCS probabilities over subtropical South America.

A final step in examining the modeled relationships between continental and oceanic SACZ precipitation and LLCS probability throughout subtropical South America is to analyze the spatial variability of the *relative* magnitude of the modeled continental and oceanic SACZ precipitation coefficients. Figure 4.17 is a map of the difference between the absolute value of the continental and oceanic SACZ precipitation coefficients at each point in the domain; regions where the continental SACZ precipitation coefficient is greater in magnitude than the oceanic SACZ precipitation coefficient are shaded red, and regions where the association between oceanic SACZ precipitation and LLCS probability is stronger than that of continental SACZ precipitation are shaded blue. The *type* of relationship between SACZ domain precipitation and LLCS probability at each point (e.g. LLCS probability increases with increasing continental SACZ precipitation but decreases with increasing oceanic SACZ precipitation) is indicated by hatching at locations where both continental and oceanic SACZ precipitation coefficients are statistically significant.

As expected, the continental SACZ precipitation coefficient is much more strongly tied to LLCS probability over the continental SACZ domain, while the oceanic SACZ precipitation coefficient is much greater in magnitude over the oceanic SACZ domain (Fig. 4.17). More interestingly, the area of stronger continental SACZ relationship with LLCS probability is mostly confined to the northern sections of the domain, over central Brazil, southern Bolivia, and northern Paraguay. There is also a tongue of higher relative magnitude of the continental SACZ

coefficient extending from the southeast coast of Brazil southward across the South Atlantic Ocean to the west of the oceanic SACZ domain and a region of stronger continental SACZ relationship over the Andes of west-central Argentina. Over the rest of the La Plata basin, across the southern half of Paraguay, the southern Brazilian Highlands, northern Argentina, Uruguay, and the South Atlantic Ocean offshore of the La Plata estuary, the relationship between oceanic SACZ precipitation and LLCS probability is stronger than that of continental SACZ precipitation.

Notably, this borderline between regions of relatively stronger oceanic versus continental SACZ relationship with LLCS probability runs from the gap in the Brazilian Highlands along the southeast coast of Brazil (see Fig. 1.1), identified in section 2.1e as a potential pathway for moisture flux from the Brazil Current into the La Plata basin, through the valleys of the Paranapanema and Paraná rivers into eastern Paraguay. This dividing line also closely approximates the southern border of the region of highest positive precipitable water anomalies found during continental SACZ events (Fig. 4.2c). These observations suggest that LLCS probability north of this line in southern Bolivia, northern Paraguay, and western Brazil is closely tied to moisture flux from the Amazon basin related to periods of enhanced precipitation over the continental SACZ region. South of this dividing line over much of the central La Plata basin, oceanic SACZ activity, likely tied to lower-tropospheric flow over the Brazil Current, is more strongly associated with variability in LLCS probability. If low-level winds over the Brazil Current are easterly, moisture flux toward the La Plata basin and LLCS probability in the region increases; if these low-level winds over the Brazil Current are westerly, oceanic SACZ precipitation is increased at the expense of La Plata basin LLCS activity.

### 4.3 LLCS moisture source analysis

Analyses of atmospheric circulation associated with subtropical South American LLCSs detailed in the previous two sections have suggested that South Atlantic and Pacific moisture sources may contribute to LLCS development in addition to the more widely recognized SALLJ moisture transport regime. This hypothesis is further supported by maps of climatological precipitable water values for all warm season months (Fig. 4.18), which show a distinct pool of atmospheric moisture off the southeast coast of Brazil (over the Brazil Current discussed in section 2.1d) with PWAT values equal to slightly less than those observed over the southern Amazon basin. Additionally, these maps show a relatively moist region over the Pacific Ocean west of Chile with PWAT values that are substantially less than those in the Amazon and South Atlantic, but could still potentially supply moisture to convection in subtropical South America. These observations motivated a more detailed investigation of the moisture source regions of LLCSs in the region, which was performed using the HYSPLIT back trajectory methodology described in section 3.2d.

Overview maps of the 5866 parcel back trajectories terminating at 6-hourly LLCS centroids for all three trajectory levels (Figs. 4.19, 4.20, and 4.21) show a variety of pathways taken by air parcels into LLCS events. A substantial amount of near-surface (10m above ground level [AGL]) parcels originated in the southern Amazon basin and flowed southward toward the La Plata basin and Brazilian Highlands, while many tracked from the tropical South Atlantic Ocean south of 10°S toward Brazil, and still others originated over the eastern Pacific Ocean and South Atlantic Ocean south of 40°S and flowed eastward and northward toward South America. At the next level in the atmosphere (1000m AGL), the distance traveled by air parcels into LLCSs increased (likely because these parcels travel at higher speeds due to less frictional interaction with the land surface), and more parcels at this level appeared to traverse the Amazon

basin. The Amazon origin of parcels is also prominent at the final trajectory level examined (2500m AGL), along with an increase in the number of parcels originating over the eastern Pacific Ocean and a marked decrease in parcels originating from the Atlantic Ocean south of 40°S. These patterns are more clearly highlighted by trajectory density maps for each parcel level (Figs. 4.22, 4.23, and 4.24), calculated using the procedure described in section 3.2d. These maps show that LLCS back trajectories at 10m AGL were most dense over southern Brazil, eastern Paraguay, far northeastern Argentina, and Uruguay (Fig. 4.22), with the region of highest parcel density shifting northwestward into the southern Amazon Basin, eastern Bolivia, western Brazil, and Paraguay at the 1000m AGL (Fig. 4.23) and 2500m AGL (Fig. 4.24) trajectory levels.

In order to examine the variability of LLCS moisture sources across subtropical South America in greater detail, back trajectories were grouped into the six sub-domains shown in Fig. 3.13 according to the location of their LLCS centroid endpoint. At 10m AGL, the majority of parcels feeding LLCSs in the “West La Plata” domain (Fig. 4.25a) originated in the South Atlantic Ocean off the coast of Argentina, Uruguay, and southern Brazil. Back trajectories at 10m AGL for the “East La Plata” domain (Fig. 4.25b) appear to be sourced from the Brazil Current region of the South Atlantic Ocean and the southern Amazon Basin in roughly equal amounts, while back trajectories for the “Amazon” domain predictably tended to arrive from the western Amazon basin (Fig. 4.25c). Over the “continental SACZ” domain (Fig. 4.25d), parcel pathways appear to be almost evenly split between northwesterly flow from the Amazon basin and easterly flow from the tropical Atlantic Ocean, while the majority of 10m AGL parcels for “oceanic SACZ” LLCSs flowed from the tropical Atlantic (Fig. 4.25e). Finally, parcel trajectories for “oceanic other” domain LLCSs (Fig. 4.25f) tended to come from either the

eastern Pacific Ocean (passing over the Brazil Current), the area of the South Atlantic to the east of the Brazil coast, or the higher latitudes of the South Atlantic north of Antarctica.

Higher in the troposphere, at the 1000m and 2500m levels, there were a few notable differences in the patterns of parcel trajectories associated with LLCs in each sub-domain. For LLCs in the “West La Plata” domain, a majority of 1000m AGL parcel trajectories (Fig. 4.26a) still tended to originate over the Brazil Current or the eastern Pacific, but substantially more parcels than at 10m AGL showed a SALLJ signature, traversing due south from the Amazon basin along the eastern slopes of the Andes. At 2500m AGL (Fig. 4.27a), most parcel trajectories came from either the SALLJ region or the eastern Pacific. For the “East La Plata” domain, the vast majority of parcels at 1000m AGL (Fig. 4.26b) and 2500m AGL (Fig. 4.27b) were indicative of northerly SALLJ flow, while trajectories for “Amazon” LLCs at 1000m (Fig. 4.26c) and 2500m (Fig. 4.27c) were consistent with the 10m trajectories in showing northerly or northeasterly flow from the Amazon basin. Parcel trajectories at 1000m AGL and 2500m AGL for the “Continental SACZ” and “Oceanic SACZ” domains were broadly similar to those found for the 10m AGL trajectories, while 1000m AGL and 2500m AGL trajectories for the “Oceanic other” domain (Figs. 4.26f and 4.27f, respectively) were substantially more likely to originate from the South American continent than 10m AGL parcels.

The last step in the examination of subtropical South America LLC moisture source regions was to visualize back trajectory density grouped by the number of days preceding the LLC valid time, in order to investigate the temporal progression of air parcel movement toward LLC centroids. These temporally-grouped trajectory density plots were created separately for each of the six sub-domains (Figs. 4.28 through 4.33). For LLCs in the “West La Plata” domain (Fig. 4.28), near-surface parcels (top row) most often originated over the La Plata estuary and the

adjacent Brazil Current, then migrated westward across Uruguay and northern Argentina. At 1000m AGL (middle row), parcels were most densely concentrated to the northeast of the near-surface parcels, flowing from far southern Brazil southwestward into central Argentina, while 2500m AGL parcels (bottom row) tended to migrate from either the eastern Pacific or the SALLJ region toward the “West La Plata” domain. Near-surface trajectories for “East La Plata” LLCs (top row of Fig. 4.29) had dual centers of highest density, one located in the SALLJ region east of the Andes and one over the southern Brazil coast suggestive of moisture flux from the Brazil Current through the gap in the Brazilian Highlands described in section 2.1e. At 1000m (middle row of Fig. 4.29) and 2500m AGL (bottom row), trajectory densities associated with “East La Plata” LLCs showed a clear SALLJ signature, migrating from the Amazon basin southward to the La Plata basin. With regard to the remaining four sub-domains, the most interesting result revealed by the trajectory density plots was the substantial proportion of trajectories for both “Continental SACZ” (Fig. 4.31) and “Oceanic SACZ” (Fig. 4.32) LLCs that originated over the warm waters of the tropical Atlantic off the northeast coast of Brazil.

In interpreting the results of these parcel trajectory analyses, it is important to keep in mind several sources of uncertainty regarding the moisture sources of LLCs in subtropical South America. First, the relatively coarse-resolution NCEP-NCAR Reanalysis 1 dataset used to model the parcel trajectories reduces confidence in the accuracy of the trajectories, particularly over the complex topography of the Andes and Brazilian Highlands. Moreover, only one parcel trajectory was used to model the airflow into each 6-hourly merged LLC cloud shield, which is an oversimplification of the complex atmospheric circulation patterns associated with these large, highly dynamic convective complexes. Considering the size of these systems, it is quite plausible that at any one time they are receiving inflow at a given level from source regions

hundreds or thousands of kilometers apart. Finally, atmospheric moisture transport is a complex phenomenon with many intricacies (e.g. uplift along isentropic surfaces, upstream rainout, land surface – boundary layer interactions) that are likely not adequately modeled by a simple parcel trajectory.

With these caveats noted, the results of this LLCS back trajectory study still reveal several aspects of moisture transport over subtropical South America that have not been documented in previous studies. Most importantly, the tendency of modeled parcels terminating at La Plata basin LLCS centroids just above ground level to originate over the South Atlantic Ocean off the coasts of eastern Argentina, Uruguay, and southern Brazil confirms that the warm waters of the Brazil Current provide at least some of the necessary atmospheric moisture for organized La Plata basin convection in many instances. At higher levels in the atmosphere (1000m and 2500m AGL), parcels tended to originate over the Amazon Basin and flow southward toward La Plata basin LLCSs, which shows that SALLJ activity is more pronounced above the immediate boundary layer. Additionally, a substantial percentage of trajectories for convection over central Argentina originated over the eastern Pacific Ocean, which suggests that these mid-latitude events may sometimes be fed by Pacific moisture. Viewed in conjunction with the atmospheric circulation analyses detailed in the previous two sections, these results show that the oft-repeated assumption that the Amazonian SALLJ is the primary moisture source for all large-scale organized convection in the La Plata basin is, in a nontrivial number of cases, potentially inaccurate. Further research will be needed to determine how these South Atlantic and Pacific moisture contributions compare to those of the SALLJ.

#### 4.4 Moisture sources and case studies of central Argentina LLCS events

The last major objective of this study was the investigation of LLCS events in central Argentina that Durkee (2008) suggested may occur in the absence of SALLJ transport of Amazonian moisture. All LLCS events whose centroids fell inside the central Argentina domain shown in Fig. 3.14 at any point in their life cycle were examined according the procedure described in section 3.2e to determine if any of the 6-hourly LLCS back trajectories at each level (10m, 1000m, and 2500m AGL) passed through the SALLJ domain shown in Fig. 3.14. Overall, a plurality of central Argentina LLCS events (42%) did not exhibit a SALLJ connection at any trajectory level, while 25% of events had parcel trajectories that passed through the SALLJ domain at two of the three levels and 21% had SALLJ parcel trajectories at all three levels (Table 4.5). As Fig. 4.34 shows, central Argentina LLCS events that did not exhibit a SALLJ connection were most common during all months except March. The proportion of events with all trajectory levels connected to the SALLJ was maximized during the December-March peak of the warm season, while a large majority of LLCS events during May showed no SALLJ connection.

As Figs. 4.35 and 4.36 and Table 4.5 show, the size and duration of central Argentina LLCS events increased as the number of trajectories passing through the SALLJ domain increased. Differences in mean LLCS maximum area and duration across SALLJ connection categories, with the exception of duration and maximum area differences between category 1 (one trajectory level with SALLJ connection) and category 0 (no levels with SALLJ connection) and the maximum area difference between category 3 and category 2, were all statistically significant as determined by Tukey's Honestly Significant Difference Test (Table 4.6). These tests confirm a strong tendency for central Argentina LLCSs with inflow from the SALLJ to be both larger and longer-lasting than "non-SALLJ" central Argentina LLCS events.

To illustrate the variability in moisture sources that feed these central Argentina LLCSs and the difficulty involved in determining which moisture source was dominant for a given system, two case studies of central Argentina LLCS events are now presented. The first case study LLCS event initiated along the eastern slopes of the Andes in north-central Argentina around 0000 UTC 15 October 2001 (Fig. 4.37a). At this initiation time, 925-hPa winds over the Brazil Current were easterly and their progress inland toward the La Plata basin was blocked by the Highlands of far southern Brazil, causing one branch of this easterly 925-hPa flow to be diverted through the gap in the Highlands between Curitiba and São Paulo and the other branch to curve southwest then west across Uruguay and the southern tip of Brazil. A tongue of elevated precipitable water extended from the southern coast of Brazil through Uruguay and into central Argentina as a result of this easterly flow, with a separate pool of elevated PWAT extending from the northern La Plata basin southward through northern Argentina in association with northeasterly flow along the eastern periphery of the Chaco Low in southern Bolivia. HYSPLIT trajectories at the lower two levels (10m and 1000m AGL) originated south of the system and progressed northeastward before encountering the moist easterly flow off the Brazil Current and turning westward over far southern Brazil and Uruguay.

Twelve hours later at 1200 UTC 15 October 2011, the LLCS had progressed eastward into eastern Argentina and grown considerably larger (Fig. 4.37b). At this point, the bifurcation of low-level flow around the southern Brazilian Highlands was still evident, as the 10m parcel trajectory approached the LLCS centroid via the pathway south of the Highlands in far southern Brazil and Uruguay, and the 1000m parcel trajectory approached from the northeast under the apparent influence of the northeasterly flow through the aforementioned gap in the Brazilian Highlands. There were also increasing indications of moisture from the Amazon basin flowing

southward into the system, as there was a coherent area of northerly flow extending from central Brazil southward into the La Plata basin and the 2500m parcel trajectory flowed southward from eastern Bolivia into the LLCS centroid. By 0000 UTC 16 October 2001 (Fig. 4.37c), two separate LLCS cloud shields were present, with one located over far northern Argentina and southern Bolivia and the other a continuation of the existing system over far southern Brazil. The new Bolivia system initiated in a moisture pool formed by the convergence of southerly flow originating over the Brazil Current and northerly flow around the Chaco Low, while the previously existing system was maintained by a combination of low-level easterly winds from the Brazil Current and elevated SALLJ flow. Finally, at 1200 UTC 16 October 2001 (Fig. 4.37d), the original system had dissipated to below LLCS criteria, and the Bolivia system had progressed northeastward and appeared to be primarily supported by moist northeasterly flow from the Amazon. This system went on to grow quite large over the western Amazon basin before dissipating around 0600 UTC 17 October 2001.

The second case study (Fig. 4.38) exemplifies a very different type of central Argentina LLCS event, one that initiated along a plume of moisture flowing from the Pacific before progressing eastward with support from moisture contributions by all three sources (Pacific, South Atlantic, and Amazonian SALLJ). It first developed around 1800 UTC 11 April 2004, along a narrow but rich plume of moisture extending from the central Pacific to the southern coast of Chile (Fig. 4.38a). HYSPLIT trajectories at all three levels showed evidence of Pacific origin before funneling through a gap in the Andes along the Chile-Argentina border. This gap flow was particularly pronounced 12 hours later (Fig. 4.38b), as the 925-hPa wind vectors associated with the Pacific moisture plume converged along the Andes of the Chile-Argentina border region and were channeled through gaps in the mountains, accelerating on the eastern side

and bringing a tongue of elevated PWAT toward the LLCS. At this point the LLCS appeared to also be receiving moisture from the Brazil Current as a result of fast northerly flow on the west side of a strong South Atlantic subtropical anticyclone, and potentially from the SALLJ as well, as northerly flow extended all the way from the southern Amazon basin to the LLCS centroid. By the last two timesteps (Fig. 4.38c and Fig. 4.38d), the LLCS had tracked far into the South Atlantic and its primary moisture source appeared to be the Brazil Current. Also notable during this LLCS event was the well-defined SACZ signature in elevated PWAT extending diagonally from central Brazil southeastward through the South Atlantic Ocean off the coast of Brazil at all timesteps. All three days (11-13 April 2004) were classified as continental SACZ days, and 11 April 2004 was classified as an oceanic SACZ day as well.

These case studies demonstrate the variety of moisture sources that can feed LLCSs over subtropical South America and the difficulty in determining the relative moisture contribution of each source region. Both the October 2001 and the April 2004 events appeared to receive moisture from different sources throughout their life cycle, and HYSPLIT back trajectories tracing the movement of air parcels into these systems often originated from distinctly different regions depending on the level in the atmosphere at which the modeled trajectory terminated. This type of ambiguity is common to LLCS events over central Argentina and throughout the South American subtropics, a fact which once again reinforces the importance of considering South Atlantic and Pacific moisture sources in addition to the South American Low-Level Jet.

**Table 4.1.** Number of days during the Oct–May 1997–2008 POR that were classified in each SACZ category.

	<b>Neither SACZ active</b>	<b>Continental SACZ active only</b>	<b>Oceanic SACZ active only</b>	<b>Both SACZ active</b>
<b>Number of days in POR</b>	1463 (67%)	329 (15%)	308 (14%)	89 (4%)

**Table 4.2.** Number of 6-hourly timesteps during the Oct–May 1997–2008 POR that were classified in each LLCS category. Note that these percentages sum to over 100 because these categories are not mutually exclusive.

	<b>No active La Plata LLCS</b>	<b>Active LLCS in either La Plata domain</b>	<b>Active LLCS in E La Plata domain</b>	<b>Active LLCS in W La Plata domain</b>
<b>Number of 6- hourly timesteps in POR</b>	5116 (58%)	3640 (42%)	3136 (36%)	1705 (19%)

**Table 4.3.** Output generated by logistic regression model for the “continental” representative point (-22.875S, -55.125W).

```
glm(formula = LLCS_dummy ~ cont_pcp + oc_pcp, family = "binomial",
    data = SACZ_precip_LLCS_presence)
```

Deviance Residuals:

Min	1Q	Median	3Q	Max
-0.9599	-0.6537	-0.5651	-0.4427	2.2767

Coefficients:

	Estimate	Std. Error	z value	Pr(> z )
(Intercept)	-1.511613	0.141306	-10.697	< 2e-16 ***
cont_pcp	0.010326	0.002047	5.045	4.53e-07 ***
oc_pcp	-0.012549	0.002070	-6.062	1.35e-09 ***

---

Signif. codes: 0 '\*\*\*' 0.001 '\*\*' 0.01 '\*' 0.05 '.' 0.1 ' ' 1

(Dispersion parameter for binomial family taken to be 1)

Null deviance: 2017.5 on 2188 degrees of freedom  
 Residual deviance: 1962.8 on 2186 degrees of freedom  
 AIC: 1968.8

Number of Fisher Scoring iterations: 4

**Table 4.4.** Output generated by logistic regression model for the “oceanic” representative point (-31.125S, -41.125W).

```
glm(formula = LLCs_dummy ~ cont_pcp + oc_pcp, family = "binomial",
    data = SACZ_precip_LLCs_presence)
```

Deviance Residuals:

Min	1Q	Median	3Q	Max
-0.4480	-0.3055	-0.2233	-0.1618	3.0873

Coefficients:

	Estimate	Std. Error	z value	Pr(> z )
(Intercept)	-4.787055	0.391542	-12.226	<2e-16 ***
cont_pcp	-0.002156	0.004173	-0.517	0.605
oc_pcp	0.025513	0.004790	5.327	1e-07 ***

---

Signif. codes: 0 '\*\*\*' 0.001 '\*\*' 0.01 '\*' 0.05 '.' 0.1 ' ' 1

(Dispersion parameter for binomial family taken to be 1)

Null deviance: 633.30 on 2188 degrees of freedom

Residual deviance: 600.84 on 2186 degrees of freedom

AIC: 606.84

Number of Fisher Scoring iterations: 7

**Table 4.5.** Number of “Central Argentina” LLCS events and their mean maximum area and duration across SALLJ connection categories.

<b>Number of trajectory levels with SALLJ connection (out of 3)</b>	<b>0</b>	<b>1</b>	<b>2</b>	<b>3</b>
Number of LLCS events	146 (42%)	41 (12%)	86 (25%)	72 (21%)
Mean LLCS maximum area (km <sup>2</sup> )	213,181	248,894	410,030	427,678
Mean LLCS duration (hrs.)	11.8	12.6	25.8	31.4

**Table 4.6.** Tukey's Honestly Significant Difference Test results for differences in mean Central Argentina LLCS maximum area and duration between pairs of SALLJ connection categories.

SALLJ connection categories	<i>LLCS maximum area</i>		<i>LLCS duration</i>	
	Difference in means (km <sup>2</sup> )	p-value	Difference in means (hrs.)	p-value
1 - 0	35,712	0.68	0.79	0.98
2 - 0	196,849	0.00	14.0	0.00
3 - 0	214,496	0.00	19.6	0.00
2 - 1	161,136	0.00	13.2	0.00
3 - 1	178,784	0.00	18.8	0.00
3 - 2	17,647	0.93	5.67	0.02

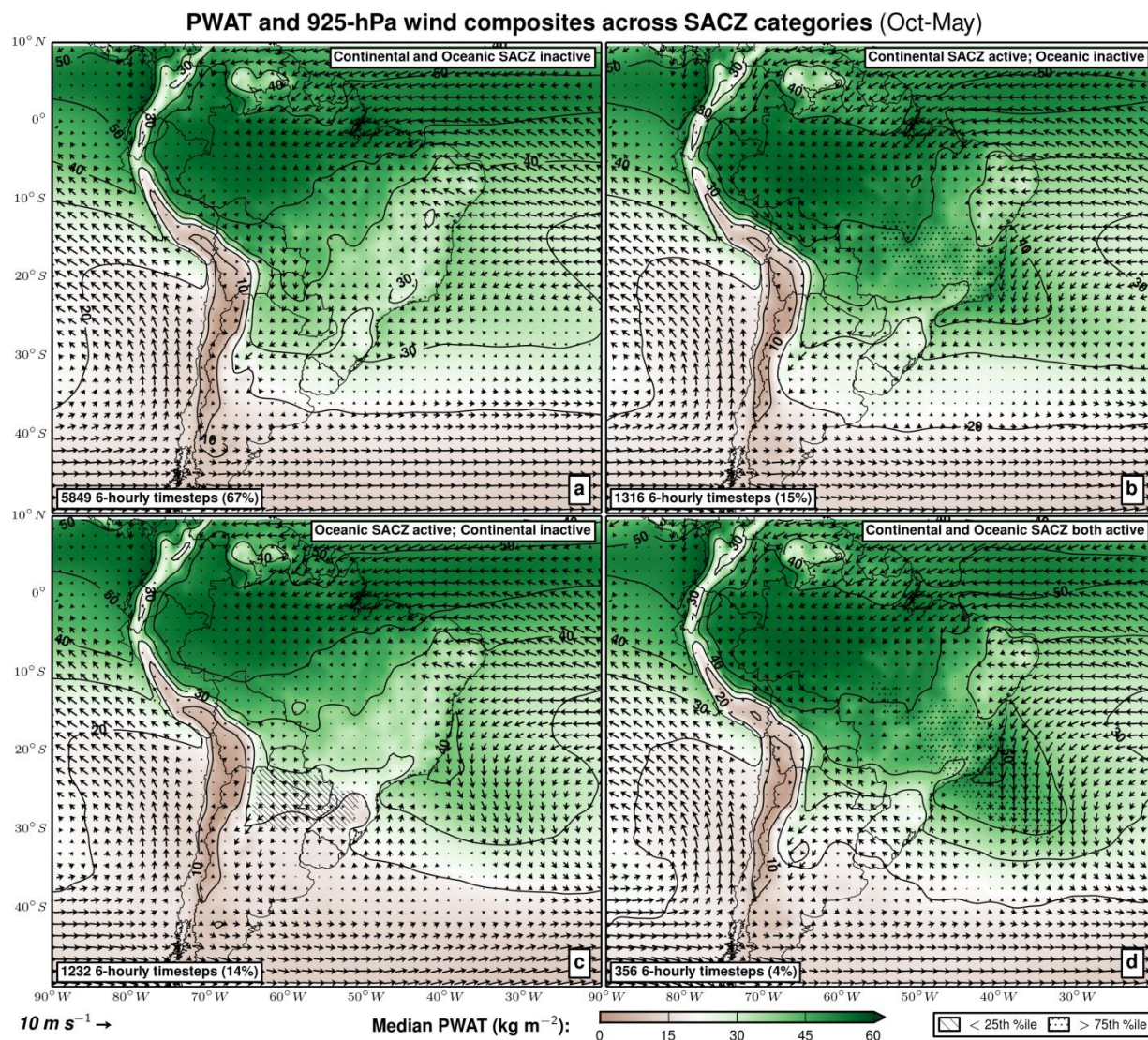


**Fig. 4.1.** Median precipitable water (fill;  $\text{kg m}^{-2}$ ) and 925-hPa wind (arrows;  $\text{m s}^{-1}$ ) for subsets of SACZ activity: (a) continental and oceanic SACZ both inactive, (b) continental SACZ active only, (c) oceanic SACZ active only, (d) continental and oceanic SACZ both active. Dotted areas indicate regions with precipitable water greater than the 75<sup>th</sup> climatological percentile and diagonal lines indicate regions with precipitable water less than the 25<sup>th</sup> climatological percentile.

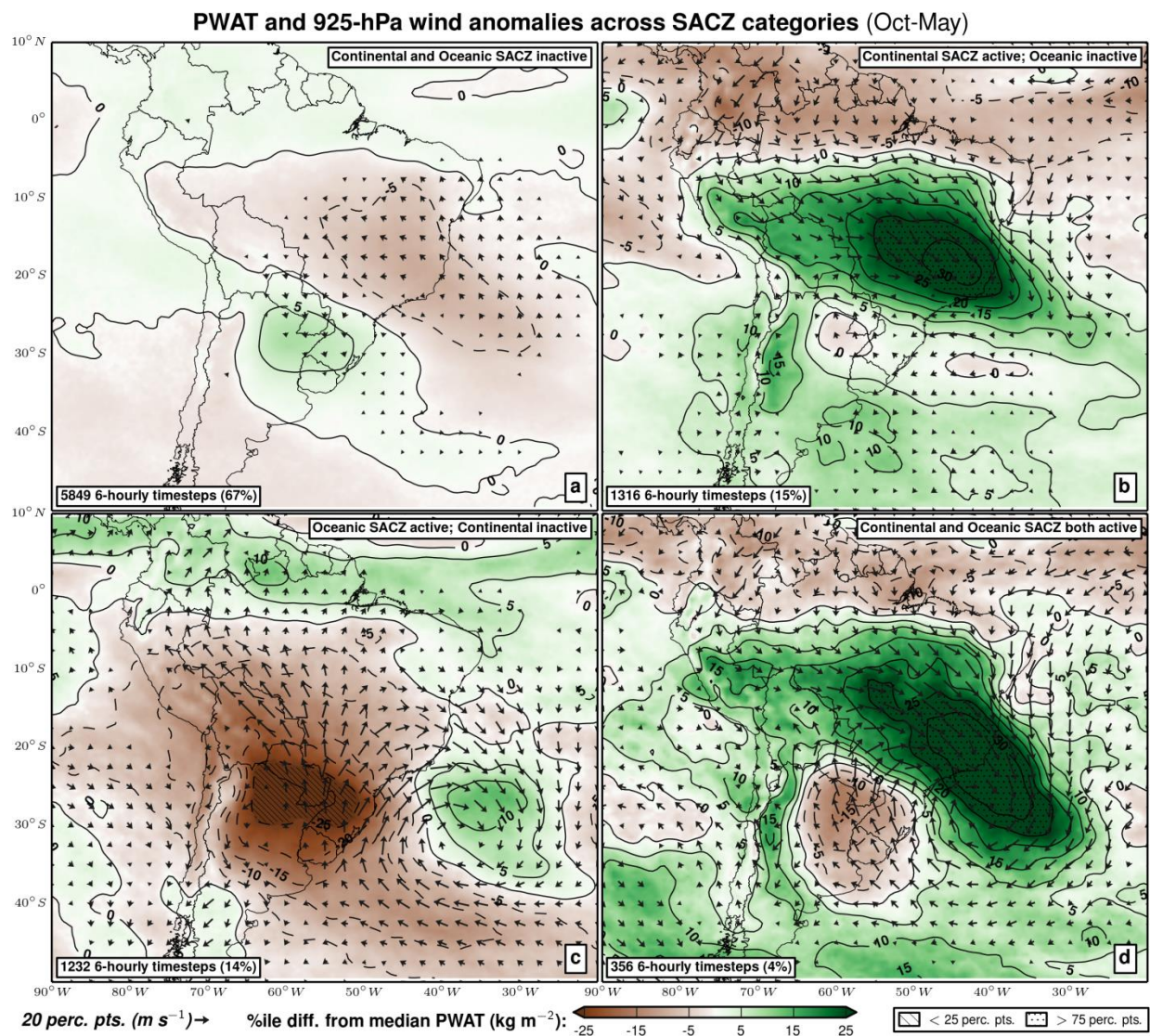


**Fig. 4.2.** Composite PWAT and 925-hPa wind anomalies (percentile departure from Oct–May 1998–2007 climatological median) across subsets of SACZ activity described in Fig. 4.1. Dotted areas indicate regions with precipitable water greater than the 75<sup>th</sup> climatological percentile and diagonal lines indicate regions with precipitable water less than the 25<sup>th</sup> climatological percentile.

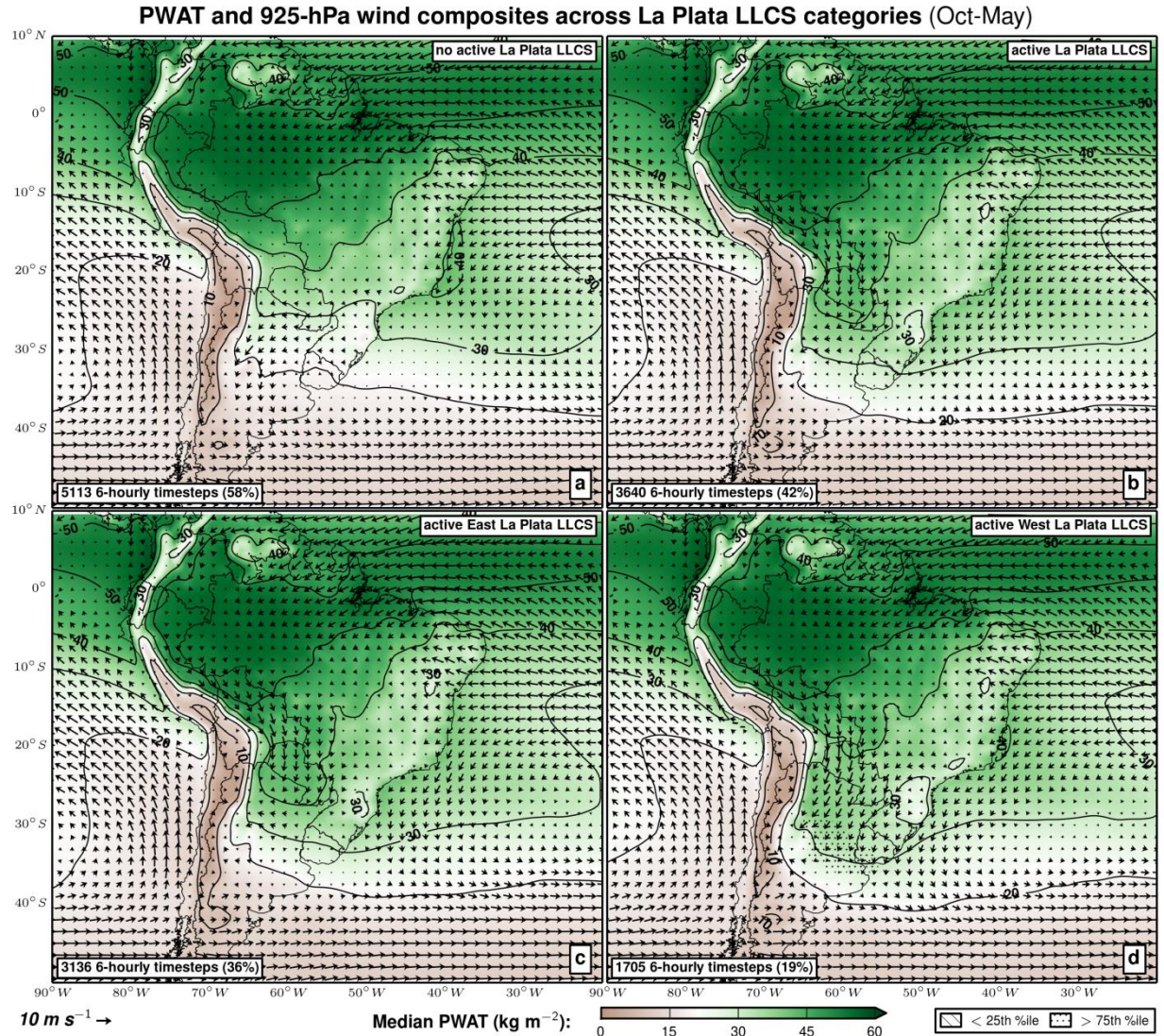


**Fig. 4.3.** As in Fig. 4.1 but for subsets of La Plata domain LLCS activity: (a) no active LLCS in La Plata domain, (b) active LLCS anywhere in domain, (c) active LLCS in East La Plata domain only, (d) active LLCS in West La Plata domain only.

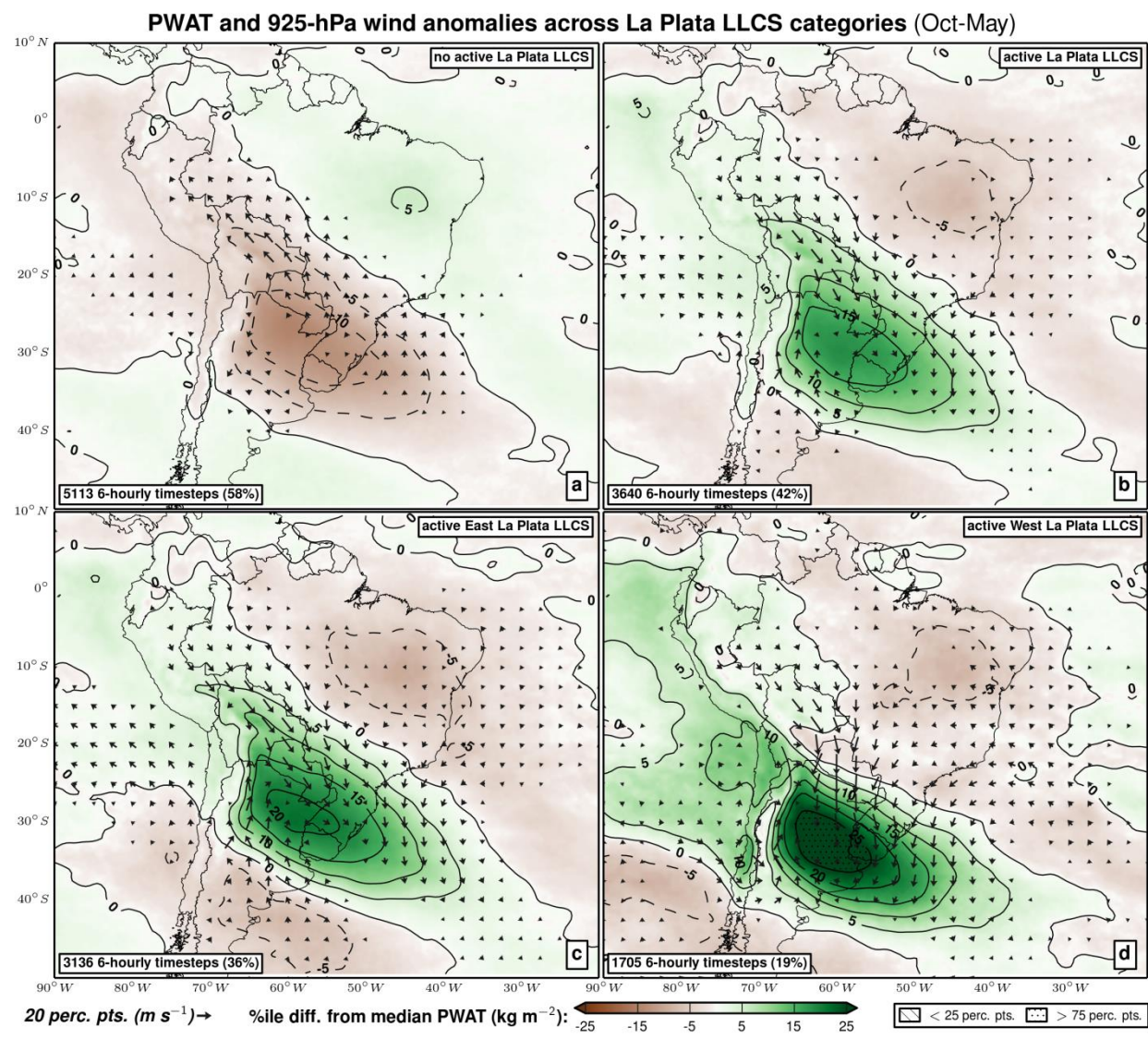


**Fig. 4.4.** As in Fig. 4.2 but for subsets of La Plata domain LLCS activity described in Fig. 4.3.

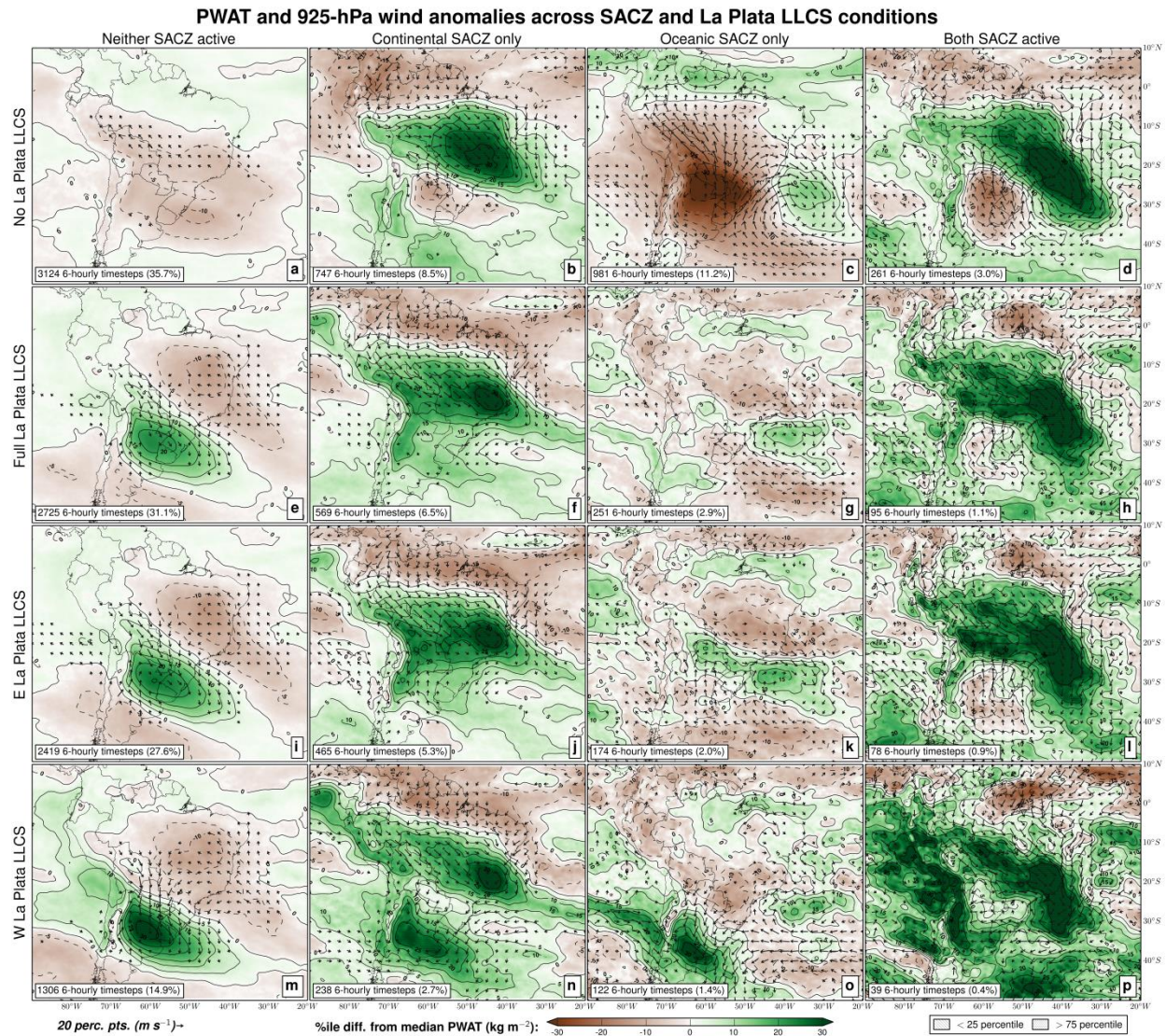


**Fig. 4.5.** Composite PWAT and 925-hPa wind anomalies across subsets of SACZ (columns) and La Plata LLCS (rows) activity. Dotted areas indicate regions with precipitable water greater than the 75<sup>th</sup> climatological percentile and diagonal lines indicate regions with precipitable water less than the 25<sup>th</sup> climatological percentile.

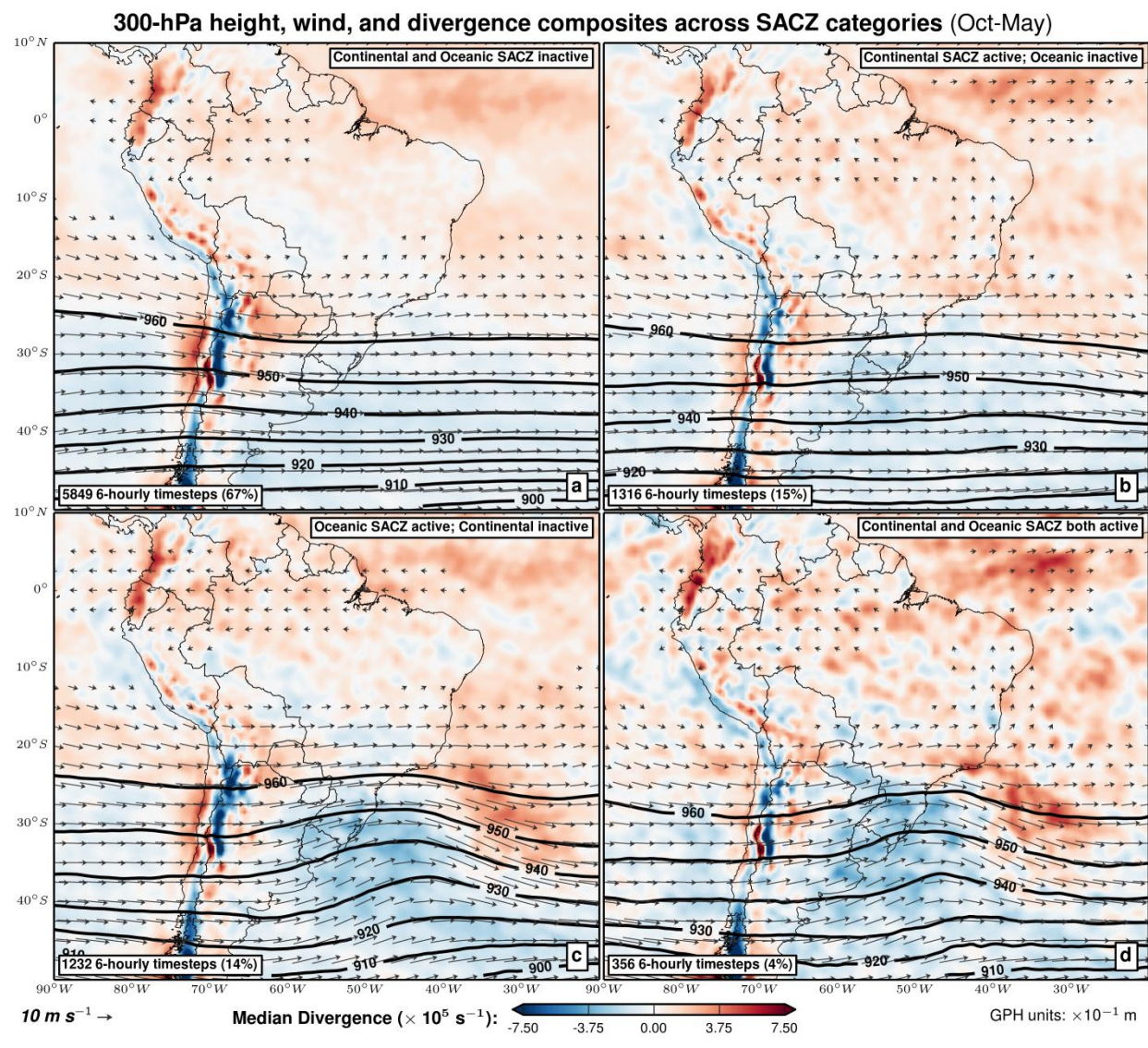


**Fig. 4.6.** Median 300-hPa geopotential height (contour lines;  $\times 10^{-1} \text{ m}$ ), wind (arrows;  $\text{m s}^{-1}$ ), and divergence (fill;  $\times 10^5 \text{ s}^{-1}$ ) for subsets of SACZ activity described in Fig. 4.1.

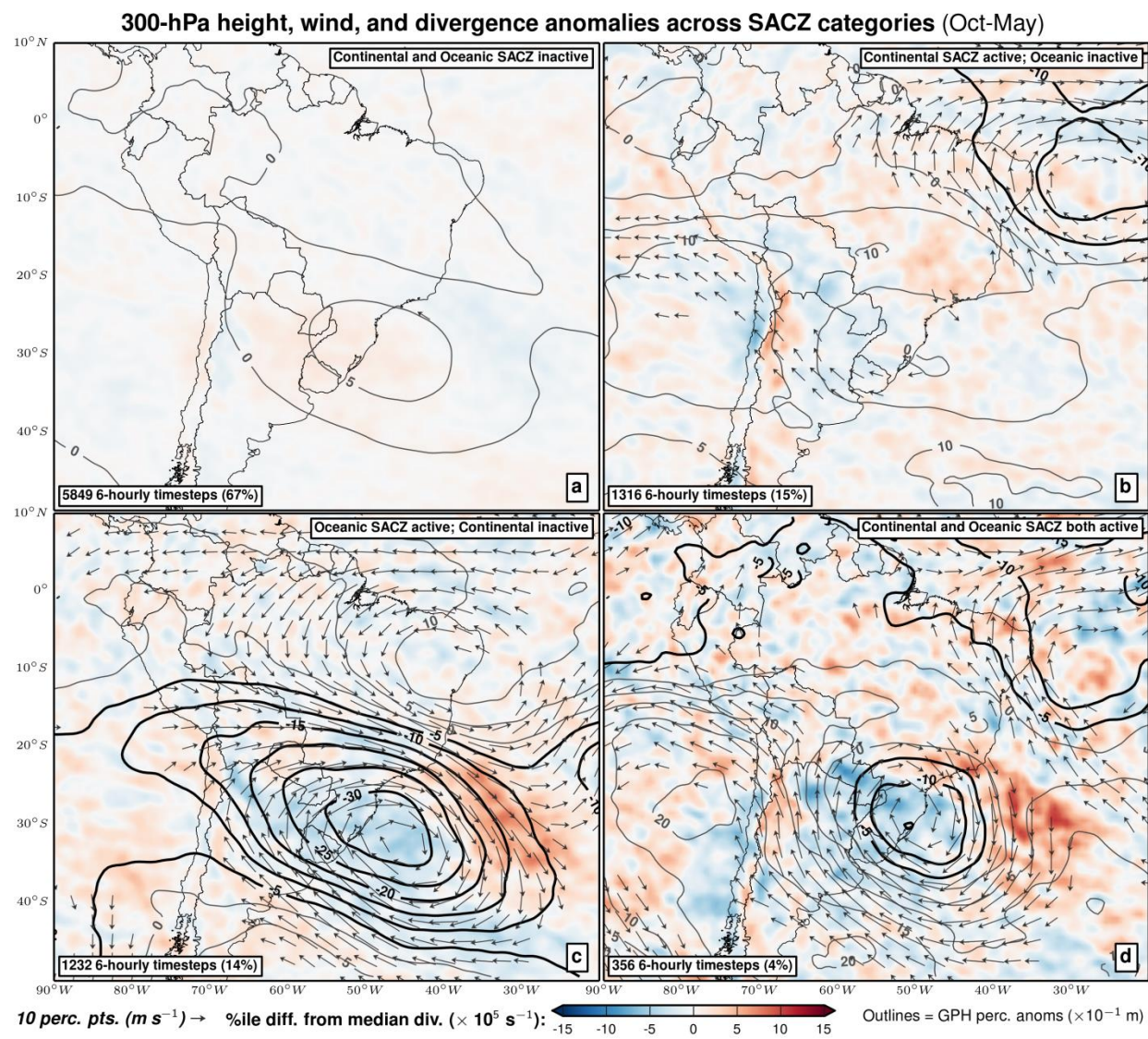


**Fig. 4.7.** Composite anomalies of 300-hPa height (contour lines), wind (arrows), and divergence (fill) across subsets of SACZ activity described in Fig. 4.1. Positive height anomalies are drawn with thin gray lines and negative height anomalies with thick black lines.

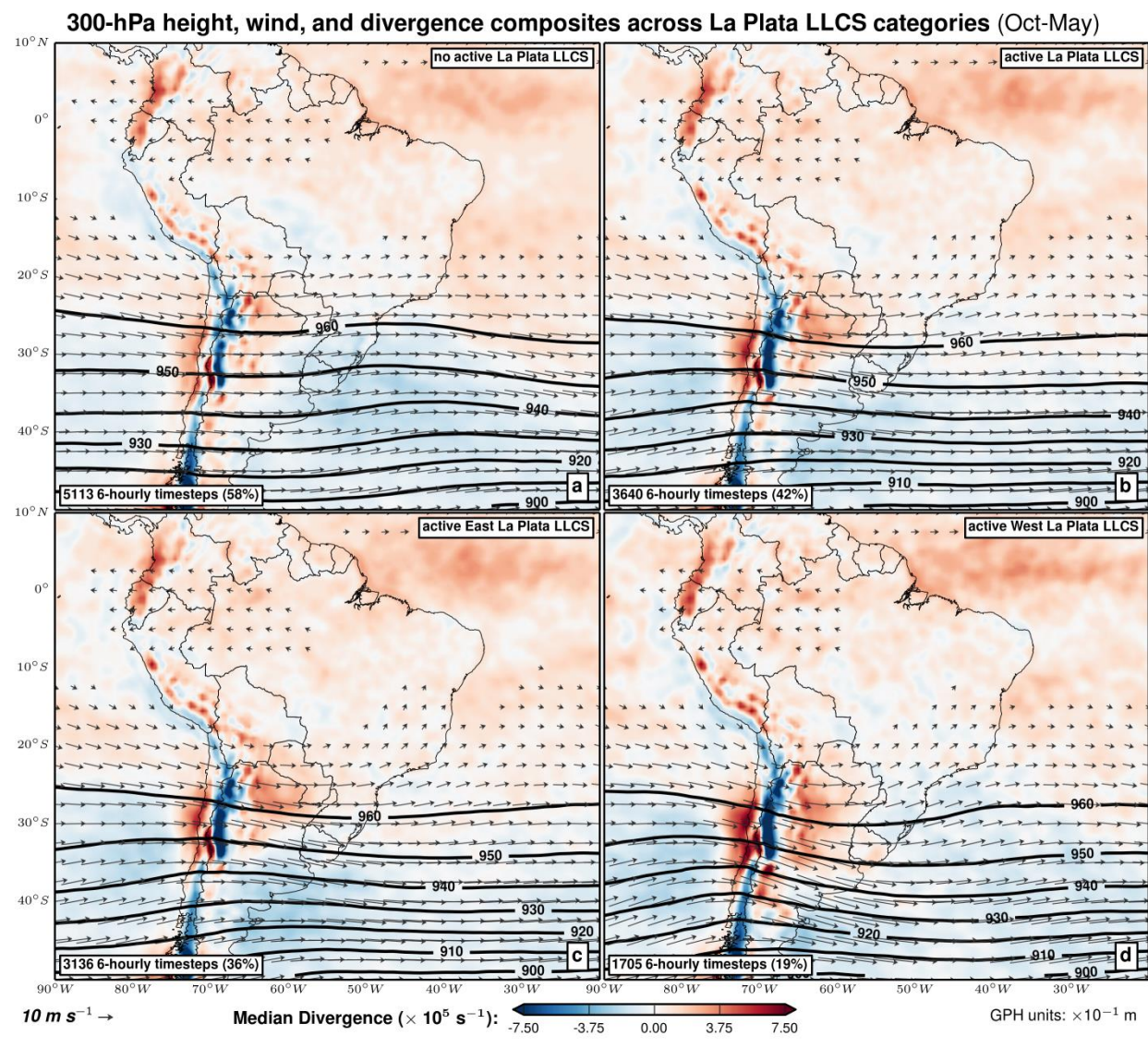


**Fig. 4.8.** As in Fig. 4.6 but for subsets of LLCS activity described in Fig. 4.3.

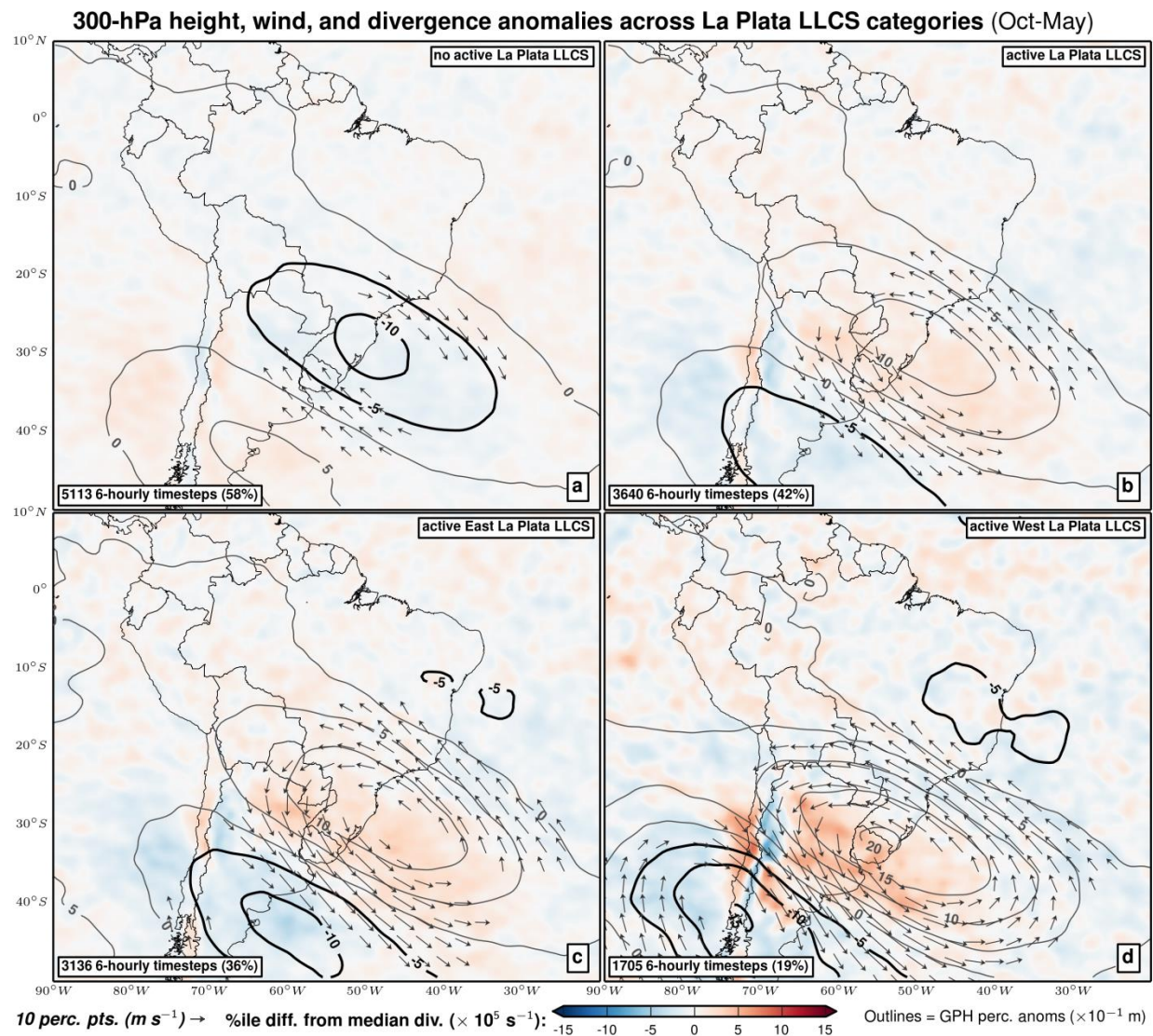


**Fig. 4.9.** As in Fig. 4.7 but for subsets of LLCS activity described in Fig. 4.3.

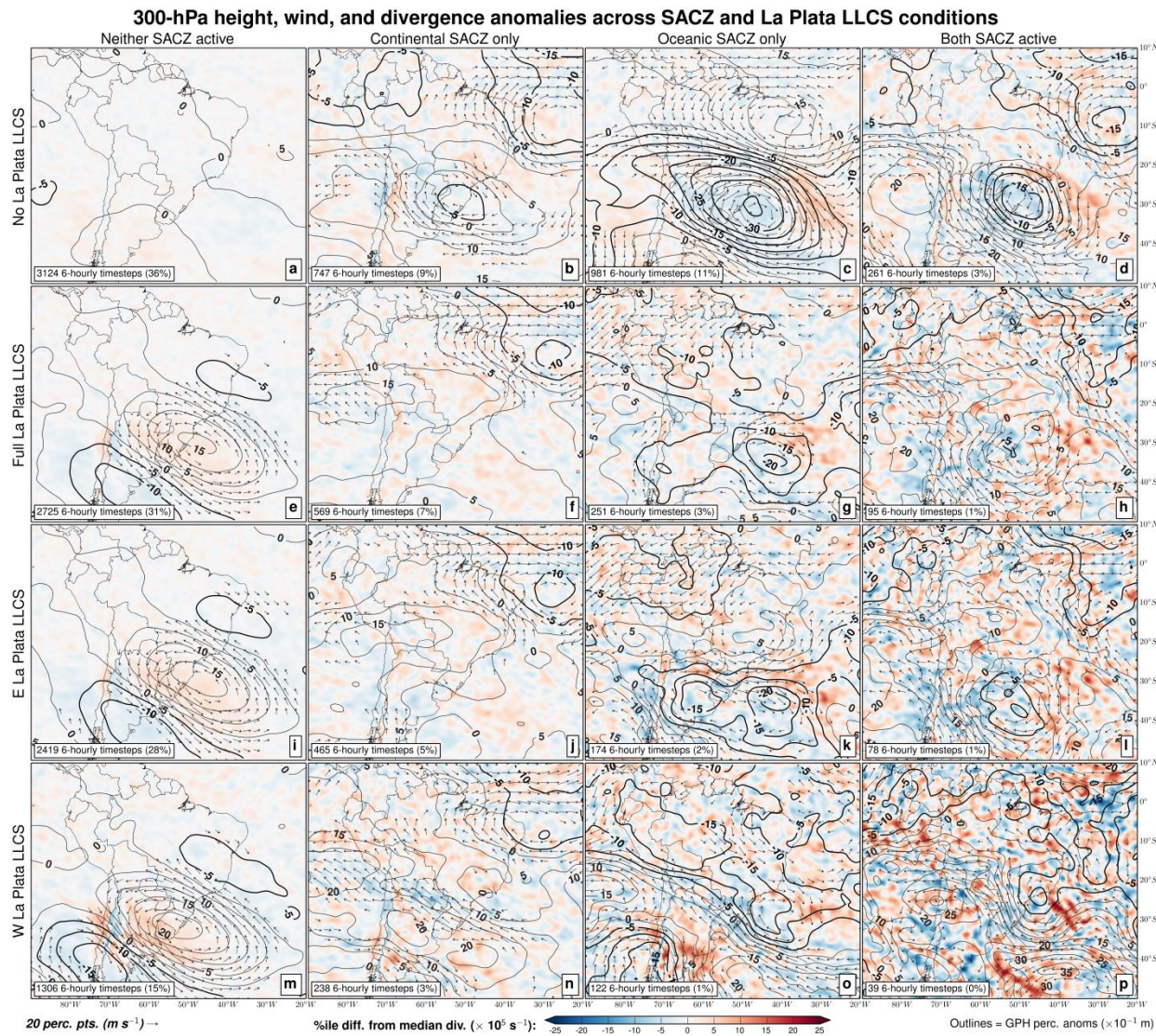


**Fig. 4.10.** Composite 300-hPa height, wind, and divergence anomalies across subsets of SACZ (columns) and La Plata LLCS (rows) activity. Positive height anomalies are drawn with thin gray lines and negative height anomalies with thick black lines.

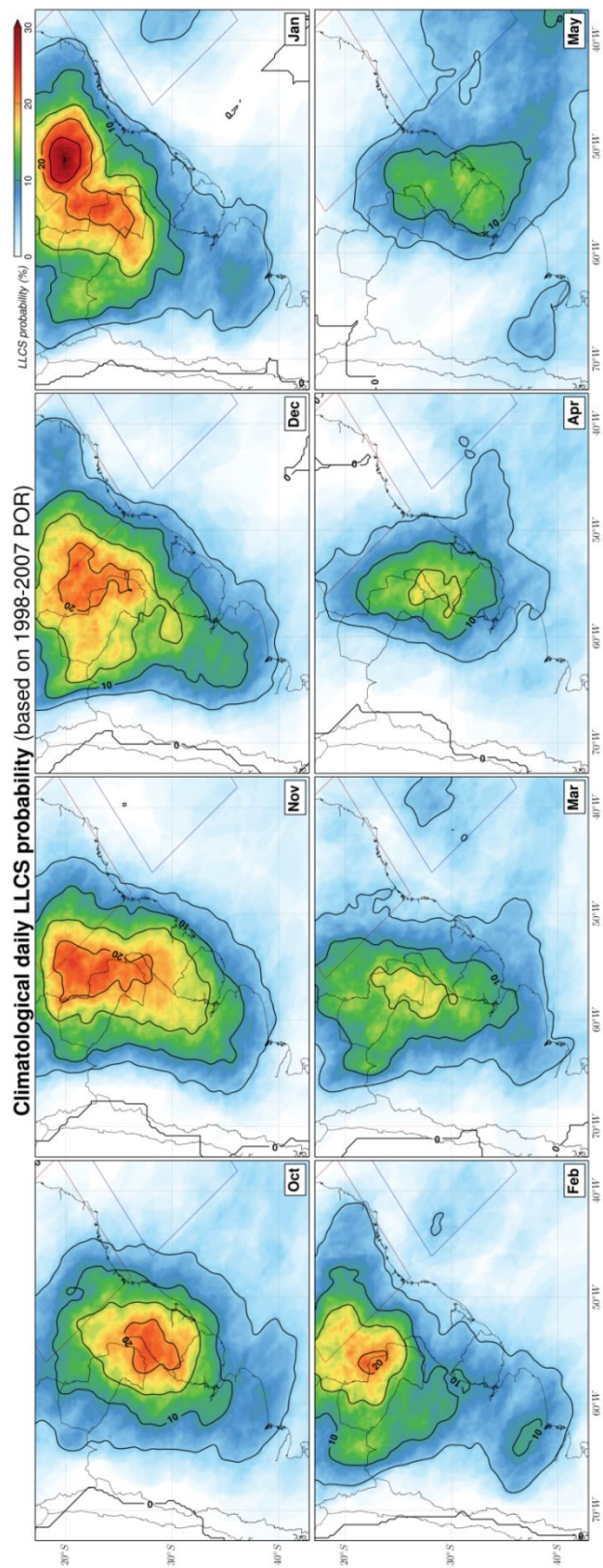


**Fig. 4.11.**  $0.25^\circ \times 0.25^\circ$  gridded probability of LLCS occurrence for each month during the Oct–May austral warm season (based on 1998–2007 study period).

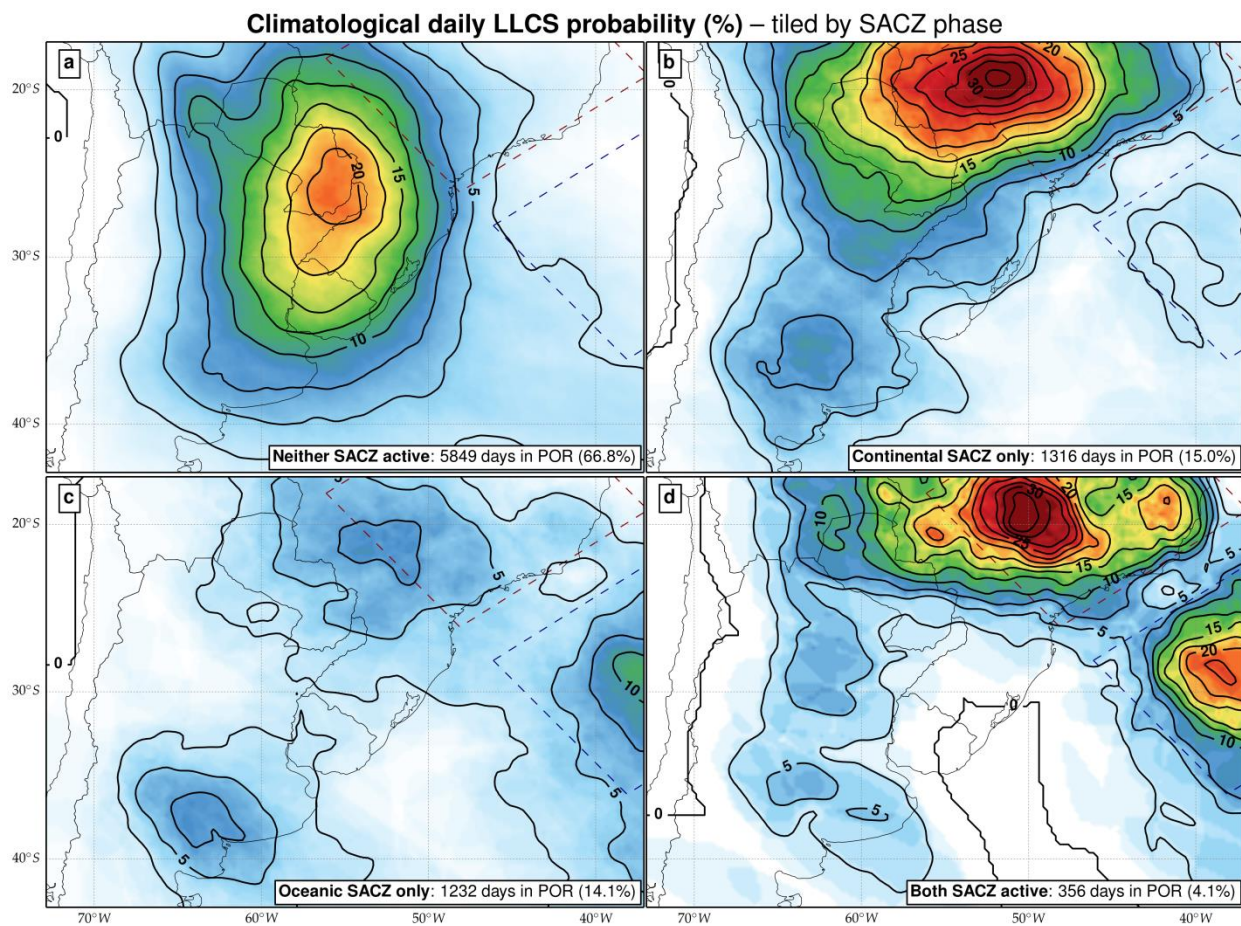


**Fig. 4.12.**  $0.25^\circ \times 0.25^\circ$  gridded probability of LLCS occurrence across SACZ phases: (a) neither SACZ active, (b) continental active only, (c) oceanic active only, and (d) both active.

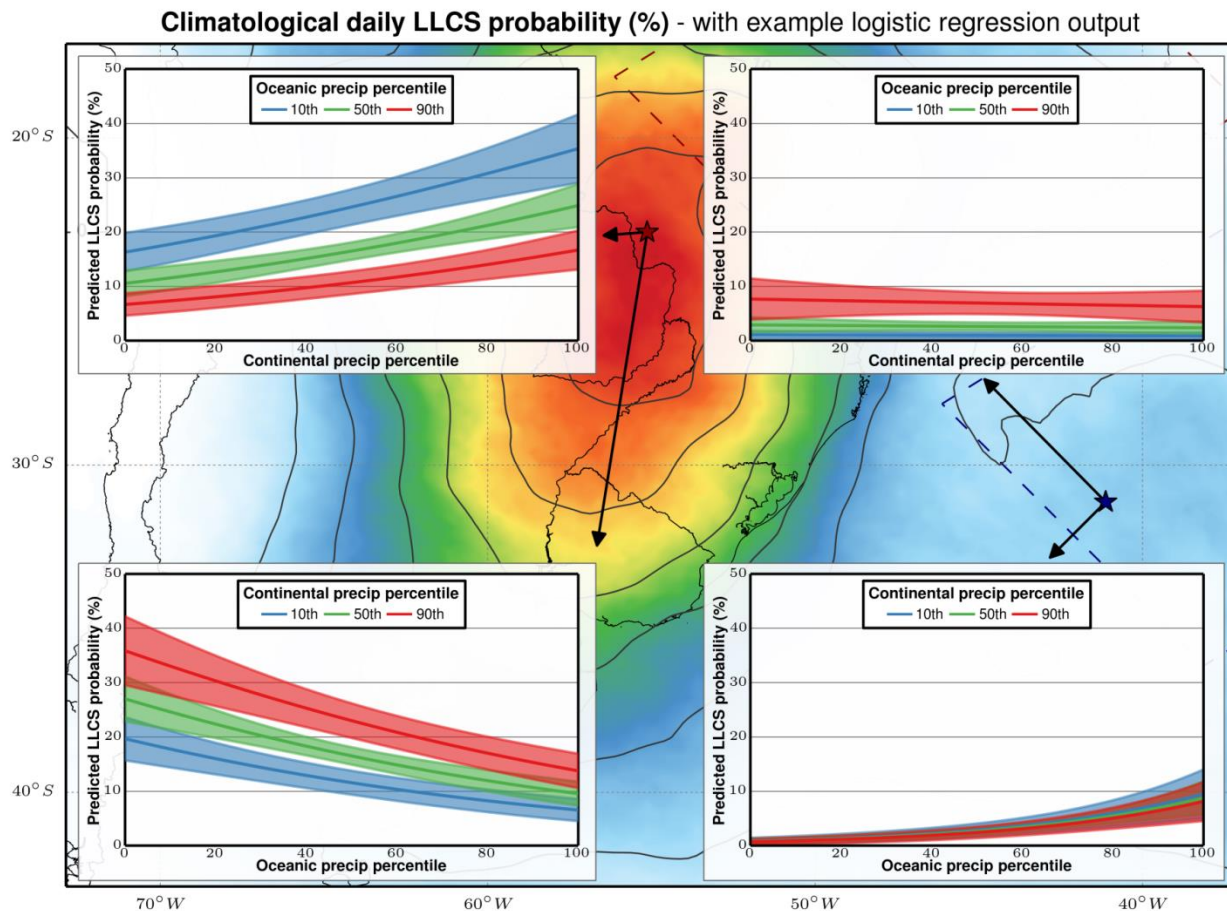


**Fig. 4.13.** Logistic regression predicted daily LLCS probability for “continental” representative point (left side plots) and “oceanic” representative point (right side plots) across all percentiles of oceanic SACZ precipitation (top plots) and continental SACZ precipitation (bottom plots). Separate curves on each top row (bottom row) plot represent predicted LLCS probability with oceanic (continental) precipitation held at its 10<sup>th</sup>, 50<sup>th</sup>, and 90<sup>th</sup> percentiles, and shading around each line indicates standard error of predicted probability values. Shading of map background is austral warm season (Oct–May) 1998–2007 climatological LLCS probability.

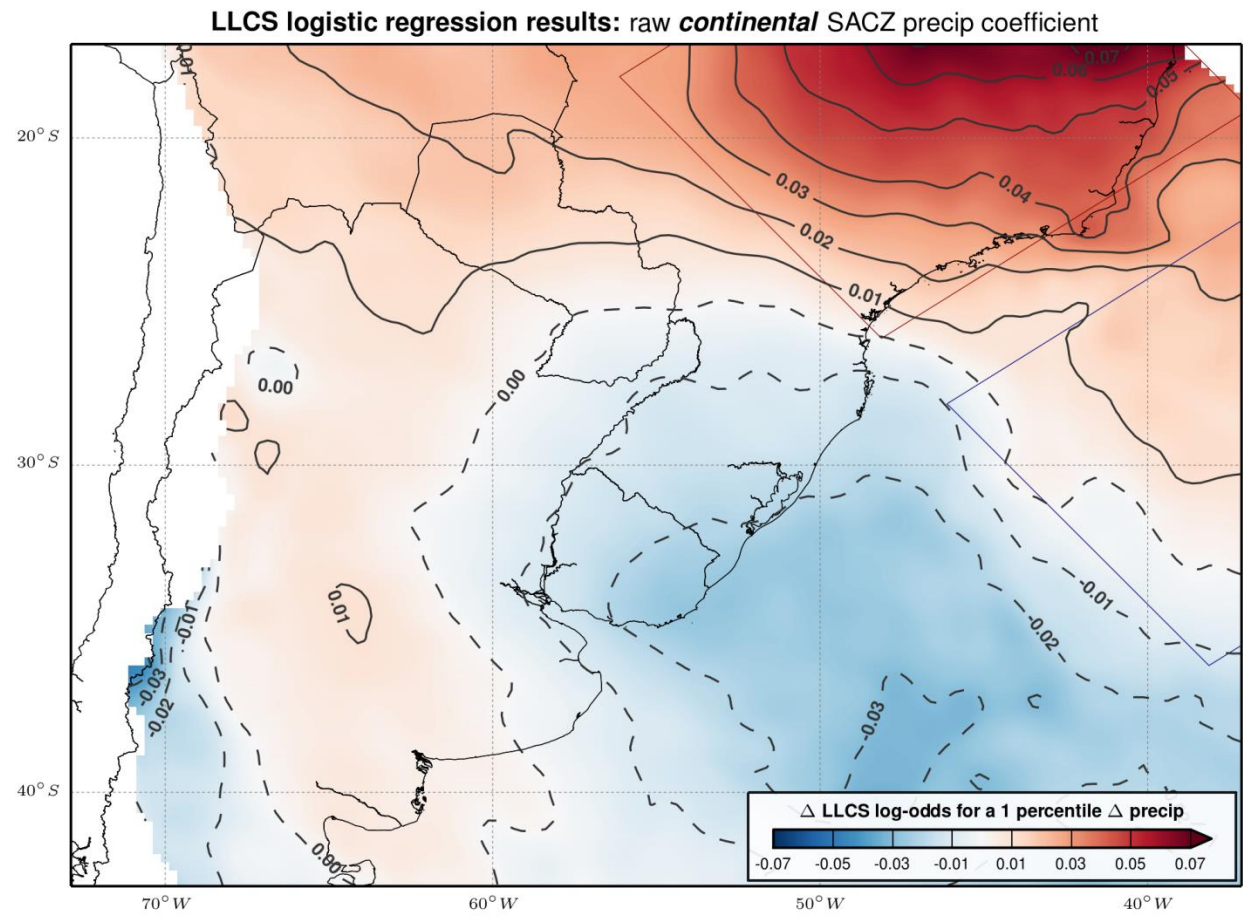


**Fig. 4.14.**  $0.25^\circ \times 0.25^\circ$  gridded logistic regression coefficient for continental SACZ precipitation. Values represent the change in log-odds of LLCS occurrence at a given point for a one percentile increase in continental SACZ precipitation.

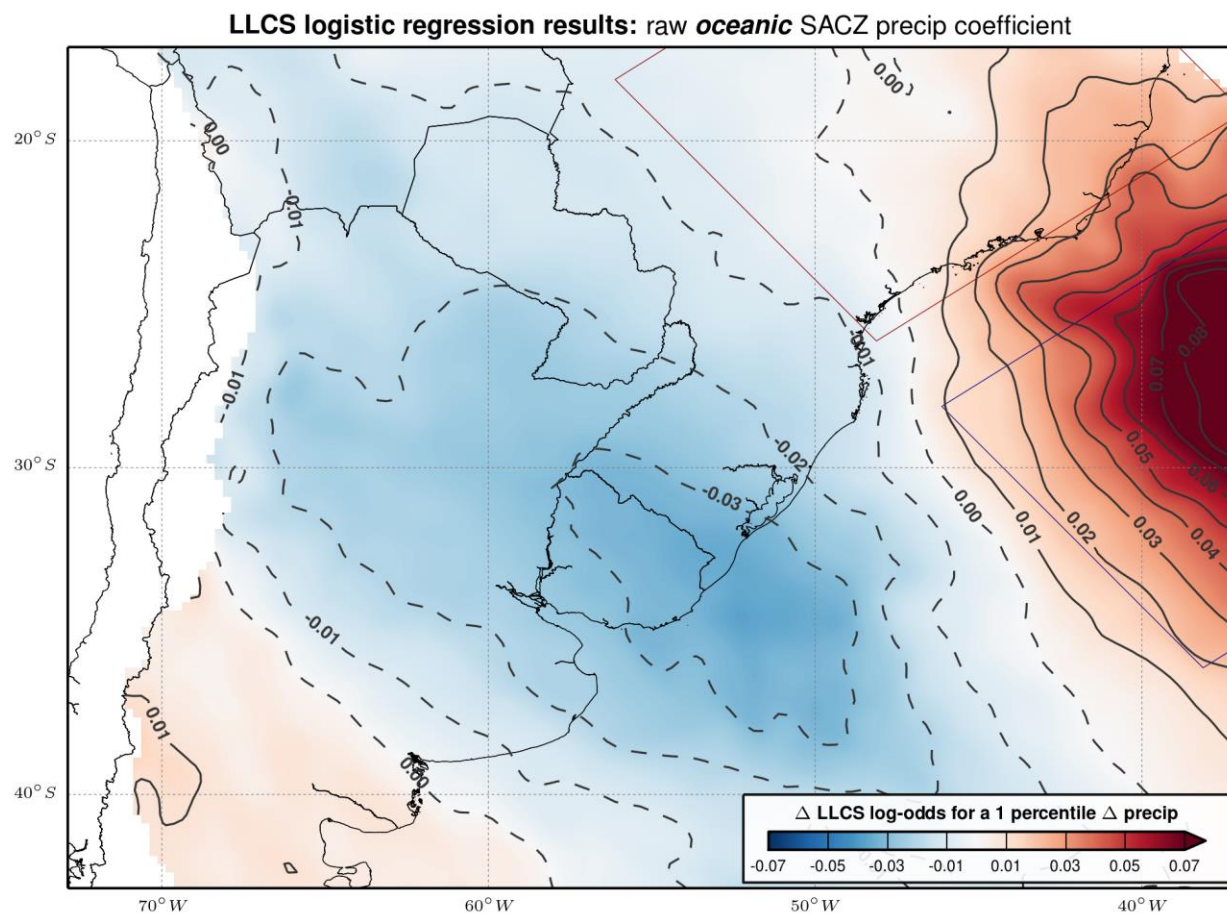


**Fig. 4.15.** As in Fig. 4.14 except for oceanic SACZ precipitation logistic regression coefficient.

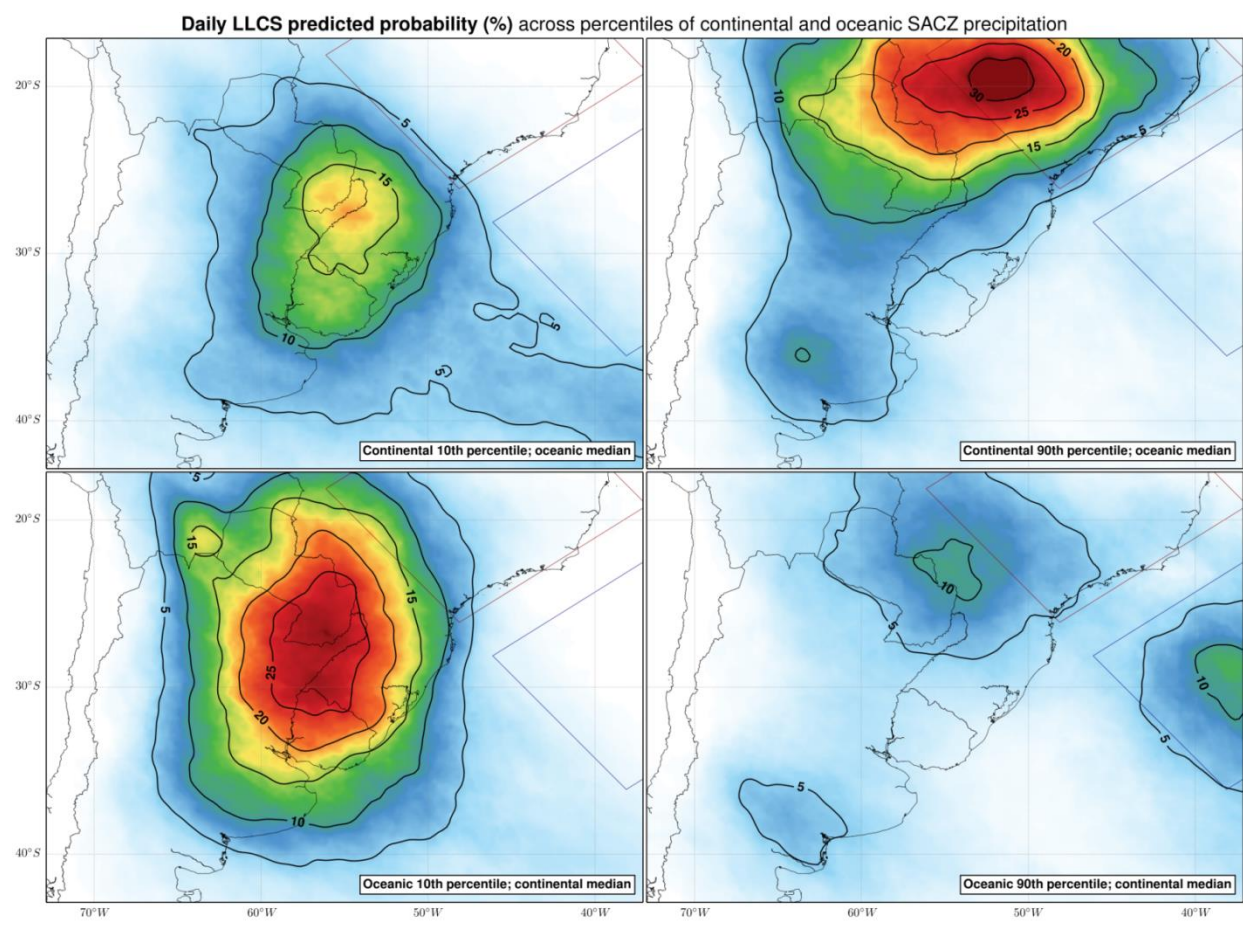


**Fig. 4.16.** Logistic regression predicted probability of LLCS occurrence across combinations of representative “low” and “high” continental (top row) and oceanic (bottom row) SACZ precipitation percentiles (10<sup>th</sup> and 90<sup>th</sup>) with precipitation over the other domain held constant at its median.

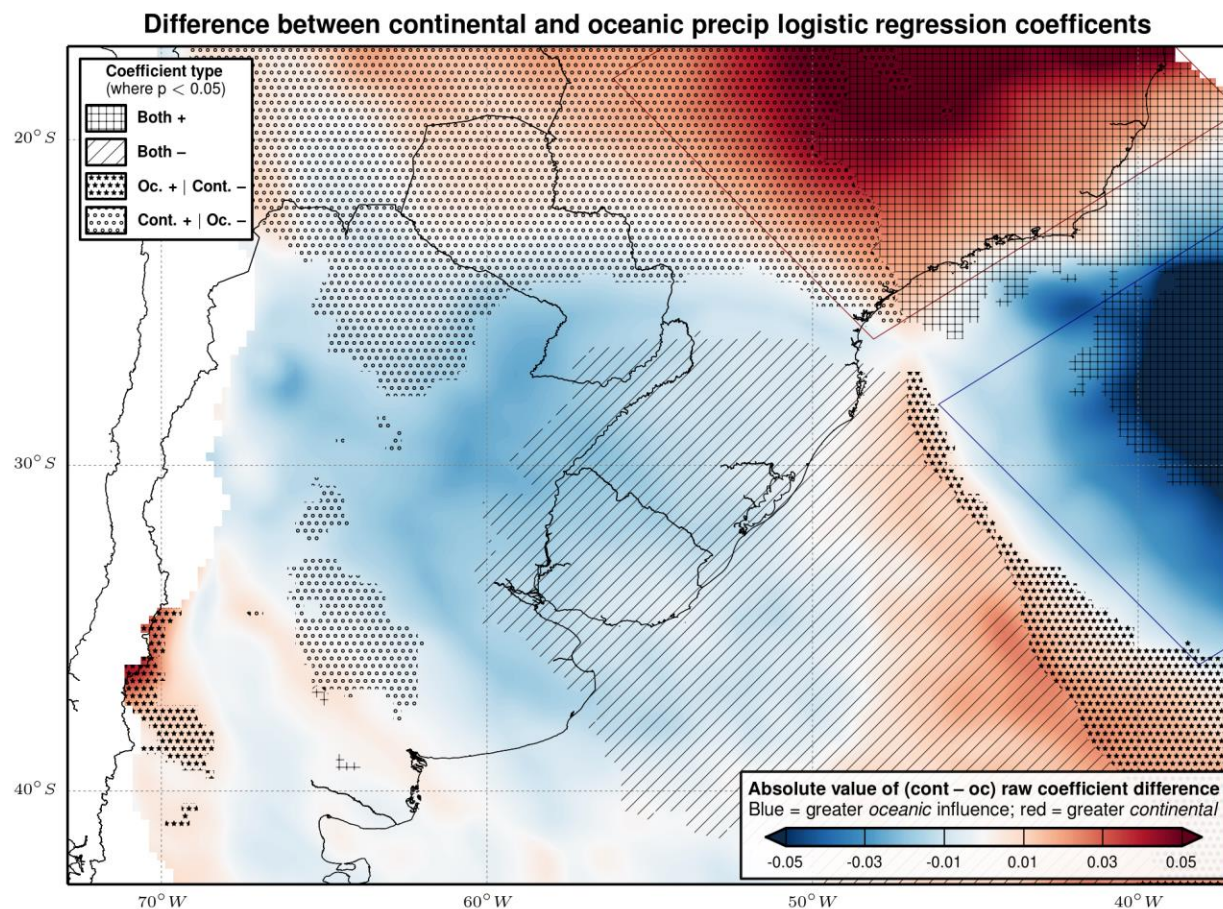


**Fig. 4.17.** Difference between the respective absolute values of the continental and oceanic SACZ precipitation coefficients. Hatching indicates the type of SACZ influence e.g. “Oc. + | Cont. -” means an increase in oceanic SACZ domain precipitation results in increased LLCS probability and an increase in continental SACZ domain precipitation results in decreased LLCS probability. Hatching only drawn where both continental and oceanic SACZ precipitation coefficients are statistically significant ( $p \leq 0.05$ ).

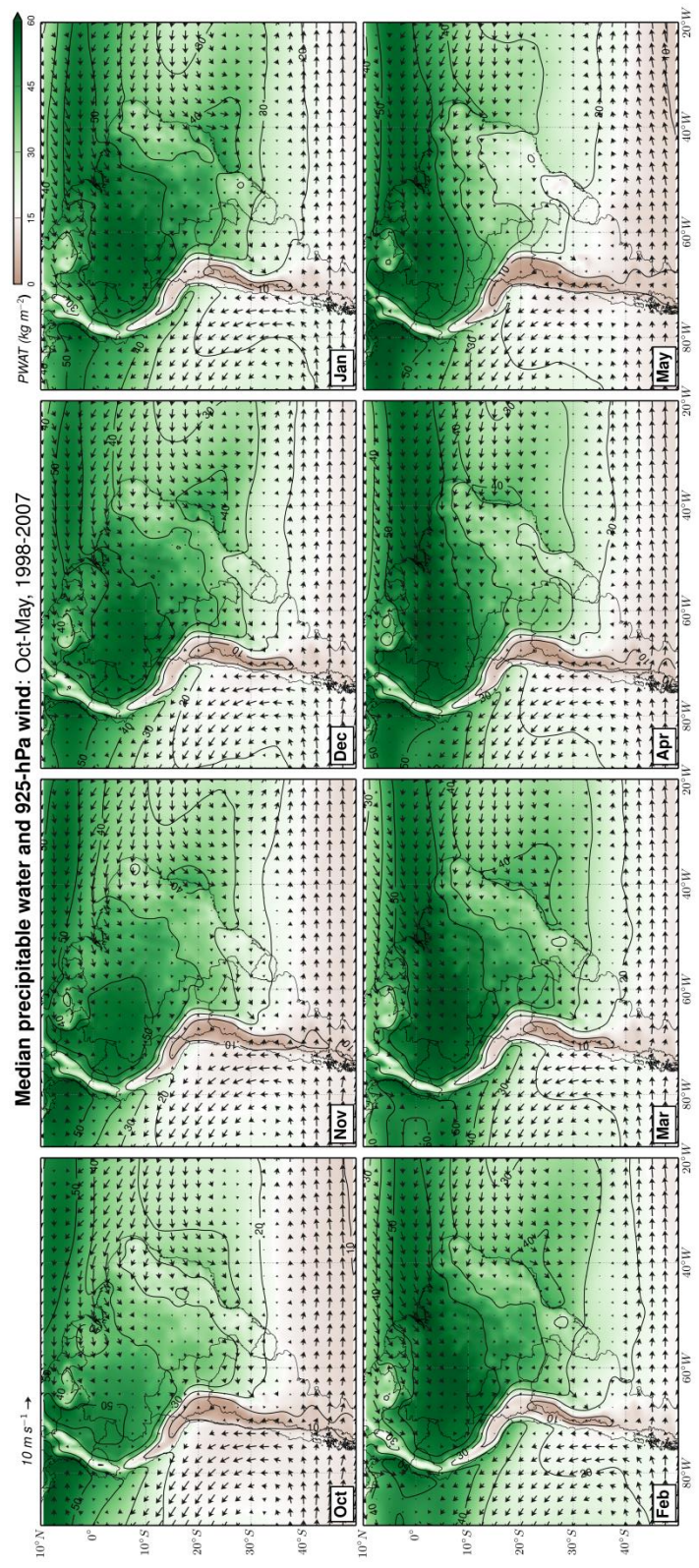


**Fig. 4.18.** Median precipitable water ( $\text{kg m}^{-2}$ ) and 925-hPa wind vectors ( $\text{m s}^{-1}$ ) for each month of the austral warm season (Oct–May) during the 1998–2007 study period.

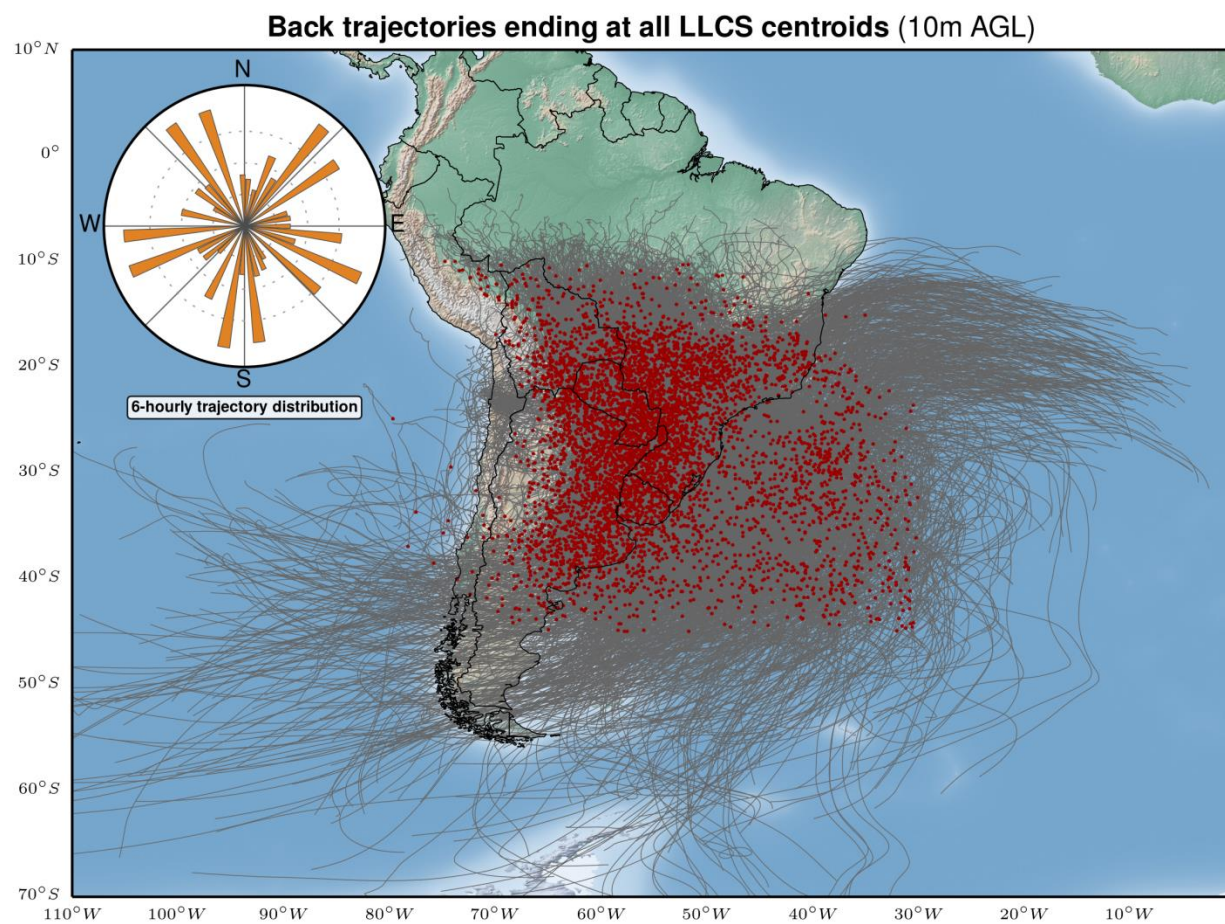


**Fig. 4.19.** Map of HYSPLIT modeled 120-hour parcel back trajectories at 10 meters above ground level for all 6-hourly merged LLCS cloud shields. Also plotted is a polar histogram of the direction from which parcel trajectories flowed.

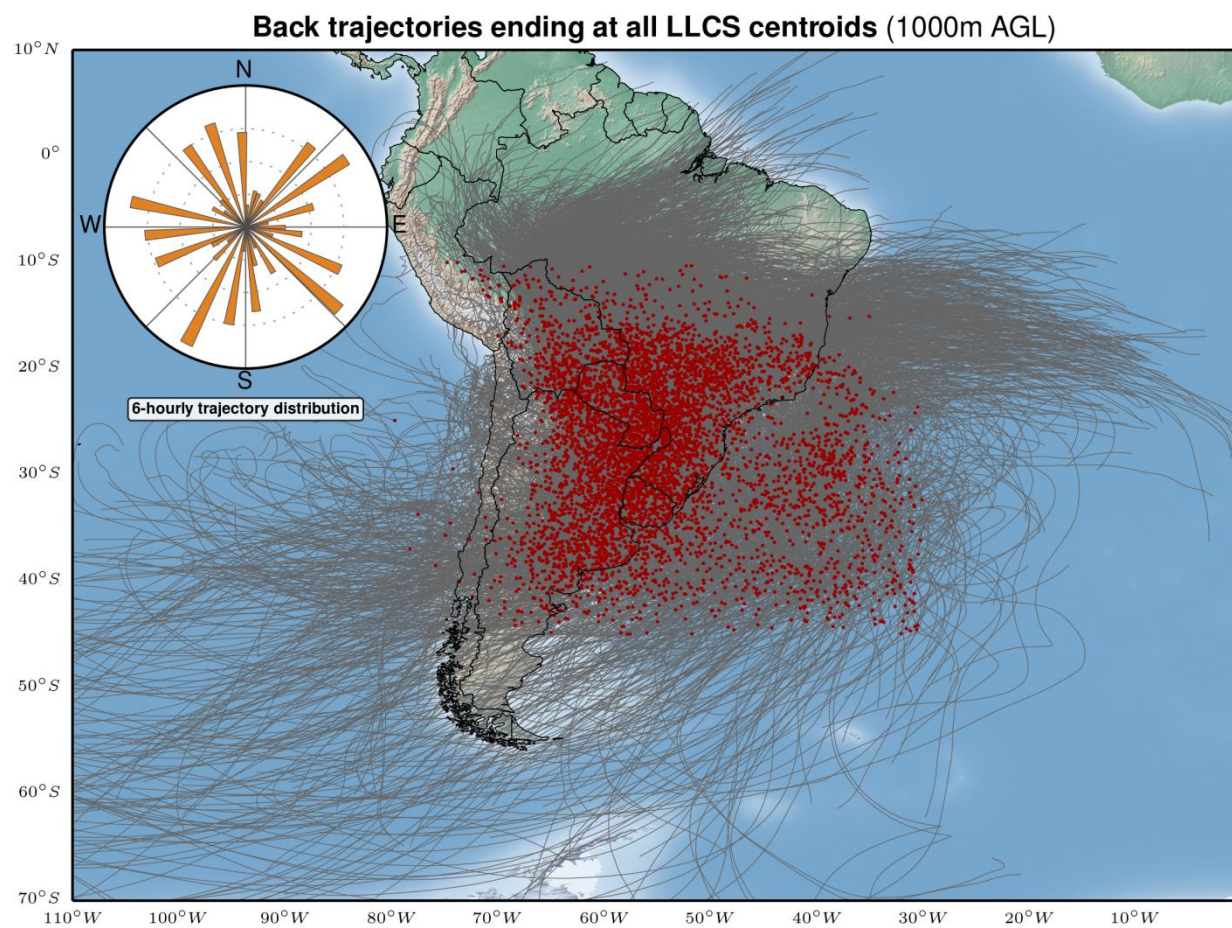


**Fig. 4.20.** As in Fig. 4.19 but for 1000m AGL trajectories.

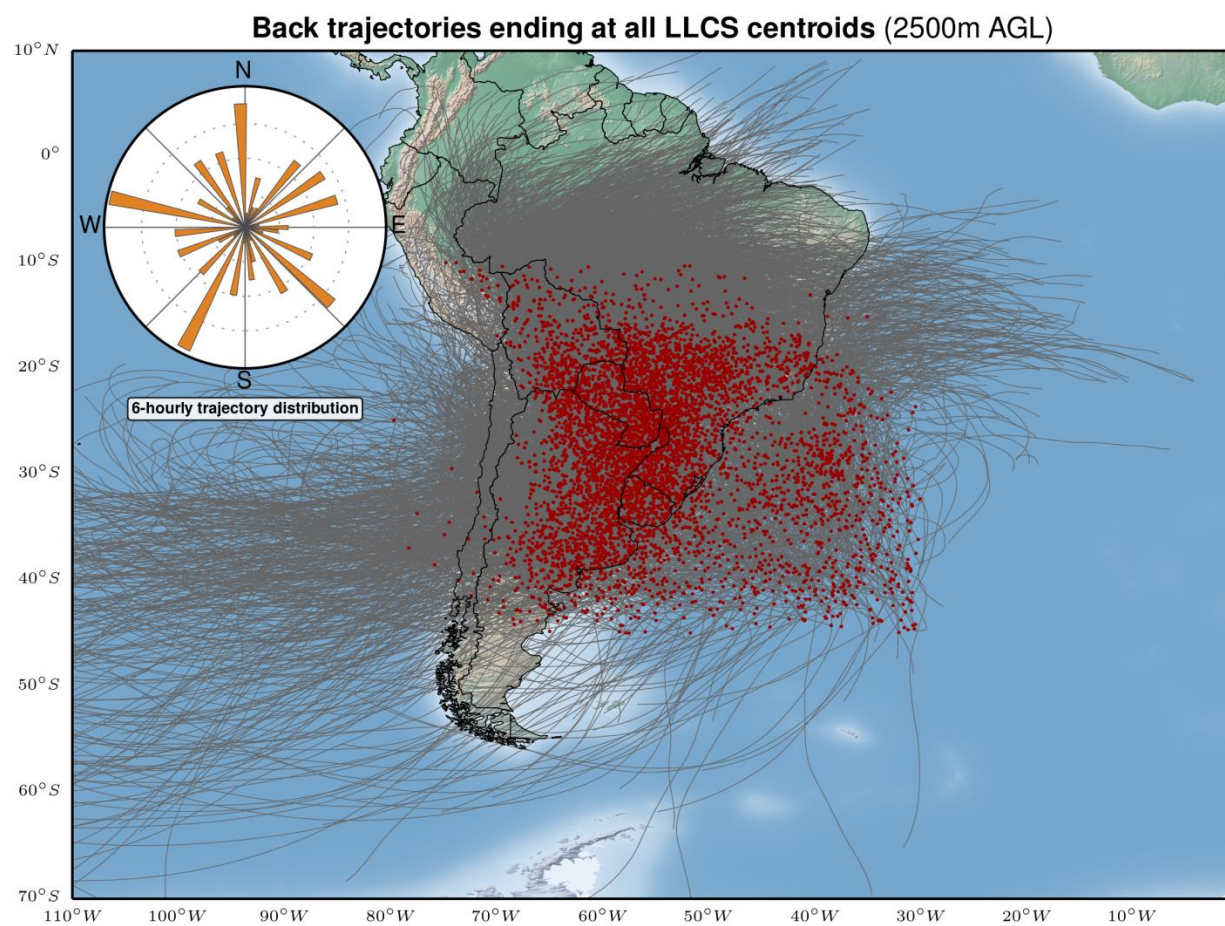


**Fig. 4.21.** As in Figs. 4.19 and 4.20 but for 2500m AGL trajectories.

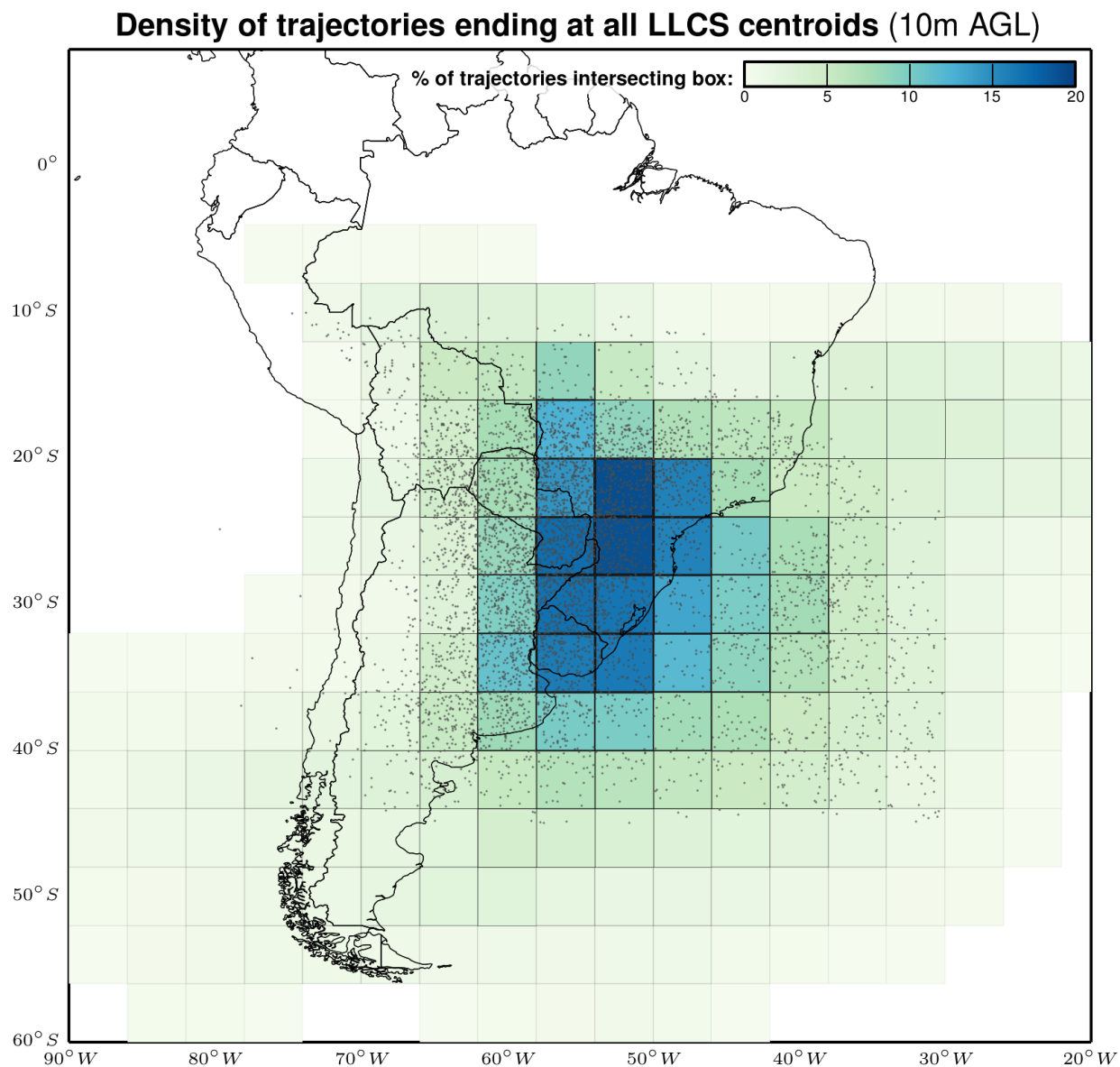


**Fig. 4.22.** Density of all 10m AGL LLCS back trajectories. Density unit is the ratio of the number of LLCS trajectories that intersected a given  $4^\circ \times 4^\circ$  box to the total number of trajectories.

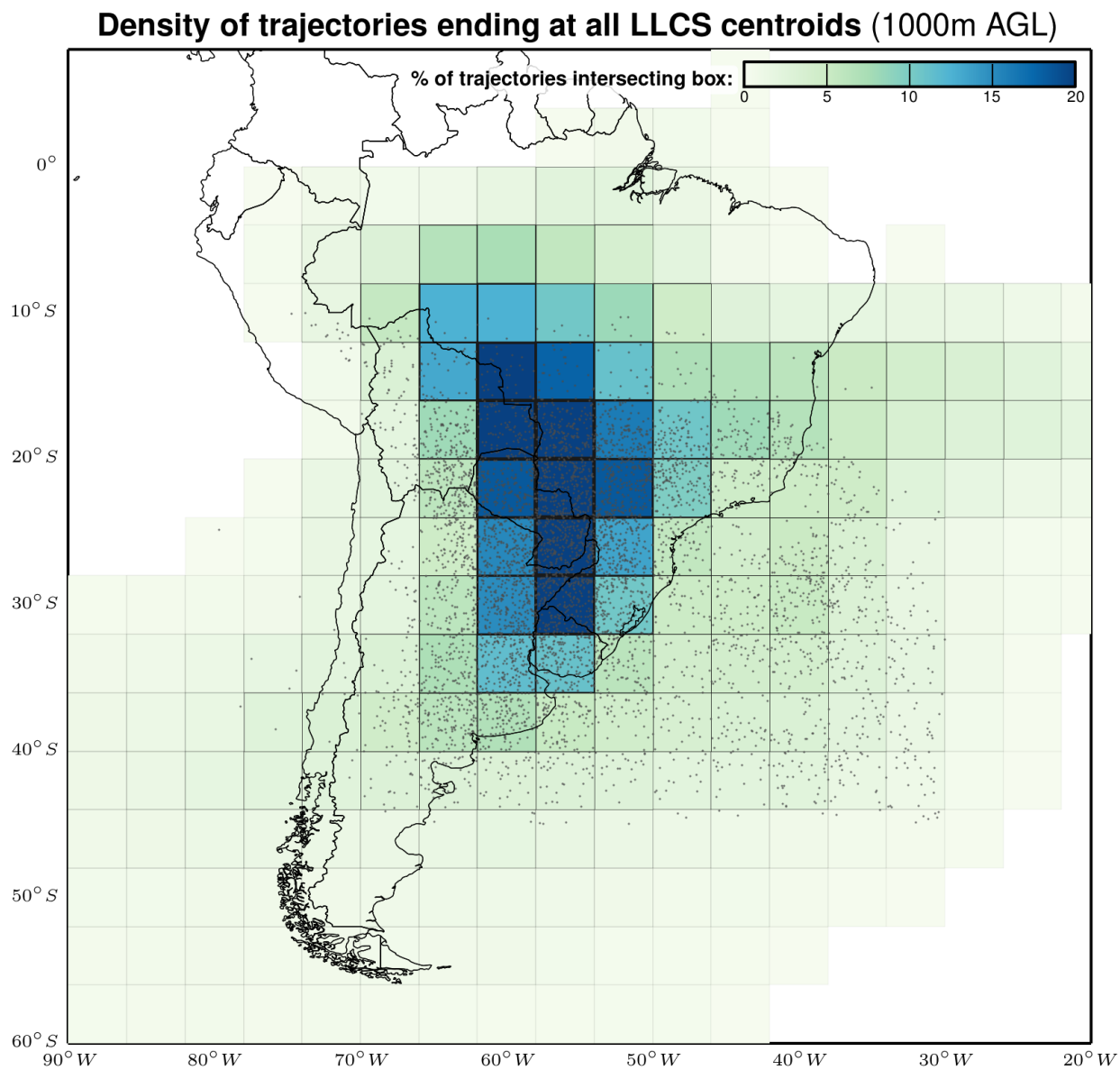


**Fig. 4.23.** As in Fig. 4.22 but for 1000m AGL trajectories.

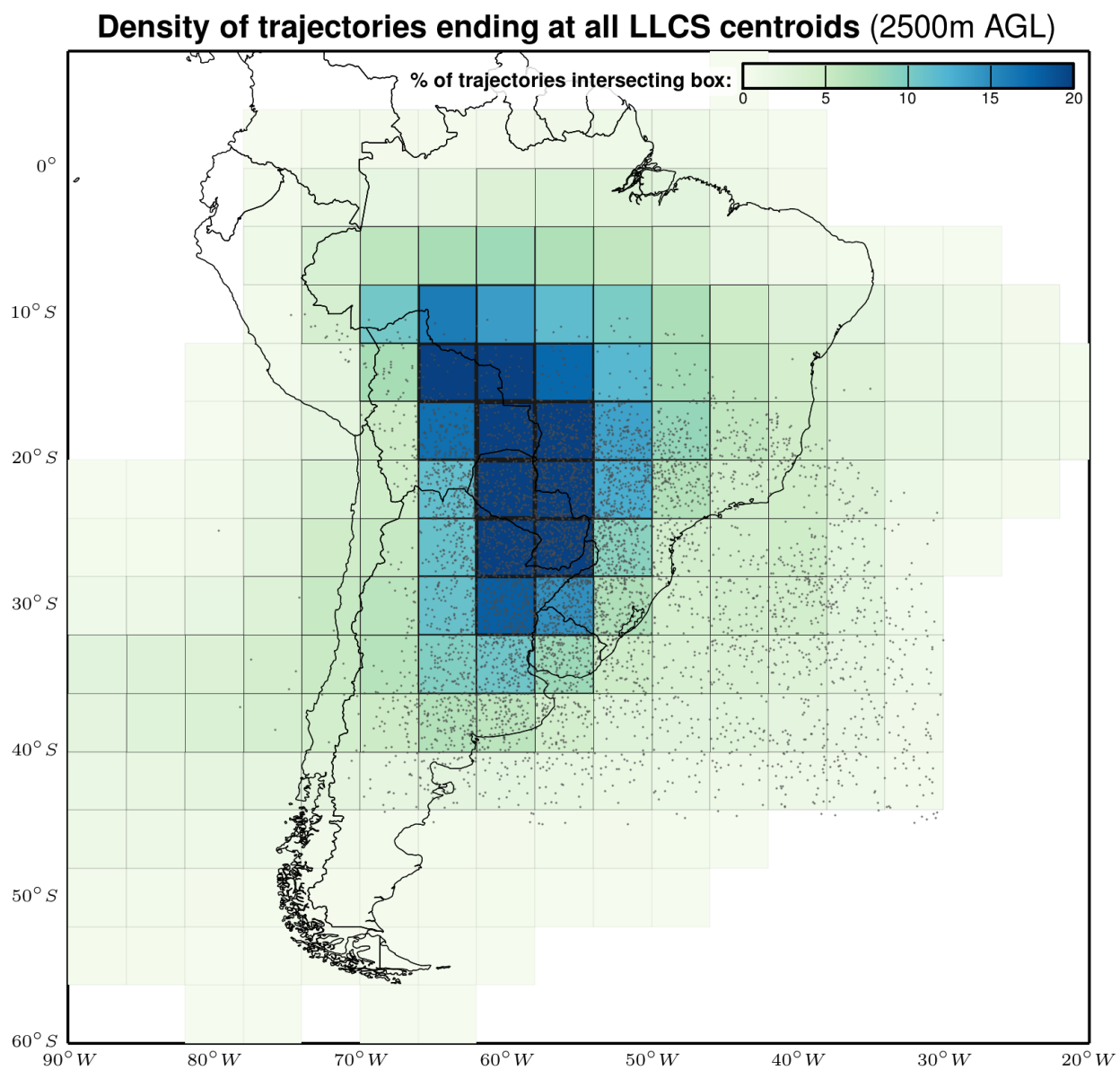


**Fig. 4.24.** As in Fig. 4.23 except for 2500m AGL trajectories.

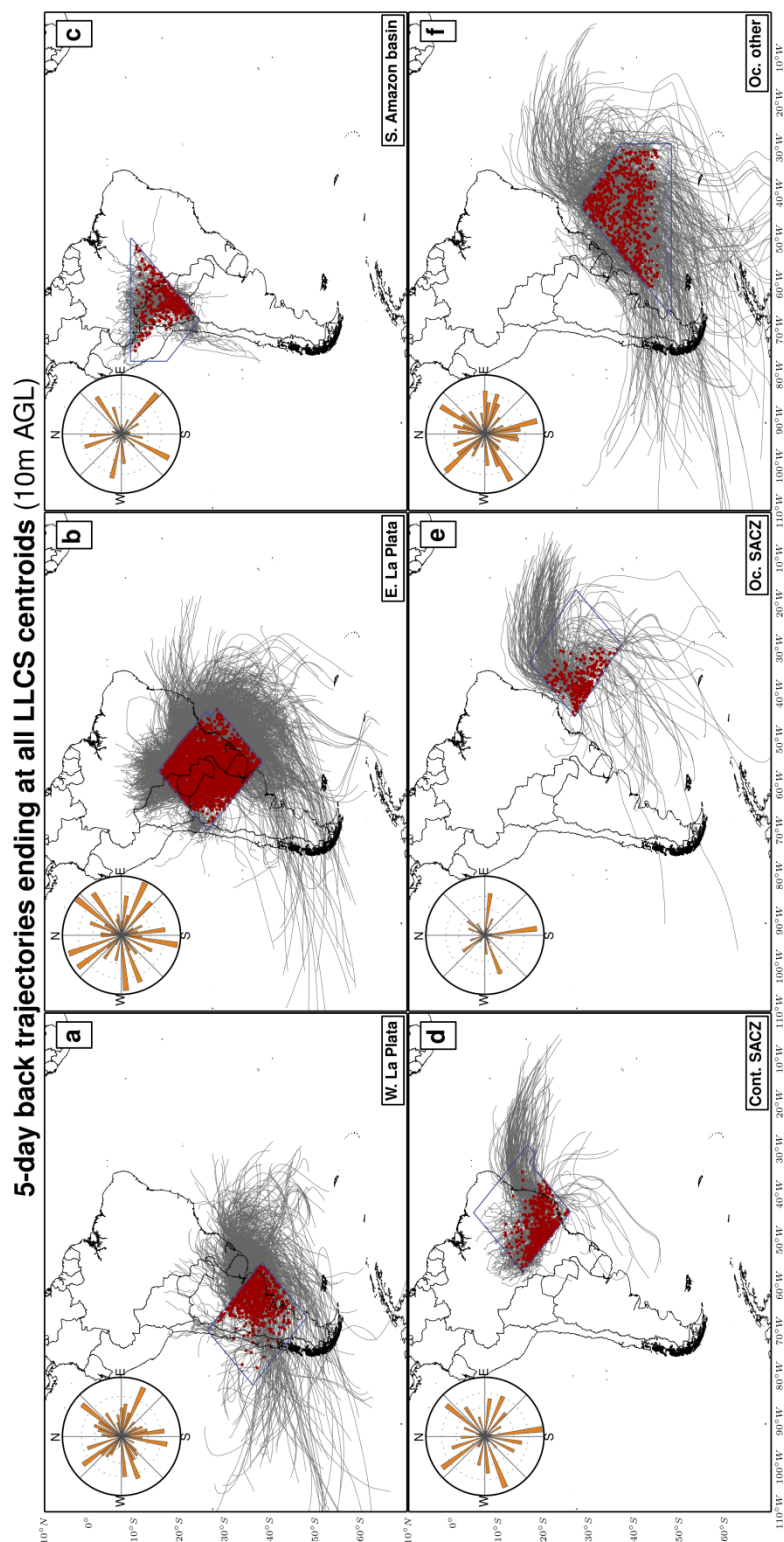


**Fig. 4.25.** HYSPLIT modeled 120-hour parcel back trajectories at 10 meters AGL for all 6-hourly merged LLCS cloud shields grouped by sub-domains: (a) West La Plata, (b) East La Plata, (c) Amazon, (d) Continental SACZ, (e) Oceanic SACZ, (f) Oceanic other.

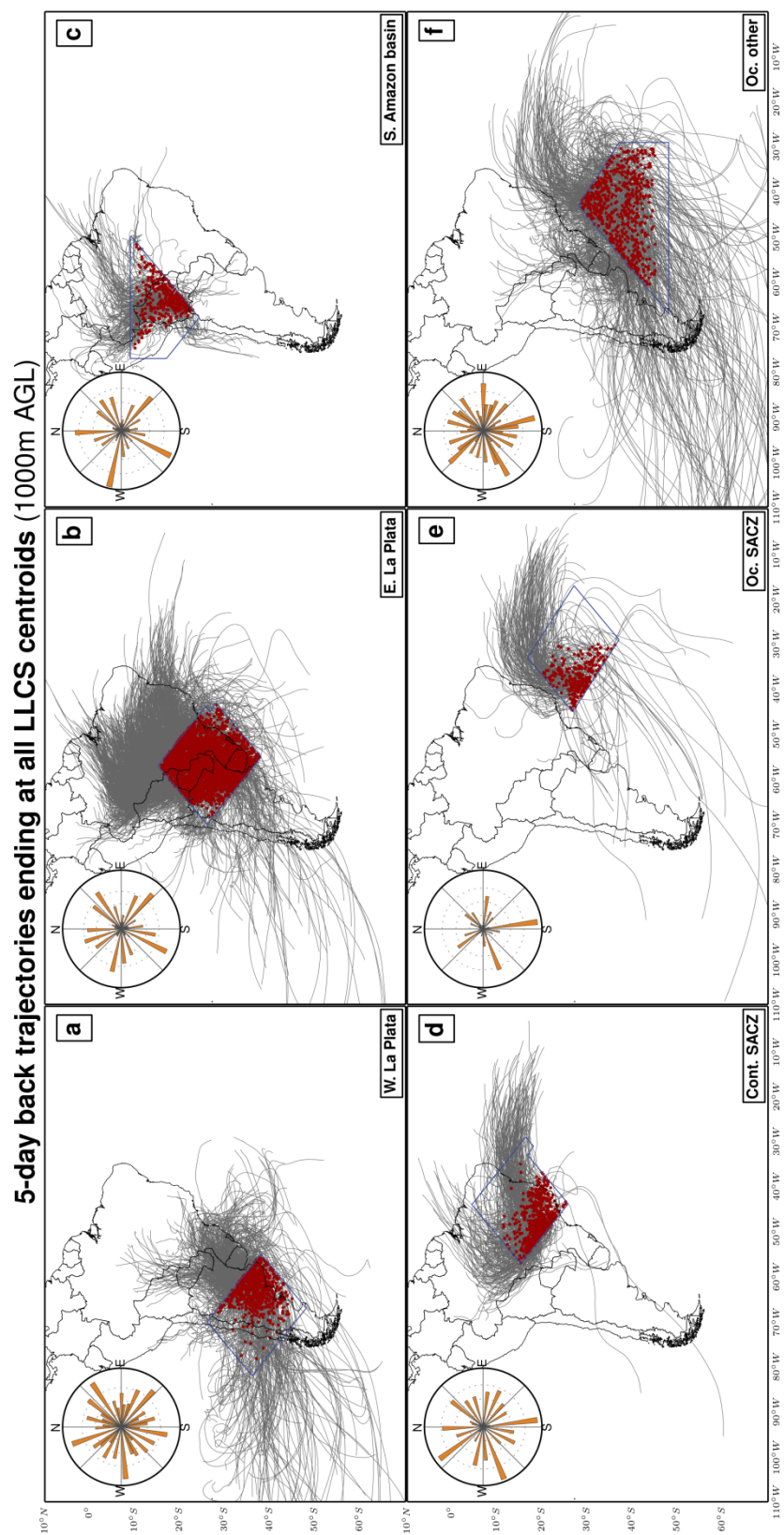


**Fig. 4.26.** As in Fig. 4.25 except for 1000m AGL trajectories.

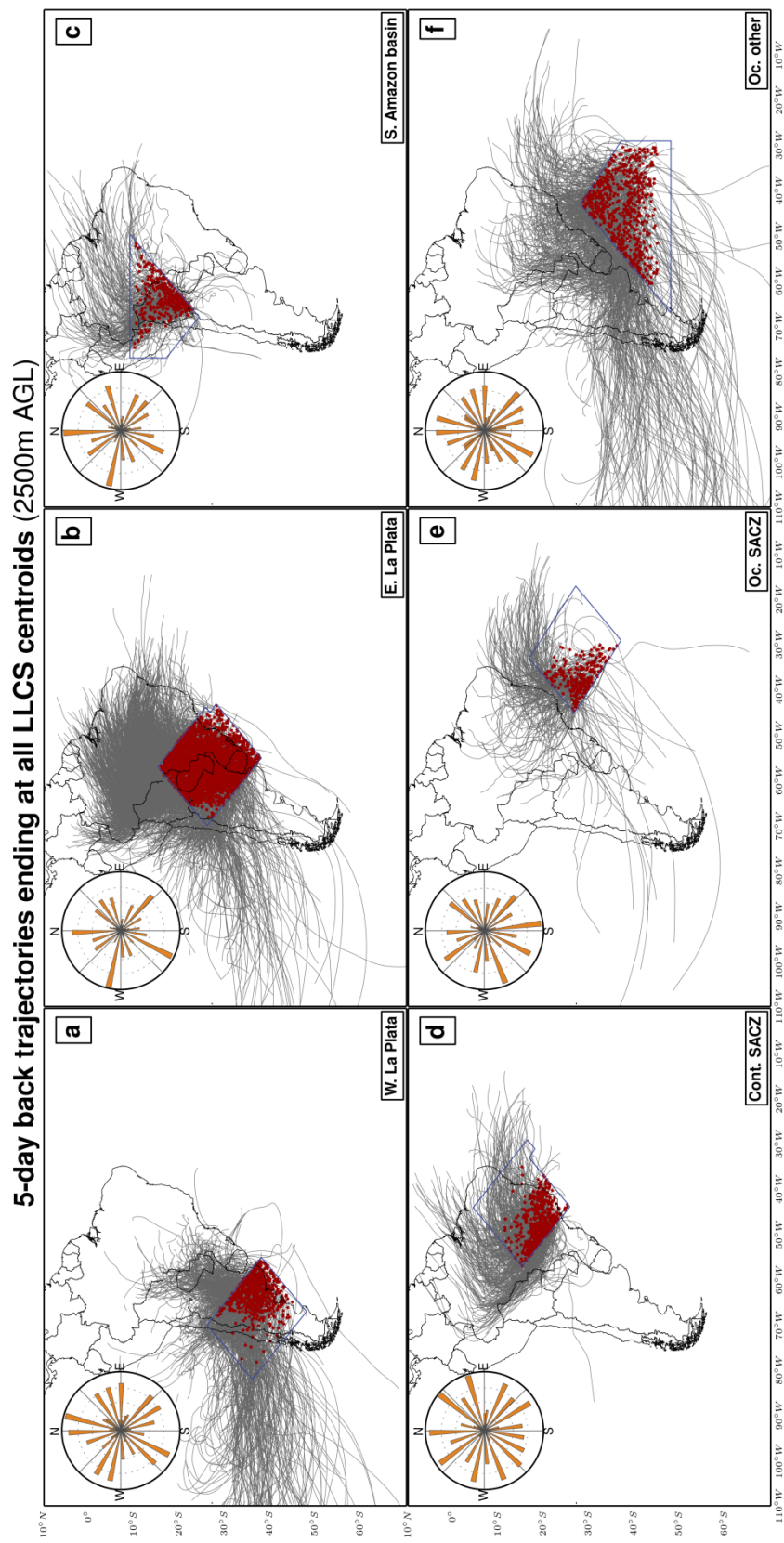


**Fig. 4.27.** As in Figs. 4.25 and 4.26 except for 2500m AGL trajectories.

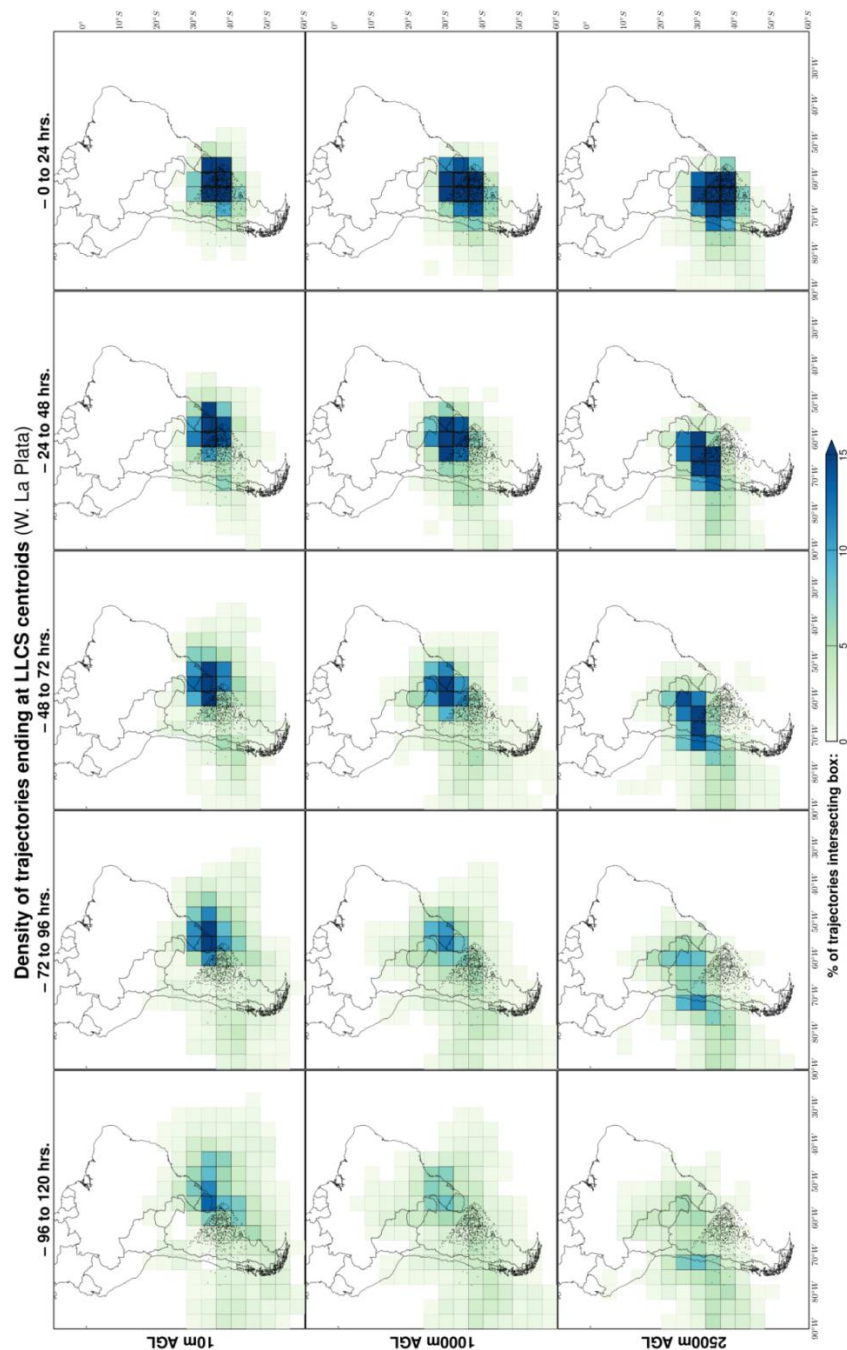


**Fig. 4.28.** Trajectory density plots for the “West La Plata” sub-domain grouped by hours preceding LLCS valid time: 96–120 hours before LLCS time (leftmost column), 72–96 hours before (second column from left), 48–72 hours before (middle column), 24–48 hours before (second column from right), and 0–24 hours before (rightmost column). Rows represent trajectory levels: 10m AGL (top row), 1000m AGL (middle row), and 2500m AGL (bottom row). On each plot, the density units are the ratio of the number of LLCS trajectories for the given timestep that intersected the given  $4^\circ \times 4^\circ$  box to the total number of trajectories for the given timestep.

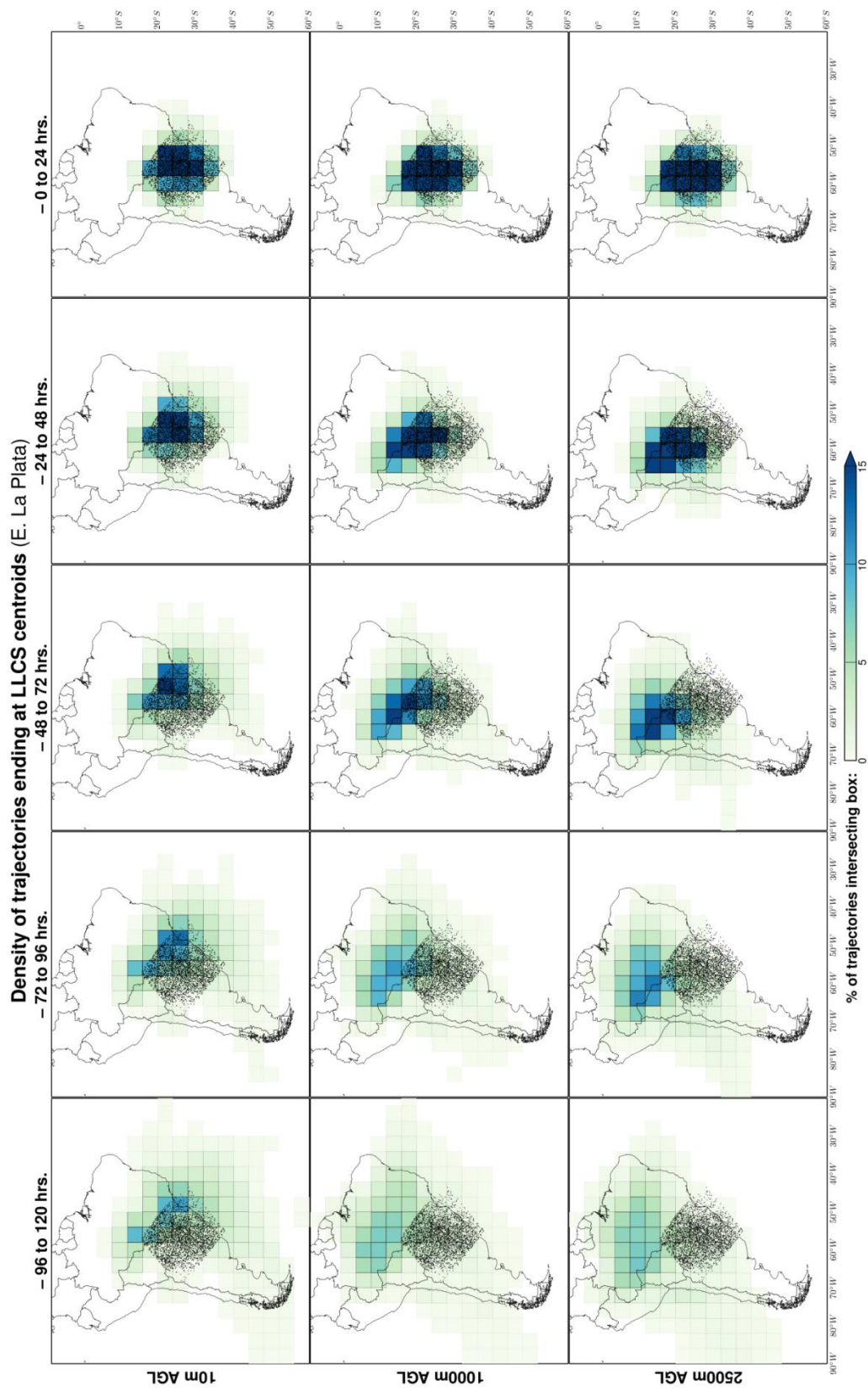


**Fig. 4.29.** As in Fig. 4.28 except for “East La Plata” sub-domain.

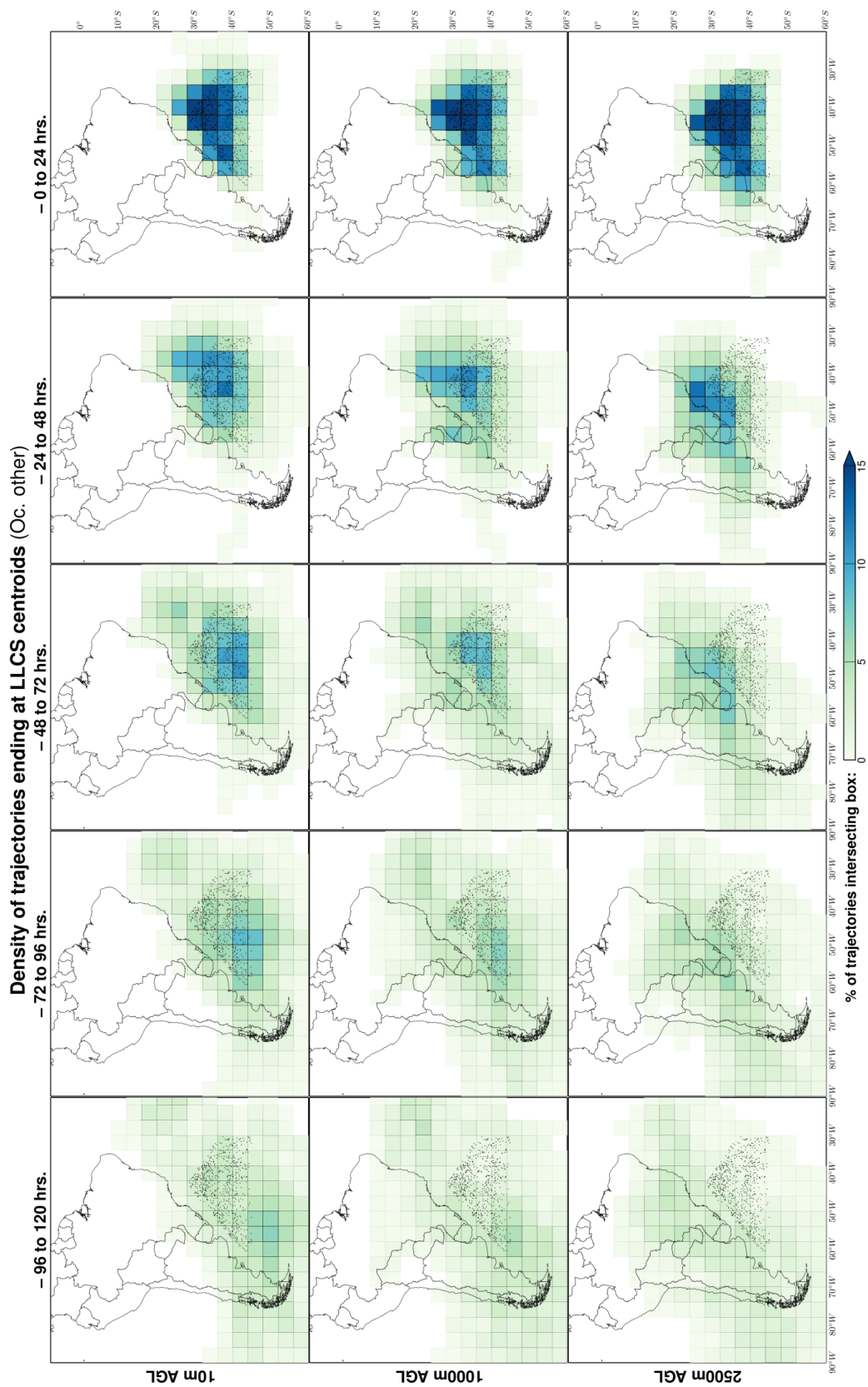


**Fig. 4.30.** As in Figs. 4.28–4.29 except for “Oceanic other” domain.

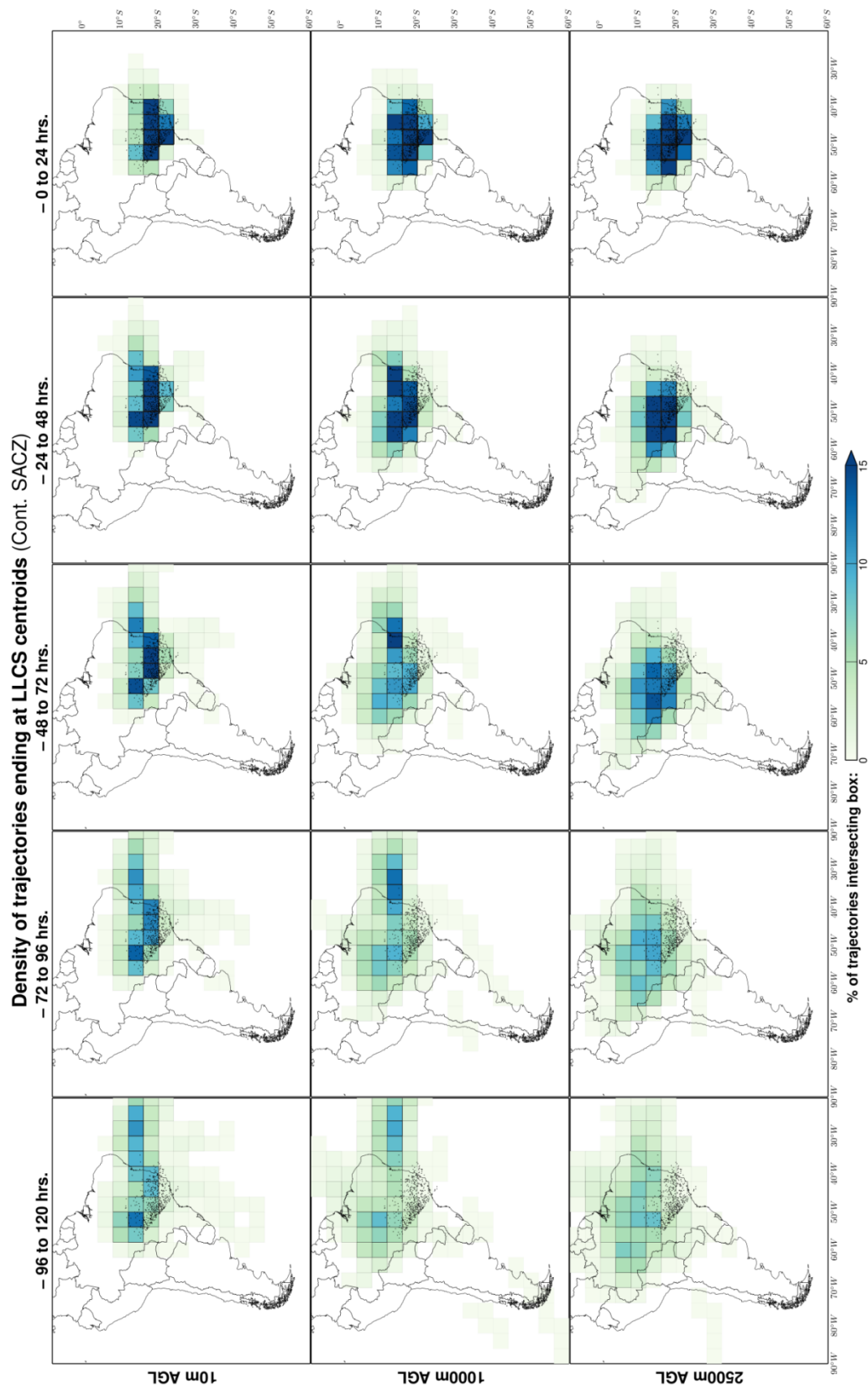


**Fig. 4.31.** As in Figs. 4.28–4.30 except for “Continental SACZ” domain.

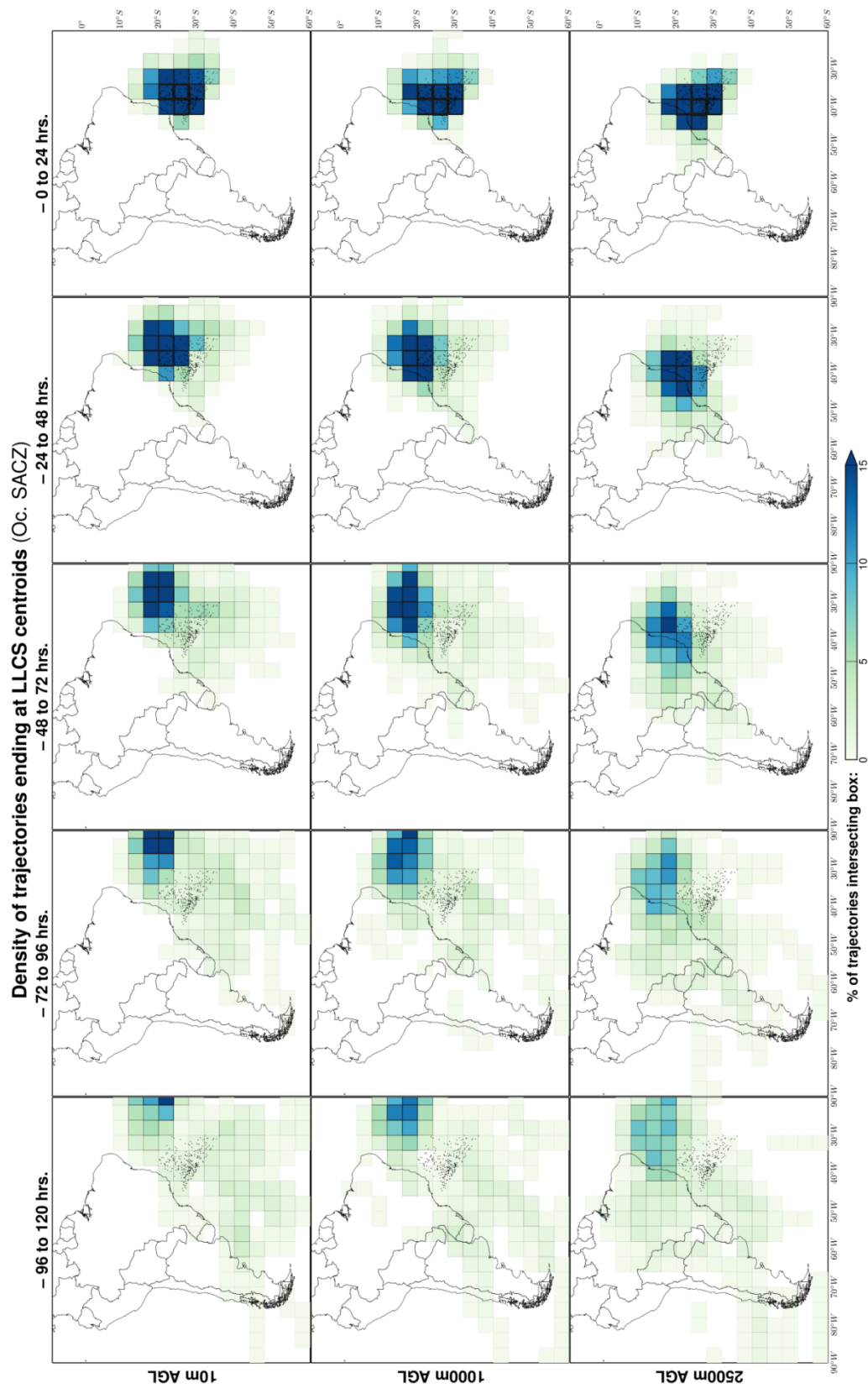


**Fig. 4.32.** As in Figs. 4.28–4.31 except for “Oceanic SACZ” domain.

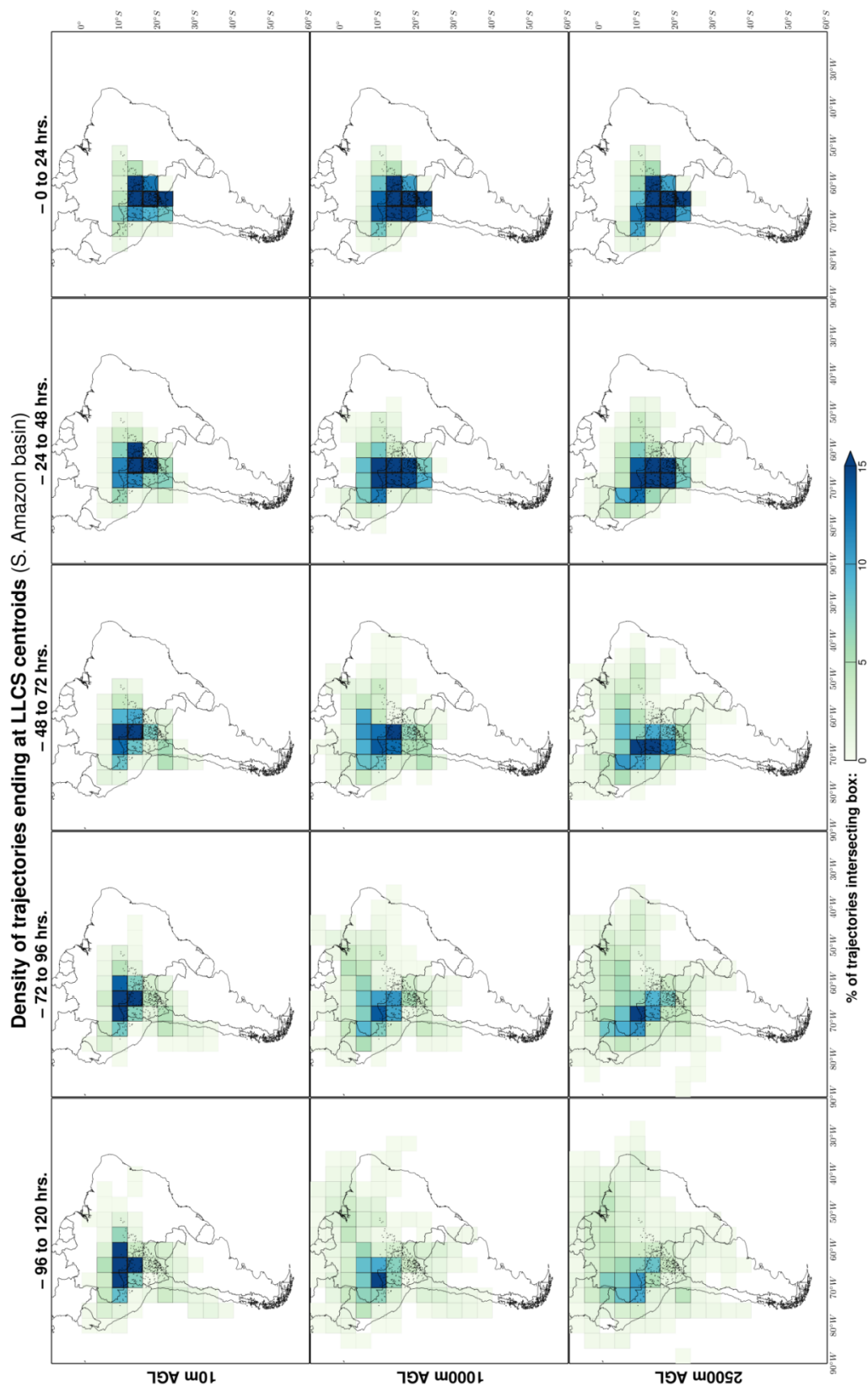


**Fig. 4.33.** As in Figs. 4.28–4.32 except for “Amazon” domain.

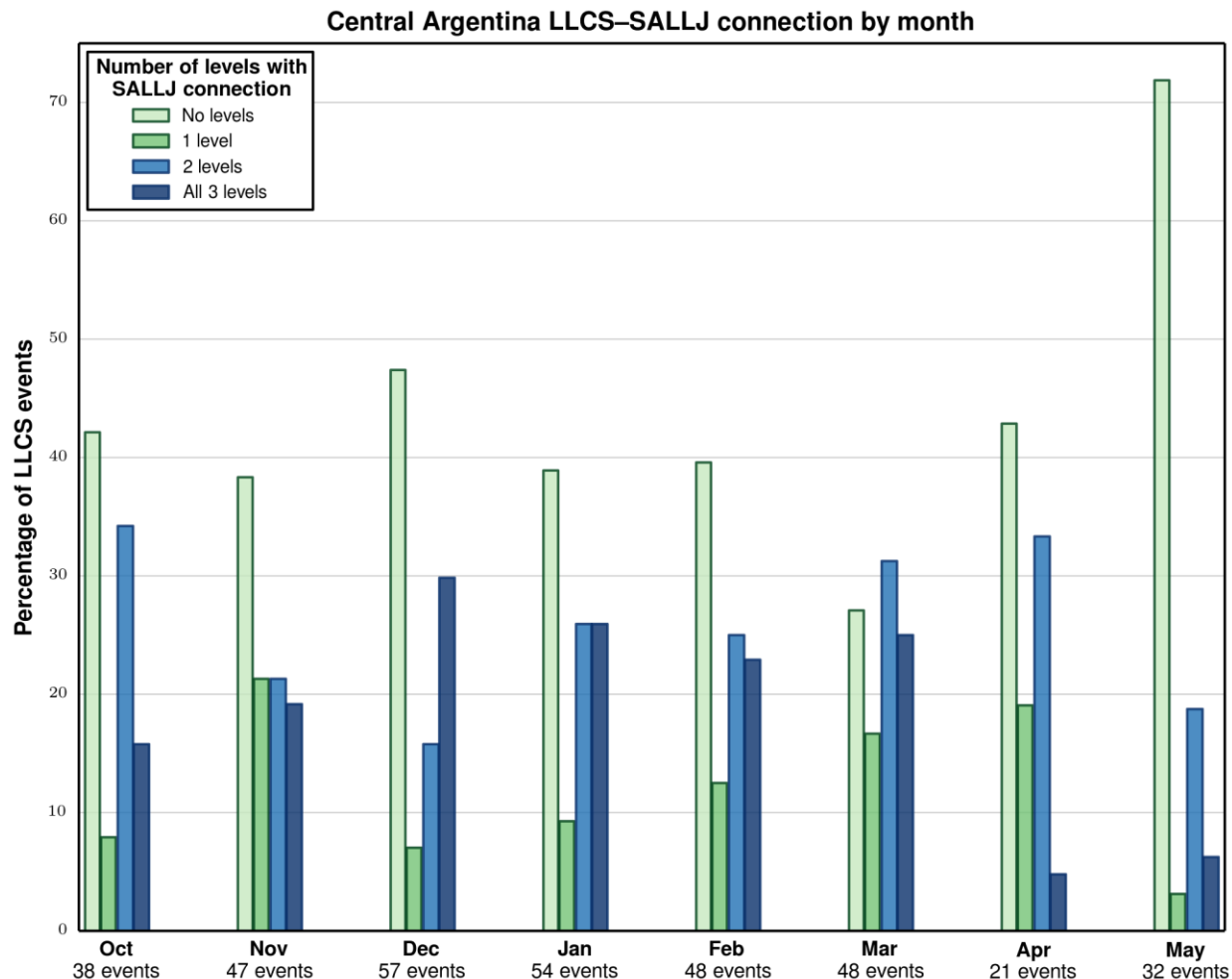


**Fig. 4.34.** Percentage of central Argentina LLCS events during each warm season month that fell each SALLJ connection category: no levels (no HYSPLIT modeled back trajectories at any of the three levels for any of the LLCS’s 6-hourly timesteps passed through the SALLJ domain), 1 level (back trajectory at 1 of 3 levels passed through the SALLJ domain), 2 levels (back trajectories at 2 of 3 levels passed through the SALLJ domain), 3 levels (back trajectories at all 3 levels passed through the SALLJ domain).

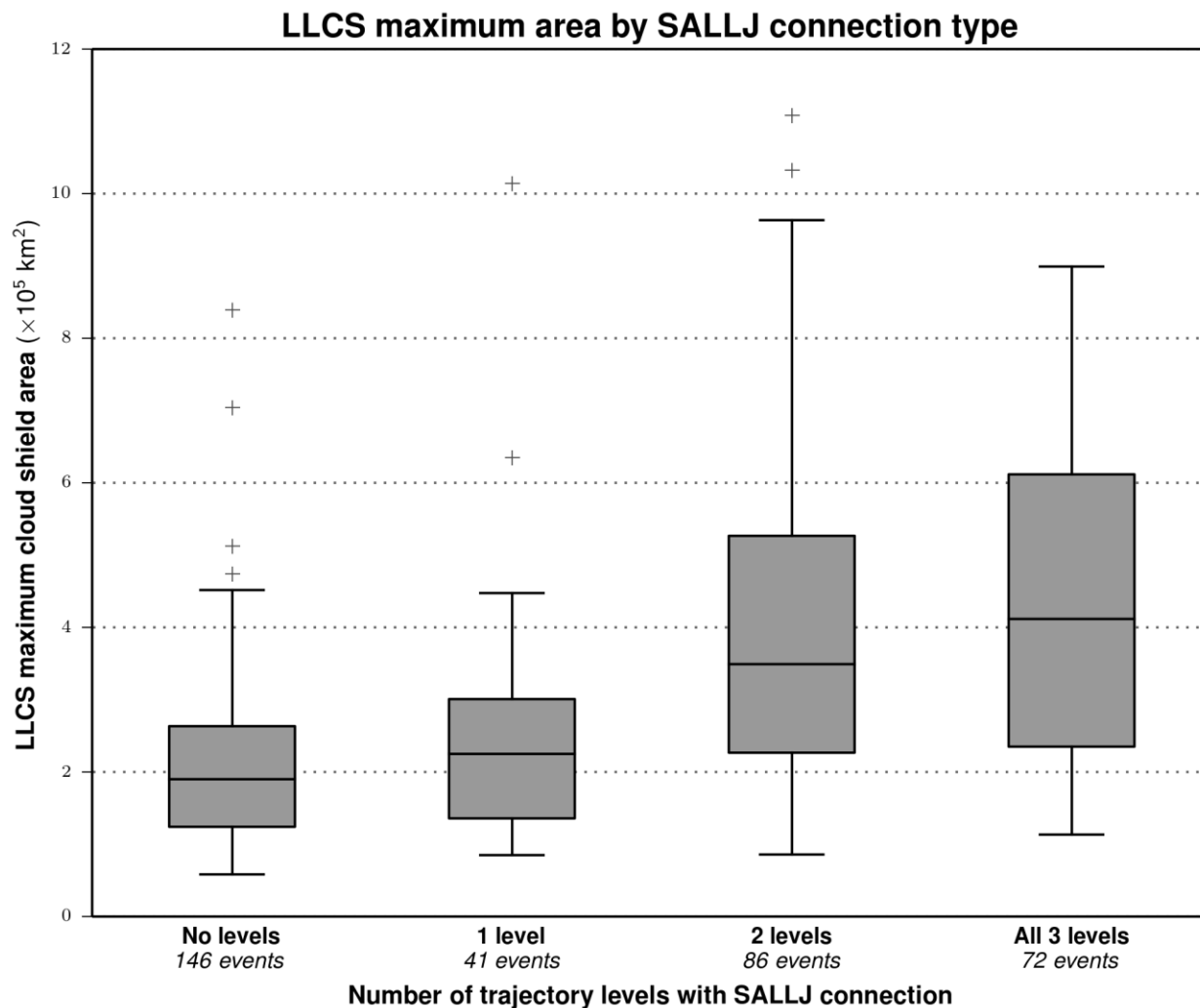


**Fig. 4.35.** Distribution of central Argentina LLCS maximum cloud shield area across same categories of SALLJ connection as in Fig. 4.34. Boxes contain the region between the lower and upper quartiles (25<sup>th</sup> and 75<sup>th</sup> percentiles) of the distribution and whiskers extend to the most extreme data point within  $\pm 1.5 \cdot (\text{interquartile range})$ .

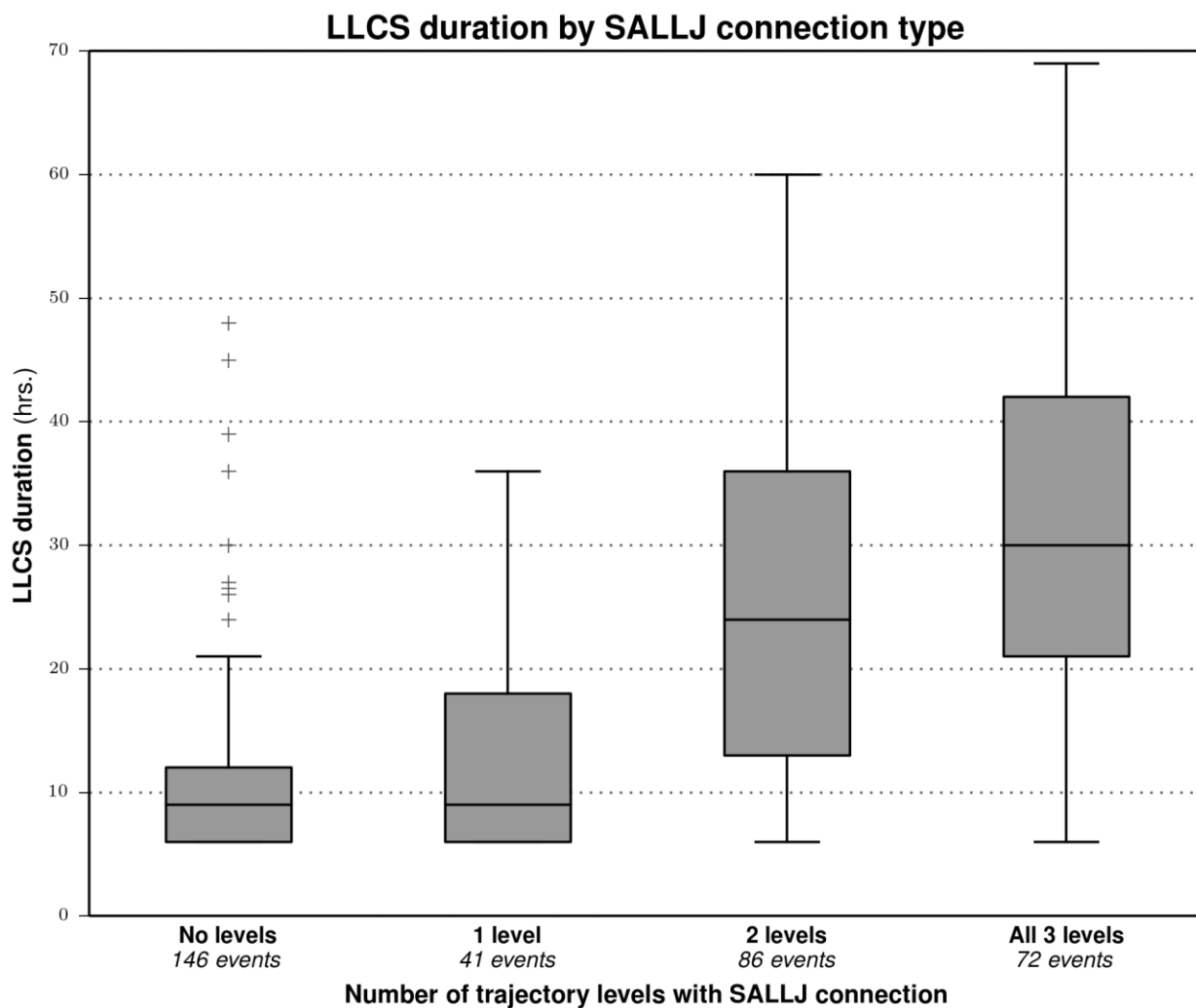


**Fig. 4.36.** As in Fig. 4.35 except for distribution of LLCS duration.

PWAT, 925-hPa wind, and HYSPLIT trajectories: October 2001 case study

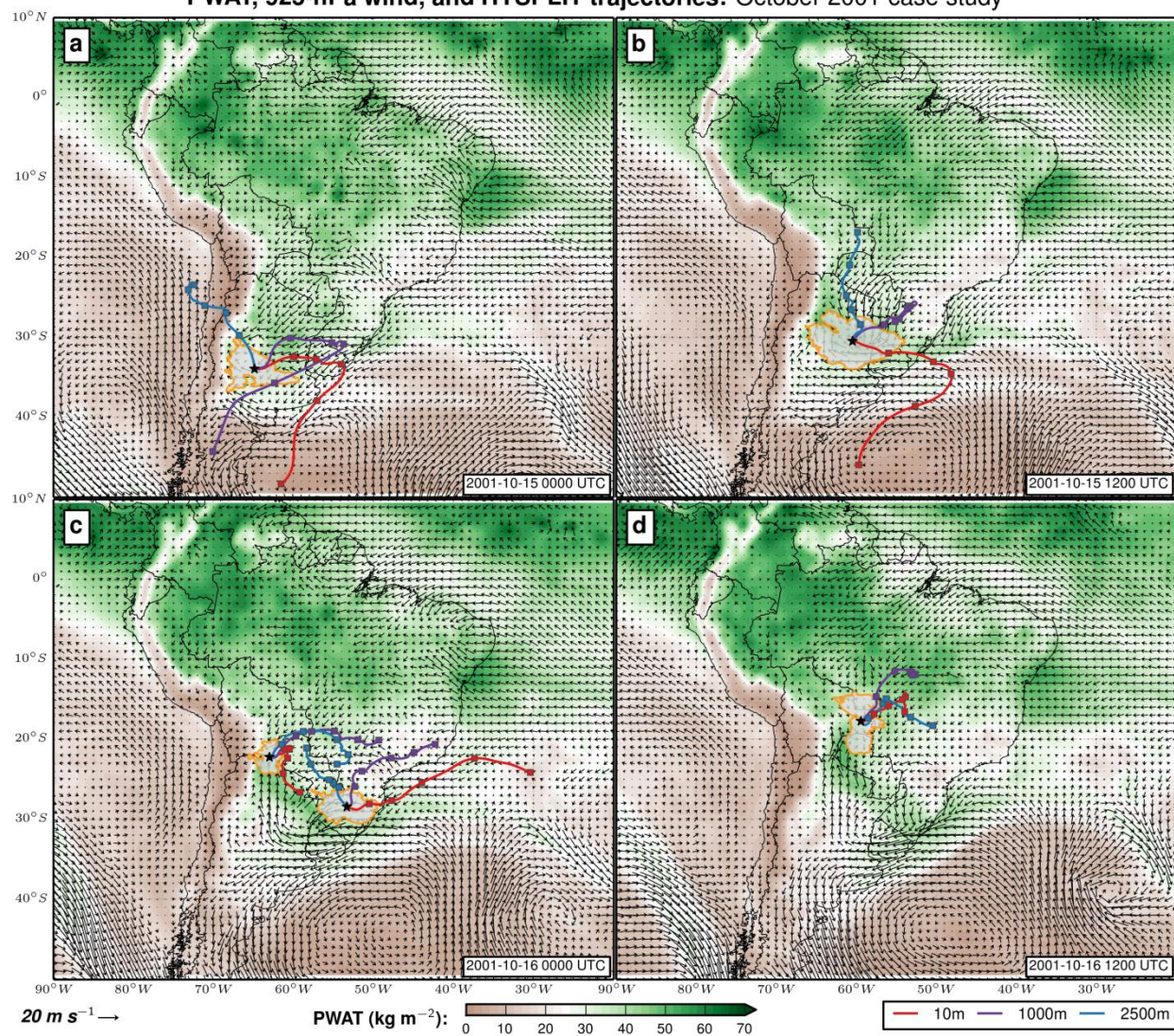


**Fig. 4.37.** Precipitable water (fill;  $\text{kg m}^{-2}$ ) and 925-hPa wind vectors ( $\text{m s}^{-1}$ ) for four timesteps during Oct 2001 case study LLCS event: (a) 0000 UTC 15 Oct 2001, (b) 1200 UTC 15 Oct 2001, (c) 0000 UTC 16 Oct 2001, (d) 1200 UTC 16 Oct 2001. Also plotted are the HYSPLIT modeled back trajectories ending at each 6-hourly merged LLCS centroid at three levels: 10m AGL (red lines), 1000m AGL (purple lines), and 2500m AGL (blue lines).

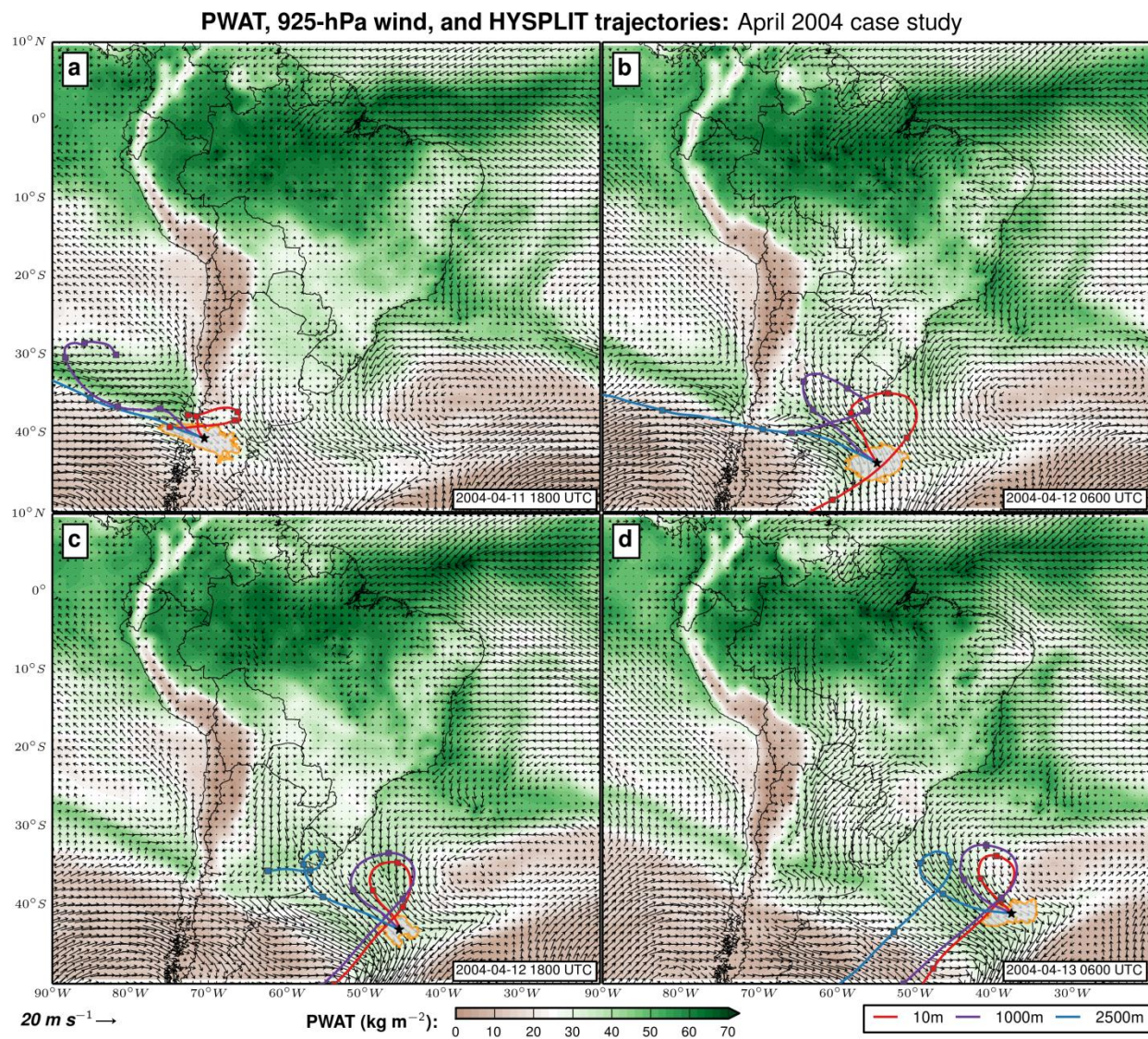


**Fig. 4.38.** As in Fig. 4.37 except for Apr 2004 case study LLCS event at timesteps: (a) 1800 UTC 11 Apr 2004, (b) 0600 UTC 12 Apr 2004, (c) 1800 UTC 12 Apr 2004, (d) 0600 UTC 13 Apr 2004.

## CHAPTER 5

### DISCUSSION AND CONCLUSIONS

#### **5.1 Discussion of major findings**

The first part this study involved a comprehensive investigation of the lower- and upper-tropospheric circulation features associated with both continental and oceanic South Atlantic Convergence Zone events and their relationships with LLCS formation over the La Plata basin of subtropical South America. This analysis yielded several insights into the atmospheric processes that govern the variability of regional hydroclimate. Continental and oceanic SACZ events were found to generally occur separately from one another as a result of distinct atmospheric flow patterns. Continental SACZ events typically occurred during the spring and summer months, under atmospheric regimes that were characterized by large-scale moisture transport from the Amazon basin to the Brazilian Highlands consistent with the warm phase of the South American monsoon. Oceanic SACZ events, on the other hand, increased in frequency during the autumn months (particularly May) and were typically associated with more dynamic atmospheric flow patterns featuring an upper-level trough over the La Plata basin and below-normal atmospheric moisture over most of South America.

These findings regarding the atmospheric flow patterns associated with continental and oceanic SACZ events proved to also hold important ramifications for LLCS activity over the La Plata basin and helped to further describe the nature of the “South American Seesaw” precipitation dipole identified in previous studies. Increases in precipitation over the continental SACZ region were found to be associated with an increase in the probability of LLCS occurrence over northern and western sections of the La Plata basin and a decrease in LLCS

probability over the southeastern La Plata basin and adjacent regions of the South Atlantic Ocean. Increased oceanic SACZ precipitation, on the other hand, was strongly associated with a decreased probability of LLCS occurrence over nearly the entire La Plata basin, with the exception of a small section of central Argentina. This negative relationship between oceanic SACZ precipitation and LLCS probability was found to be stronger than the relationships (both positive and negative) between continental SACZ precipitation and LLCS probability over most of the La Plata basin. Areas of stronger continental SACZ precipitation linkages to LLCS probability were confined to the continental SACZ domain itself and a small section of northern Paraguay and eastern Bolivia that typically receives moisture flux from the Amazon during the same times that precipitation is enhanced in the continental SACZ region. Thus the “South American Seesaw” signature, as it appears in relationships between the SACZ and La Plata basin LLCS activity, was shown to exhibit substantial variability across different regions of the La Plata basin. Over the northern and western sections of the basin, there is indeed a “Seesaw” inverse relationship between LLCS activity and *oceanic* SACZ precipitation, but there is no “Seesaw” with *continental* SACZ precipitation and increases in continental SACZ precipitation were actually associated with increased LLCS probability. Over the southeastern La Plata basin (southern Paraguay, far northeastern Argentina, far southern Brazil, and Uruguay), there is a pronounced “Seesaw” between both continental *and* oceanic SACZ precipitation and LLCS probability, as enhanced precipitation in either of the SACZ domains favors moisture transport away from this area through the mechanisms described in section 4.1.

Atmospheric circulation patterns observed in this study for periods of active SACZ and La Plata basin precipitation are broadly similar to those found in previous research (e.g. Carvalho et al. 2004; Muza et al. 2009; Carvalho et al. 2011; de Oliveira Vieira et al. 2012). However, this

study is unique in finding that oceanic SACZ precipitation shows a much stronger inverse relationship with La Plata LLCS activity compared to the continental SACZ; the few previous studies (Muza et al. 2009; Carvalho et al. 2011) that have treated the continental and oceanic SACZ as separate entities found that the “Seesaw” inverse relationship is roughly equivalent for both the continental and oceanic SACZ (see Fig. 9 of Muza et al. 2009). A likely cause of this discrepancy is the fact that these two previous studies only examined SACZ events during the austral summer months of December-February, while the present study covers October-May. As Figs. 3.6 and 3.11 show, oceanic SACZ events commonly occur during the spring and fall months. This suggests that this study captures more early- and late-warm season oceanic SACZ events than previous studies which, due to their timing away from the peak of the monsoon, are more likely to coincide with periods of reduced La Plata basin precipitation than summer oceanic SACZ events.

The most salient conclusion to be drawn from the LLCS moisture source analysis that comprised the second part of this study is that moisture transport into large-scale organized convection over subtropical South America is quite complex and likely originates from sources beyond the South American Low-Level Jet alone. Although there is a large degree of uncertainty in the results generated by the HYSPLIT back trajectory analysis of airflow into these events, it appears likely that a substantial proportion of moisture feeding LLCSs over the La Plata basin can be sourced to the Brazil Current area of the South Atlantic Ocean and / or the eastern Pacific Ocean. In the detailed analysis of central Argentina LLCS events reported in section 4.4, it was found that nearly half of them showed no evidence of receipt of moisture from the SALLJ, which confirms the suggestion of Durkee (2008) that LLCS events in this region may not be initiated by the transport of Amazonian moisture in all cases. Notably, these “non-SALLJ” systems were

significantly smaller and shorter in duration than LLCs with a connection to the SALLJ, which suggests that richer Amazonian moisture may be capable of supporting larger and longer-lasting convective events than South Atlantic and Pacific moisture sources.

## **5.2 Future research**

Most of the unresolved questions surrounding this research were raised by the LLCs moisture source portion of the study, as the relative importance of the Amazon basin, South Atlantic Ocean, and Pacific Ocean moisture source regions is still largely unknown. A necessary first step in beginning to resolve this question would be to use a more modern and high-resolution reanalysis dataset such as CFSR or ERA-Interim to generate more accurate HYSPLIT back trajectories. These trajectories should be modeled for numerous levels throughout the lower troposphere and at numerous points located within LLCs cloud shields rather than just the cloud shield centroid to create an ensemble of possible trajectories entering the system at all levels where moisture transport was potentially occurring. For a truly accurate picture of moisture transport over the region, however, spatially dense observations of moisture and wind flow throughout the depth of the troposphere would be needed across subtropical South America, particularly in areas (such as the narrowing of the Brazilian Highlands between Curitiba and São Paulo and gaps in the Argentinian Andes) that have been identified in this study as potential key moisture transport pathways. These observations would be especially useful in diagnosing the vertical structure of moisture transport for comparison with reanalysis data and numerical weather prediction simulations. An example of this type of observational study is the South American Low-Level Jet Experiment, a field campaign to observe the characteristics of the SALLJ that took place during November 2002 – February 2003 (Vera et al. 2006b).

Once the principal moisture source regions of convection over subtropical South America have been more thoroughly investigated and better understood through one or more of these

methods, future work should build upon this knowledge by exploring its scientific and societal ramifications. For example, if the South Atlantic Ocean is confirmed to in fact be a major moisture source region fueling large-scale convective precipitation in the La Plata basin, further studies would be warranted to determine the relative precipitation impacts of convective events whose primary moisture source is from the South Atlantic – do they produce as much rainfall over as wide a region as convection fed by the Amazonian SALLJ, or do they tend to be smaller and shorter in duration, as this study’s preliminary results for central Argentina suggest? A more complete picture of La Plata basin moisture sources would also aid in understanding the broader effects of droughts and deforestation in the Amazon basin. These changes may prove to be more (or less) important to economic interests in the La Plata basin than previously thought, depending on the level of dependence on Amazon-sourced atmospheric moisture the region is found to exhibit. Finally, the contribution of South Atlantic moisture to La Plata basin precipitation could prove to be an important component of the assessment of future climate change scenarios for South America and the South Atlantic Ocean. Climate model simulations (Junquas et al. 2012; Marengo et al. 2012) have predicted a future increase in precipitation across the La Plata basin. The preliminary results of this study suggest that warming of the South Atlantic Ocean could potentially be a factor in this predicted trend by leading to increased amounts of water vapor available for La Plata basin convection, but further research is needed to confirm that South Atlantic moisture is indeed a major contributor to precipitation in subtropical South America.

## REFERENCES

- Anderson, C. J., and R. W. Arritt, 1998: Mesoscale convective complexes and persistent elongated convective systems over the United States during 1992 and 1993. *Monthly Weather Review*, **126**, 578–599.
- Augustine, J. A., 1985: An automated method for the documentation of cloud-top characteristics of mesoscale convective systems. National Oceanic and Atmospheric Administration, Environmental Research Laboratories, Environmental Sciences Group.
- Augustine, J. A., and K. W. Howard, 1988: Mesoscale convective complexes over the United States during 1985. *Monthly Weather Review*, **116**, 685–701.
- Bischof, B., A. J. Mariano, and E. H. Ryan, 2003: The North Brazil Current. Available online at <http://oceancurrents.rsmas.miami.edu/atlantic/north-brazil.html>.
- Bischof, B., E. Rowe, A. J. Mariano, and E. H. Ryan, 2004: The Brazil Current. Available online at <http://oceancurrents.rsmas.miami.edu/atlantic/brazil.html>.
- Bombardi, R. J., L. M. V. Carvalho, C. Jones, and M. S. Reboita, 2014: Precipitation over eastern South America and the South Atlantic Sea surface temperature during neutral ENSO periods. *Climate Dynamics*, **42**, 1553–1568.
- Carvalho, L., C. Jones, and B. Liebmann, 2002: Extreme precipitation events in southeastern South America and large-scale convective patterns in the South Atlantic convergence zone. *Journal of Climate*, **15**, 2377–2394.
- Carvalho, L. M. V., C. Jones, and B. Liebmann, 2004: The South Atlantic convergence zone: Intensity, form, persistence, and relationships with intraseasonal to interannual activity and extreme rainfall. *Journal of Climate*, **17**, 88–108.
- Carvalho, L. M. V., A. E. Silva, C. Jones, B. Liebmann, P. L. Silva Dias, and H. R. Rocha, 2011: Moisture transport and intraseasonal variability in the South America monsoon system. *Climate Dynamics*, **36**, 1865–1880.
- Carvalho, L. M. V., C. Jones, A. N. D. Posadas, R. Quiroz, B. Bookhagen, and B. Liebmann, 2012: Precipitation characteristics of the South American monsoon system derived from multiple datasets. *Journal of Climate*, **25**, 4600–4620.

- Chen, T. C., S. P. Weng, and S. Schubert, 1999: Maintenance of austral summertime upper-tropospheric circulation over tropical South America: The Bolivian High-Nordeste Low system. *Journal of the Atmospheric Sciences*, **56**, 2081–2100.
- Cook, K. H., 2000: The South Indian convergence zone and interannual rainfall variability over southern Africa. *Journal of Climate*, **13**, 3789–3804.
- Delvenne, P., F. Vasen, and A. M. Vara, 2013: The “soy-ization” of Argentina: the dynamics of the “globalized” privatization regime in a peripheral context. *Technology in Society*, **35**, 153–162.
- Diaz, A. F., C. D. Studzinski, and C. R. Mechoso, 1998: Relationships between precipitation anomalies in Uruguay and southern Brazil and sea surface temperature in the Pacific and Atlantic Oceans. *Journal of Climate*, **11**, 251–271.
- Díaz, A., and P. Aceituno, 2003: Atmospheric circulation anomalies during episodes of enhanced and reduced convective cloudiness over Uruguay. *Journal of Climate*, **16**, 3171–3185.
- Doyle, M. E., and V. R. Barros, 2002: Midsummer low-level circulation and precipitation in subtropical South America and related sea surface temperature anomalies in the South Atlantic. *Journal of Climate*, **15**, 3394–3410.
- Draxler, R. R., and G. D. Hess, 1997: Description of the HYSPLIT\_4 modeling system. NOAA Tech. Memo. ERL ARL-224, NOAA Air Resources Laboratory, Silver Spring, MD, 24 pp.
- Durkee, J. D., 2008: Assessing the role of warm-season mesoscale convective complexes in subtropical South American precipitation variability. Dissertation, University of Georgia, 150 pp.
- Durkee, J. D., and T. L. Mote, 2009: A climatology of warm-season mesoscale convective complexes in subtropical South America. *International Journal of Climatology*, **30**, 418–431.
- Durkee, J. D., T. L. Mote, and J. M. Shepherd, 2009: The contribution of mesoscale convective complexes to rainfall across subtropical South America. *Journal of Climate*, **22**, 4590–4605.
- Food and Agriculture Organization of the United Nations (FAO), 2014: FAOSTAT. Available online at [http://faostat3.fao.org/faostat-gateway/go/to/browse/Q/\\*/E](http://faostat3.fao.org/faostat-gateway/go/to/browse/Q/*/E).

- Feng, F., Z. Li, M. Zhang, S. Jin, and Z. Dong, 2013: Deuterium and oxygen 18 in precipitation and atmospheric moisture in the upper Urumqi River Basin, eastern Tianshan Mountains. *Environmental Earth Sciences*, **68**, 1199–1209.
- Gan, M., V. Kousky, and C. Ropelewski, 2004: The South America monsoon circulation and its relationship to rainfall over west-central Brazil. *Journal of Climate*, **17**, 47–66.
- Garreaud, R. D., 2000: Cold air incursions over subtropical South America: Mean structure and dynamics. *Monthly Weather Review*, **128**, 2544–2559.
- Garreaud, R. D., M. Vuille, R. Compagnucci, and J. Marengo, 2009: Present-day South American climate. Palaeogeography, Palaeoclimatology, *Palaeoecology*, **281**, 180–195.
- Goldfarb, L. and A. Zoomers, 2013: The Drivers Behind the Rapid Expansion of Genetically Modified Soya Production into the Chaco Region of Argentina. *Biofuels - Economy, Environment and Sustainability*. Prof. Zhen Fang (Ed.), ISBN: 978-953-51-0950-1, InTech, DOI: 10.5772/53447. Available online at <http://www.intechopen.com/books/biofuels-economy-environment-and-sustainability/the-drivers-behind-the-rapid-expansion-of-genetically-modified-soya-production-into-the-chaco-region>.
- Guan, H., X. Zhang, G. Skrzypek, Z. Sun, and X. Xu, 2013: Deuterium excess variations of rainfall events in a coastal area of South Australia and its relationship with synoptic weather systems and atmospheric moisture sources. *Journal of Geophysical Research: Atmospheres*, **118**, 1123–1138.
- Hamilton, L., 1992: *Regression with Graphics*. Cengage Learning, 363 pp.
- Hoke, G. D., J. N. Aranibar, M. Viale, D. C. Araneo, and C. Llano, 2013: Seasonal moisture sources and the isotopic composition of precipitation, rivers, and carbonates across the Andes at 32.5–35.5° S. *Geochemistry, Geophysics, Geosystems*, **14**, 962–978.
- Hu, Z. Z., A. Kumar, B. Huang, J. Zhu, and Y. Guan, 2014: Prediction Skill of North Pacific Variability in NCEP Climate Forecast System Version 2: Impact of ENSO and Beyond. *Journal of Climate*, **27**, 4263–4272.
- Huffman, G. J., and Coauthors, 2007: The TRMM Multisatellite Precipitation Analysis (TMPA): Quasi-global, multiyear, combined-sensor precipitation estimates at fine scales. *Journal of Hydrometeorology*, **8**, 38–55.

- Insel, N., C. J. Poulsen, C. Sturm, and T. A. Ehlers, 2013: Climate controls on Andean precipitation  $\delta^{18}\text{O}$  interannual variability. *Journal of Geophysical Research: Atmospheres*, **118**, 9721–9742.
- International Service for the Acquisition of Agri-Biotech Applications (ISAAA), 2014: *ISAAA Brief 46-2013: Executive Summary*. Available online at <http://www.isaaa.org/resources/publications/briefs/46/executivesummary/default.asp>.
- Jirak, I. L., W. R. Cotton, and R. L. McAnelly, 2003: Satellite and radar survey of mesoscale convective system development. *Monthly Weather Review*, **131**, 2428–2449.
- Jouzel, J., G. Delaygue, A. Landais, V. Masson-Delmotte, C. Risi, and F. Vimeux, 2013: Water isotopes as tools to document oceanic sources of precipitation. *Water Resources Research*, **49**, 7469–7486.
- Junquas, C., C. Vera, L. Li, and H. Le Treut, 2012: Summer precipitation variability over Southeastern South America in a global warming scenario. *Climate Dynamics*, **38**, 1867–1883.
- Kalnay, E., and Coauthors, 1996: The NCEP/NCAR 40-year reanalysis project. *Bulletin of the American Meteorological Society*, **77**, 437–471.
- Kodama, Y. M., T. Sagawa, S. Ishida, and T. Yoshikane, 2012: Roles of the Brazilian Plateau in the formation of the SACZ. *Journal of Climate*, **25**, 1745–1758.
- Lenters, J., and K. Cook, 1997: On the origin of the Bolivian high and related circulation features of the South American climate. *Journal of the Atmospheric Sciences*, **54**, 656–678.
- Lenters, J., and K. Cook, 1999: Summertime precipitation variability over South America: Role of the large-scale circulation. *Monthly Weather Review*, **127**, 409–431.
- Liebmann, B., G. N. Kiladis, J. Marengo, T. Ambrizzi, and J. D. Glick, 1999: Submonthly convective variability over South America and the South Atlantic convergence zone. *Journal of Climate*, **12**, 1877–1891.
- Liebmann, B., G. N. Kiladis, C. S. Vera, A. C. Saulo, and L. M. V. Carvalho, 2004: Subseasonal variations of rainfall in South America in the vicinity of the low-level jet east of the Andes and comparison to those in the South Atlantic convergence zone. *Journal of Climate*, **17**, 3829–3842.

- Maddox, R. A., 1980: Mesoscale convective complexes. *Bulletin of the American Meteorological Society*, **61**, 1374–1387.
- Marengo, J. A., and Coauthors, 2012: Development of regional future climate change scenarios in South America using the Eta CPTEC/HadCM3 climate change projections: Climatology and regional analyses for the Amazon, São Francisco and the Parana River Basins. *Climate Dynamics*, **38**, 1829–1848.
- Mattingly, K. S., 2012: Large, long-lived convective systems over subtropical South America and their relationships with atmospheric teleconnections. Undergraduate thesis, Western Kentucky University, 74 pp.
- McHugh, M. J., and J. C. Rogers, 2001: North Atlantic oscillation influence on precipitation variability around the southeast African convergence zone. *Journal of Climate*, **14**, 3631–3642.
- Mechoso, R. C., P. S. Días, W. Baetghen, V. Barros, E. H. Berbery, R. Clarke, H. Cullen, C. Ereño, B. Grassi, and D. Lettenmaier, 2001: Climatology and Hydrology of the La Plata Basin. Document of VAMOS/CLIVAR. 56. Available online: [http://www.atmos.umd.edu/~berbery/lpb/science\\_plan.html](http://www.atmos.umd.edu/~berbery/lpb/science_plan.html).
- Muza, M. N., L. M. V. Carvalho, C. Jones, and B. Liebmann, 2009: Intraseasonal and interannual variability of extreme dry and wet events over southeastern South America and the subtropical Atlantic during austral summer. *Journal of Climate*, **22**, 1682–1699.
- National Center for Atmospheric Research (NCAR) Staff (Eds), 2013a: The Climate Data Guide: NCEP-NCAR (R1): An Overview. Available online at <https://climatedataguide.ucar.edu/climate-data/ncep-ncar-r1-overview>.
- National Center for Atmospheric Research (NCAR) Staff (Eds), 2013b: The Climate Data Guide: Climate Forecast System Reanalysis (CFSR). Available online at <https://climatedataguide.ucar.edu/climate-data/climate-forecast-system-reanalysis-cfsr>.
- Nieto-Ferreira, R., T. M. Rickenbach, and E. A. Wright, 2011: The role of cold fronts in the onset of the monsoon season in the South Atlantic convergence zone. *Quarterly Journal of the Royal Meteorological Society*, **137**, 908–922.
- Nogués-Paegle, J., and K. C. Mo, 1997: Alternating wet and dry conditions over South America during summer. *Monthly Weather Review*, **125**, 279–291.

- Nogués-Paegle, J., K. C. Mo, and J. Paegle, 2002: Progress in Pan American CLIVAR research: Understanding the South American Monsoon. *Meteorologica*, **27**, 3–32.
- de Oliveira Vieira, S., P. Satyamurty, and R. V. Andreoli, 2012: On the South Atlantic Convergence Zone affecting southern Amazonia in austral summer. *Atmospheric Science Letters*, **14**, 1–6.
- Penalba, O. C., and F. A. Robledo, 2010: Spatial and temporal variability of the frequency of extreme daily rainfall regime in the La Plata Basin during the 20th century. *Climatic Change*, **98**, 531–550.
- Pezzi, L. P., R. B. d. Souza, M. S. Dourado, C. A. E. Garcia, M. Mata, and M. Silva-Dias, 2005: Ocean-atmosphere in situ observations at the Brazil-Malvinas Confluence region. *Geophysical Research Letters*, **32**, L22603.
- Pezzi, L. P., R. B. de Souza, O. Acevedo, I. Wainer, M. M. Mata, C. A. Garcia, and R. de Camargo, 2009: Multiyear measurements of the oceanic and atmospheric boundary layers at the Brazil-Malvinas confluence region. *Journal of Geophysical Research: Atmospheres (1984–2012)*, **114**, D19103.
- Rasmussen, K. L., and R. A. Houze Jr, 2011: Orographic convection in subtropical South America as seen by the TRMM satellite. *Monthly Weather Review*, **139**, 2399–2420.
- Romatschke, U., and R. A. Houze Jr, 2013: Characteristics of precipitating convective systems accounting for the summer rainfall of tropical and subtropical South America. *Journal of Hydrometeorology*, **14**, 25–46.
- Saha, S., and Coauthors, 2010: NCEP Climate Forecast System Reanalysis (CFSR) 6-hourly Products, January 1979 to December 2010. Research Data Archive at the National Center for Atmospheric Research, Computational and Information Systems Laboratory, Boulder, CO. Available online at <http://dx.doi.org/10.5065/D69K487J>. Accessed 04 Apr 2014.
- Saraceno, M., C. Provost, A. R. Piola, J. Bava, and A. Gagliardini, 2004: Brazil Malvinas Frontal System as seen from 9 years of advanced very high resolution radiometer data. *Journal of Geophysical Research: Oceans (1978–2012)*, **109**, C05027.
- Saulo, A., M. Nicolini, and S. C. Chou, 2000: Model characterization of the South American low-level flow during the 1997–1998 spring–summer season. *Climate Dynamics*, **16**, 867–881.

- Seluchi, M. E., A. C. Saulo, M. Nicolini, and P. Satyamurty, 2003: The northwestern Argentinean low: A study of two typical events. *Monthly Weather Review*, **131**, 2361–2378.
- Silva Dias, M. A., 2011: An Increase in the Number of Tornado Reports in Brazil. *Weather, Climate & Society*, **3**, 209–217.
- Siqueira, J. R., W. B. Rossow, L. A. T. Machado, and C. Pearl, 2005: Structural Characteristics of Convective Systems over South America Related to Cold-Frontal Incursions. *Monthly Weather Review*, **133**, 1045–1064.
- Stopa, J. E., and K. F. Cheung, 2014: Intercomparison of wind and wave data from the ECMWF Reanalysis Interim and the NCEP Climate Forecast System Reanalysis. *Ocean Modelling*, **75**, 65–83.
- Tollerud, E., and R. Collander, 1993: Mesoscale convective systems and extreme rainfall in the central United States. IAHS PUBLICATION, 11–11.
- Travasso, M., G. Magrin, and G. Rodríguez, 2003: Relations between sea-surface temperature and crop yields in Argentina. *International Journal of Climatology*, **23**, 1655–1662.
- Velasco, I., and J. M. Fritsch, 1987: Mesoscale convective complexes in the Americas. *Journal of Geophysical Research: Atmospheres*, **92**, 9591–9613.
- Vera, C. S., P. K. Vighiarolo, and E. H. Berbery, 2002: Cold season synoptic-scale waves over subtropical South America. *Monthly Weather Review*, **130**, 684–699.
- Vera, C., and Coauthors, 2006a: Toward a unified view of the American monsoon systems. *Journal of Climate*, **19**, 4977–5000.
- Vera, C., and Coauthors, 2006b: The South American low-level jet experiment. *Bulletin of the American Meteorological Society*, **87**, 63–77.
- Vera, C., and G. Silvestri, 2009: Precipitation interannual variability in South America from the WCRP-CMIP3 multi-model dataset. *Climate Dynamics*, **32**, 1003–1014.
- Viale, M., and R. Garreaud, 2014: Summer Precipitation Events over the Western Slope of the Subtropical Andes. *Monthly Weather Review*, **142**, 1074–1092.

- Vimeux, F., G. Tremoy, C. Risi, and R. Gallaire, 2011: A strong control of the South American SeeSaw on the intra-seasonal variability of the isotopic composition of precipitation in the Bolivian Andes. *Earth and Planetary Science Letters*, **307**, 47–58.
- Vincent, D. G., 1994: The South Pacific convergence zone (SPCZ): A review. *Monthly Weather Review*, **122**, 1949–1970.
- Vuille, M., and Coauthors, 2012: A review of the South American Monsoon history as recorded in stable isotopic proxies over the past two millennia. *Climate of the Past Discussions*, **8**, 637–668.
- Wu, H., X. Zhang, L. Xiaoyan, G. Li, and Y. Huang, 2014: Seasonal variations of deuterium and oxygen-18 isotopes and their response to moisture source for precipitation events in the subtropical monsoon region. *Hydrological Processes*, in press.